

The role of microbial dissimilatory iron reduction in the formation of Proterozoic molar tooth structures

Malcolm S.W. Hodgskiss



Earth and Planetary Sciences

April, 2016

McGill University

Montréal, Québec, Canada

A thesis submitted to McGill University in partial fulfillment of the requirements of the degree of Master of Science

© Malcolm S.W. Hodgskiss 2016

The greater our knowledge increases, the greater our ignorance unfolds.

John F. Kennedy

Acknowledgements

I would first like to thank Galen Halverson for introducing me to the field of Proterozoic geology four years ago, and providing me with numerous opportunities, field and otherwise, since then. The questions guiding this thesis arose while measuring my first stratigraphic section with Galen in the field season of 2013.

I would also like to thank Marcus Kunzmann and Peter Crockford. Without the training Marcus has provided over the past several years, neither the field nor lab portions of this thesis would have been possible. Marcus continually gave insightful advice and discussions which helped to shape this thesis. Peter Crockford gave helpful guidance and encouragement, in addition to wading through early drafts of this thesis.

The expertise of André Poirier was crucial for the successful measurements of iron isotopes. Without André's exceptional technical knowledge and perseverance, not a single $\delta^{56}\text{Fe}$ measurement could have been made.

Finally, I would like to thank all of my friends and colleagues in PROPS, the department of Earth & Planetary Science at McGill University, GEOTOP, and elsewhere, for their continued support in my endeavours. Timothy Gibson and Clive Calver provided samples from the Boot Inlet and Humboldt Formations, respectively.

This thesis would not have been possible without the unwavering support of my family.

Field research in the Ogilvie and Wernecke Mountains, Yukon Territory, Baffin Island, Nunavut, and Finnmark, Norway was funded in part by the Northern Scientific Training Program and the Polar Continental Shelf Program.

Contents

Abstract	x
Résumé	xii
1 Introduction and Literature Review	1
1.1 Introduction	1
1.2 Physical Description	2
1.3 Temporal, Depositional, and Geographical Distribution	3
1.4 Models of Formation	5
1.4.1 Biogenic Origins	5
1.4.2 Gas Escape	5
1.4.3 Sulfate Reduction, Methanogenesis, and Organic Matter Decay	6
1.4.4 Seismites	8

1.4.5	Wave-pumping	9
1.4.6	Changing Ocean Chemistry	9
1.4.7	Evaporite Replacement	10
1.5	Research Objectives	10
2	Molar Tooth Structures in the Sedimentary Environment	15
2.1	Introduction	15
2.2	Localities Studied	16
2.2.1	Helena Formation, Belt Basin, Montana, U.S.A	16
2.2.2	Victor Bay Formation, Borden Basin, Nunavut, Canada	17
2.2.3	Båtsfjord Formation, Timan Basin, Finnmark, Norway	18
2.2.4	Other Basins	19
2.3	Variations in Depositional Environments	21
2.4	Microspar Outside of Molar Tooth Structures	22
2.5	Conclusion	22
3	Geochemistry of Molar Tooth Structures: Testing the Role of Dissimilatory Iron Reduction	41
3.1	Abstract	41
3.2	Introduction	42
3.3	Microbial Reduction of Smectite	43
3.4	Iron Isotopes	44
3.5	Sample Set	44

3.6	Methods	45
3.6.1	Sample Preparation	45
3.6.2	Total Organic Carbon and Total Sulfur	46
3.6.3	Carbon and Oxygen Isotopes	47
3.6.4	Sample Dissolution for Elemental Concentrations and Iron Isotopes .	47
3.6.5	Major/minor elements	48
3.6.6	Iron Isotopes	49
3.6.7	Scanning Electron Microscopy	51
3.7	Results	51
3.7.1	Total Organic Carbon and Total Sulfur	51
3.7.2	Carbon Isotopes	51
3.7.3	Oxygen Isotopes	52
3.7.4	Element Abundances	52
3.7.5	Iron Isotopes	54
3.7.6	Scanning Electron Microscope	57
3.8	Discussion	57
3.8.1	Preservation of Primary Signatures	57
3.8.2	Microbial Illitisation and the Formation of Molar Tooth Structures .	63
3.8.3	Effect of Clay Minerals	70
3.8.4	A Dissimilatory Iron Reduction Model for Molar Tooth Structure Formation	70
3.8.5	Abundance and Disappearance of Molar Tooth Structures	71

3.8.6	Implications for Molar Tooth Structure Formation by BSR and Methano- genesis	73
3.9	Conclusion	75
4	Concluding Thoughts and Future Work	83
	Supplementary Information	85

List of Figures and Tables

Figures

1.1	Global distribution of molar tooth structures	2
1.2	Scouring of molar tooth structures	4
2.1	Legend for all stratigraphic columns	24
2.2	Stratigraphic column of the Helena Formation	25
2.3	Map of studied area in Borden Peninsula, Baffin Island, Nunavut, Canada .	26
2.4	Stratigraphic column of the Victor Bay Formation	27
2.5	Map of studied area in Finnmark, northern Norway	28
2.6	Stratigraphic columns of the Annijokka Member, Båtsfjord Formation	29
2.7	Molar tooth structures in the Båtsfjord Formation at Syltefjorden.	30
2.8	Molar tooth structure “blob” and molar tooth structure outcrop.	31
2.9	Microspar infill of desiccation cracks, Båtsfjord Formation	32
2.10	Horizontal ribbon molar tooth structures and Båtsfjord Formation exposure	33
2.11	Molar tooth structures in the Victor Bay Formation	34
2.12	Microspar infill in the Black Canyon Creek Formation	35
2.13	Microspar infill and molar tooth structures in the Black Canyon Creek Formation	36
2.14	Ediacaran molar tooth structures, Maieberg Formation	37
3.1	Distribution of molar tooth structures in this study	46
3.2	$\delta^{56}\text{Fe}$ and $\delta^{57}\text{Fe}$ stability at signal intensity of 7.0, 3.5, 1.8, and 0.7 Volts . .	50
3.3	$\delta^{13}\text{C}$ and $\delta^{18}\text{O}$ of molar tooth structures and matrix carbonate	53
3.4	Difference in $\delta^{13}\text{C}$ and $\delta^{18}\text{O}$ of molar tooth structures and matrix carbonate	54

3.5	$\delta^{56}\text{Fe}$ of molar tooth structures, matrix carbonate, and matrix siliciclastics	55
3.6	Comparison of $\delta^{56}\text{Fe}$ of molar tooth structure, matrix carbonate, and matrix siliciclastics	56
3.7	Scanning electron microscope image of molar tooth structure	58
3.8	Mn/Sr vs Mg/Ca in molar tooth structure and matrix carbonate	59
3.9	Effects of dolomitisation of the matrix carbonate on $\delta^{13}\text{C}$ and $\delta^{18}\text{O}$	60
3.10	Effect of dolomitisation on $\delta^{56}\text{Fe}$	62
3.11	Mechanisms behind microbial dissimilatory iron reduction	67
3.12	Model for molar tooth structure formation	71
S1	Mass dependent fractionation of $\delta^{56}\text{Fe}$ and $\delta^{57}\text{Fe}$	100

Tables

3.1	Sample set details.	45
S1	Major and minor element abundances in molar tooth structures.	86
S2	Major and minor element abundances in matrix carbonate	89
S3	$\delta^{56}\text{Fe}$ in molar tooth structures	92
S4	$\delta^{56}\text{Fe}$ in matrix carbonate	93
S5	$\delta^{56}\text{Fe}$ in matrix siliciclastics	94
S6	$\delta^{13}\text{C}$ in molar tooth structures.	95
S7	$\delta^{13}\text{C}$ in matrix carbonate.	97
S8	Total organic carbon and pyrite content in bulk rock.	99

Abstract

Molar tooth structures are enigmatic carbonate structures that occur as microcrystalline calcite ribbons and blobs within argillaceous carbonates. Field observations indicate that they formed in the uppermost sediment column, prior to lithification of the host rock. Molar tooth structures have been found in numerous Proterozoic basins throughout the world, and are observed in the sedimentary record between approximately 2600-720 Ma. Despite their widespread occurrence, both their cause of formation and disappearance from the sedimentary record remain poorly understood. Although molar tooth structure occurrence is near-exclusive to clay-rich carbonate sediments, to date there has been no geochemical study exploring this relationship. Here, we present carbon, oxygen, and iron isotope analyses, in addition to major/minor element concentrations, for 77 molar tooth structure samples from eight different basins spanning approximately 700 Ma. We test a dissimilatory iron reduction hypothesis for the origin of molar tooth structures, in which microbial reduction of Fe(III) to Fe(II) occurs in Fe-rich smectites and oxides. The resulting shrinkage and deflocculation of clay minerals would create the void spaces in which molar tooth structures form, while locally increasing pore water alkalinity beyond a threshold at which microcrystalline calcite begins to precipitate. Measurements of $\delta^{56}\text{Fe}$ are supportive of a dissimilatory iron reduction mechanism

for molar tooth structure formation, with molar tooth structures typically depleted in $\delta^{56}\text{Fe}$ relative to both the carbonate minerals and siliciclastic minerals in the host sediment. $\delta^{13}\text{C}$ measurements of the molar tooth structures and matrix carbonate are indistinguishable. The findings of this study show that the appearance and disappearance of molar tooth structures are not insignificant events, but rather are reflective of an Earth in transition.

Résumé

Les structures de “dents molaires” sont des structures carbonatées énigmatiques qui surviennent lorsque de la calcite microcristalline se retrouve sous forme de filaments et de masses au sein de carbonates argileux. Les observations de terrain indiquent que les structures de “dents molaires” se forment dans la partie supérieure de la colonne sédimentaire, et ce avant la lithification de la roche mère. Ces structures se retrouvent dans de nombreux bassins du Protérozoïque à travers le monde, et sont observées dans le registre sédimentaire entre approximativement 2600-720 Ma. Malgré leur présence répandue, les raisons de leur formation et de leur disparition au sein du registre sédimentaire demeurent peu comprises. De plus, même si les structures de “dents molaires” sont presque exclusivement présentes dans des sédiments carbonatés riches en argile, aucune étude géochimique explorant cette relation n’a été réalisée jusqu’à maintenant. Ici, nous présentons des analyses isotopiques du carbone, de l’oxygène, et du fer, en plus des concentrations des éléments majeurs et mineurs, pour 77 échantillons de structures de “dents molaires”. Ces échantillons proviennent de huit bassins différents, et couvrent une période d’environ 700 Ma. Nous testons ici l’hypothèse que la réduction dissimilatrice du fer est à l’origine de la formation des structures de “dents molaires”, c’est-à-dire que la réduction microbienne du Fe(III) en Fe(II) prend en présence des oxydes

et smectites riches en fer. Cette réduction entraîne le rétrécissement et la défloculation des minéraux argileux, créant ainsi des vides ou pores dans lesquels la formation des structures de “dents molaires” peut prendre place, tout en augmentant localement l’alcalinité de l’eau interstitielle jusqu’à atteindre le seuil auquel la calcite microcristalline peut précipiter. Les mesures du $\delta^{56}\text{Fe}$ soutiennent l’hypothèse selon laquelle la réduction dissimilatrice du fer serait à l’origine de la formation des structures de “dents molaires”. En effet, ces structures sont typiquement appauvries en $\delta^{56}\text{Fe}$ par rapport aux minéraux carbonatés et siliclastiques présents dans la roche mère. Les mesures de $\delta^{13}\text{C}$ des structures de “dents molaires” et de la matrice carbonatée sont indifférenciables. Les résultats de cette étude montrent donc que l’apparition et la disparition des structures de “dents molaires” sont loin d’être des événements négligeables, et reflètent plutôt une Terre en transition.

CHAPTER 1

Introduction and Literature Review

1.1 Introduction

“Molar tooth structures” (MTS) were first discovered in southeastern British Columbia, Canada, and described as “impure limestone in which the carbonate of lime is intermingled with argillaceous patches in folds resembling the markings in the tooth of an elephant” (Bauerman, 1884). Subsequent work by others has shown that molar tooth structures are exclusive to the Precambrian (e.g. Pratt, 1998; James et al., 1998). As it stands today, the cause of their formation and disappearance in the sedimentary record remain poorly understood. In addition to addressing their restricted temporal range, any attempt to understand molar tooth structures must address two further questions: what mechanism(s) could create the void spaces in which MTS form, and what causes the precipitation of calcite cement?

MTS formation spanned almost 2 Ga, and they have been found in a broad range of depositional environments and geographical locations (Figure 1.1). The earliest documented occurrence is ~ 2.6 Ga (Bishop et al., 2006a), and the youngest are mid-Neoproterozoic (James

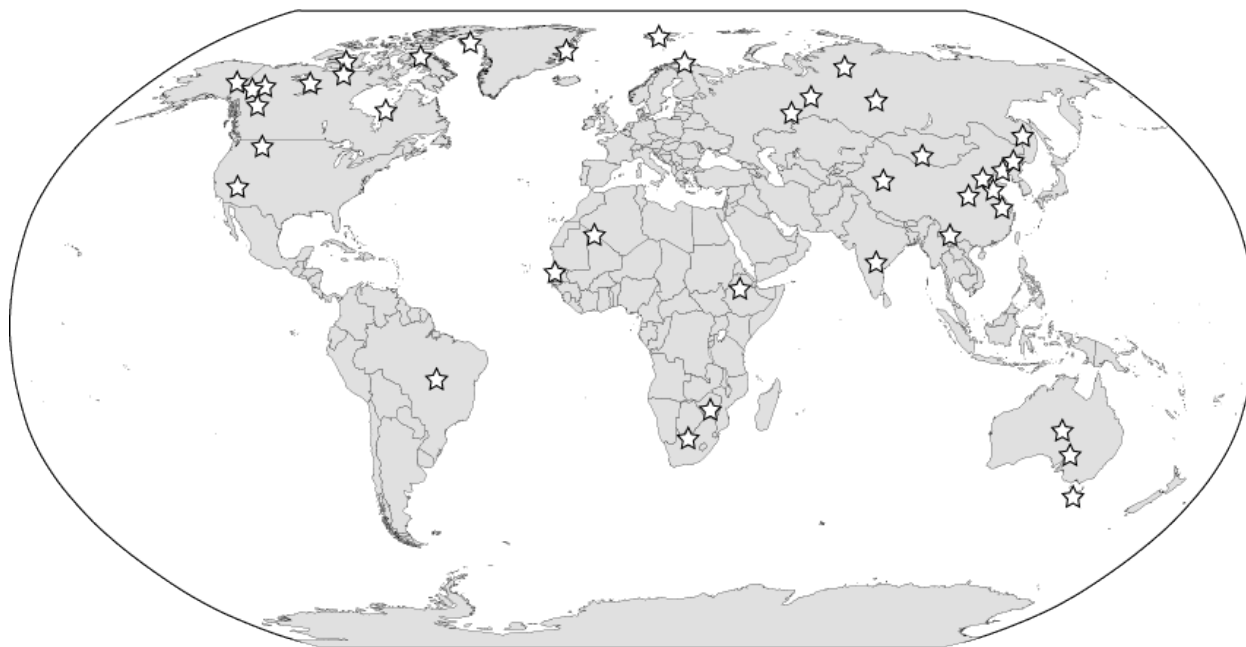


Figure 1.1 Global distribution of molar tooth structures (Personal observations; Kuang, 2014, and references therein).

et al., 1998). In a depositional environment, they may be found over a range of water depths, from below storm wave base, to the intertidal zone. Despite this, molar tooth structures are near-exclusive to argillaceous carbonate sediments. Their geographical distribution spans much of the world, reflective of their widespread occurrence in Proterozoic basins, although they are most common in Arctic Canada, Siberia, and China (Kuang, 2014, and references therein), which have thick stratigraphic successions of late Paleoproterozoic to early Neoproterozoic age.

1.2 Physical Description

Although the definition of molar tooth structure has been changed over time to accommodate new discoveries, here the definition of Furniss et al. (1998) is used, where MTS are broadly defined as vertical ribbons, horizontal ribbons, and blobs. These are filled with blocky, microcrystalline calcite grains ranging from 5-15 μm in width, referred to as microspar (Furniss et al., 1998). Boundaries between the argillaceous host sediment and the microspar

are sharp. Molar tooth structures most commonly occur as vertical ribbons, typically between 1-3 centimetres long, and several millimetres wide, although they may reach up to 20 centimetres long and 1 centimetre wide. Sediments are often compacted around molar tooth structures, and vertical ribbons range from relatively linear, to highly contorted, and may occasionally be fractured. Horizontal ribbons are typically approximately 1 centimetre in length, and 3-5 millimetres in width. They lack the ptigmatic folding exhibited in some vertical ribbons. Blobs are the most rare morphology and may be spherical to highly irregular, ranging from 1 millimetre to several centimetres in diameter.

Essential to the understanding of molar tooth structures is that they form shortly after deposition of the host sediment, but prior to lithification. Bedding is frequently compressed around molar tooth structures, with vertical shortening reaching up to 80% (Pratt, 1998). This compaction is manifested in the ptigmatic folding, fracturing, and vertical displacement often exhibited by vertical ribbons. In storm-dominated environments, molar tooth structures may be eroded to form molar tooth breccias and conglomerates (Figure 1.2). In short, molar tooth structures form early cements in unlithified marine carbonates.

1.3 Temporal, Depositional, and Geographical Distribution

The oldest reported molar tooth structures have been found in the ~2.6 Ga Monteville Fm., Transvaal Craton, South Africa, where their occurrence spans from a shallow subtidal environment to near storm wave base (Bishop et al., 2006a). In addition to the presence of MTS, an identical microspar was found filling pore space between sediment grains and forming networks of veins on sandy bedding surfaces. Some MTS were found to have internal clay laminations, interpreted as indicating that the cracks were open to the sea floor.

Molar tooth structures are rare in Paleoproterozoic successions; the two reported occurrences are in Arctic Canada (Campbell et al., 1981; Ricketts et al., 1981). In the ~1.9 Ga

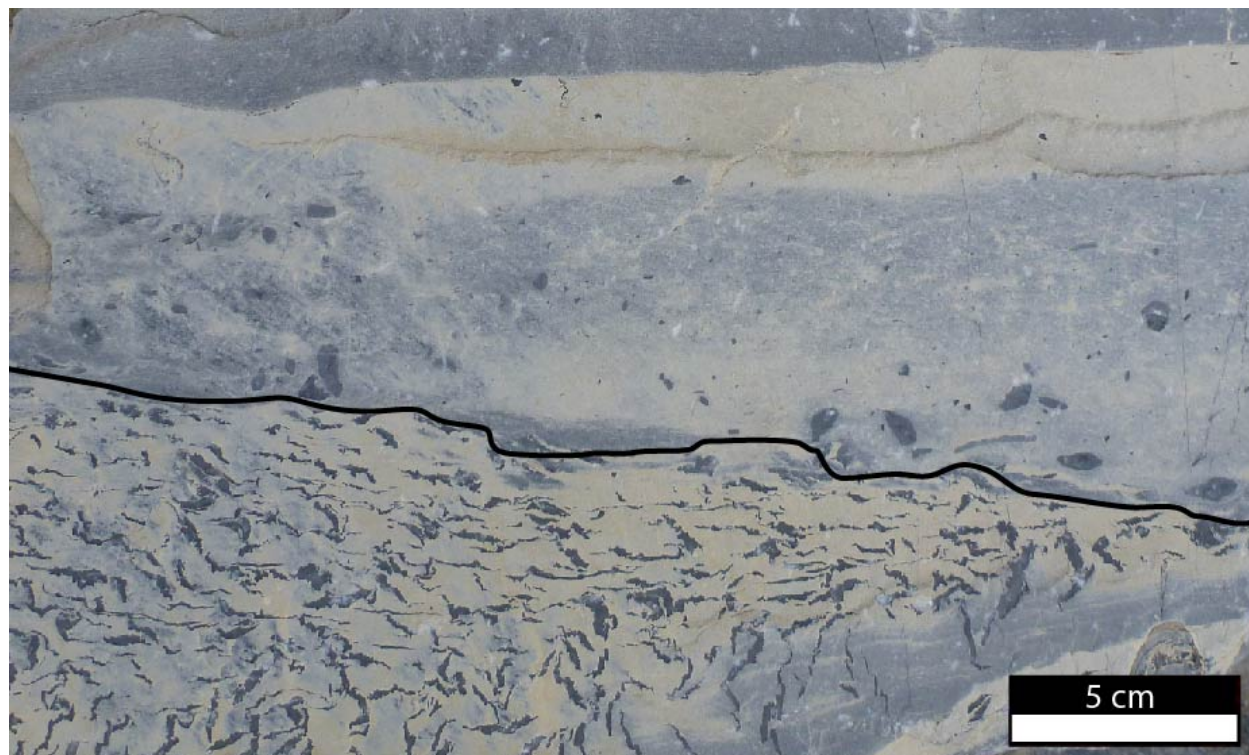


Figure 1.2 Molar tooth structures in the Mesoproterozoic Muskwa assemblage, northern British Columbia, Canada. A scour surface is indicated by a black line. Below, MTS are in situ, above, they have been reworked as clasts.

Western River Fm., Goulburn Group, Northwest Territories, Canada, molar tooth structures occur in the cores of stromatolite reef complexes and adjacent marly-carbonate, interpreted to have been deposited in a shallow subtidal setting (Campbell et al., 1981; McCormick et al., 1992). In the ~1.8 Ga Fairweather, Tukarak, and Mavor Formations, Belcher Group, Nunavut, molar tooth structures are most commonly found in dolostones and shaley dololutes. The occurrence of flaser bedding and nearby pisolites is interpreted to indicate that deposition occurred in tidal flats to shallow, subtidal environments.

The occurrence of molar tooth structures peaks in the Mesoproterozoic. Molar tooth structures are common features in carbonate sequences in North America, Siberia and China, and have also been documented in the Atar Group, Mauritania (Kuang, 2014). The majority of these occurrences are found in carbonates deposited in middle to inner ramp environments at inferred water depths spanning from shallow subtidal to below storm wave base (Personal observations; James et al., 1998).

Molar tooth structures are also common in the Neoproterozoic, and they have been reported in North America, Siberia, Asia, Australia, Africa, and to a much lesser extent, South America and northernmost Europe. The Neoproterozoic also marks the demise of MTS, as they disappear shortly before the onset of the Sturtian glaciation at ~ 720 Ma (Macdonald et al., 2010).

1.4 Models of Formation

Since their discovery, a wide array of mechanisms for the formation of molar tooth structures have been proposed. In this section, the main hypotheses will be evaluated in terms of whether they can fully explain the formation (i.e. creation of void spaces and rapid calcite precipitation) and temporal distribution of MTS.

1.4.1 Biogenic Origins

Smith (1968) noted that some occurrences of horizontal ribbon molar tooth structures seem to converge upward and merge into *Collenia* type stromatolites. This stromatolitic affinity was also reported by O'Connor (1972), who suggested that MTS are “cryptalgal” structures, where MTS morphologies are indicative of environmental factors such as water depth, wave energy, and depositional rate.

This hypothesis has been discredited, as molar tooth structures do not resemble any known organisms, either extinct or extant (Hofmann, 1976). Furthermore, molar tooth structures have been found to cross cut stromatolites and microbialaminites, indicating that they form postdepositionally rather than as primary structures (Furniss et al., 1998).

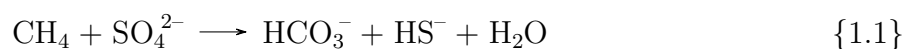
1.4.2 Gas Escape

Furniss et al. (1998) experimentally reproduced fissures remarkably similar to that of MTS, using a mixture of mud and water, with yeast and sugar added to produce carbon

dioxide. These materials were mixed into a slurry, poured into aquariums, and plaster poured on top to mimic burial underneath a nearly impermeable sediment layer. This experiment yielded gas-generated cracks that were similar in scale and morphology to some molar tooth structures. Given the similarity of some MTS to these gas-escape structures, Furniss et al. (1998) argued that MTS likely formed as the result of in-situ gas production during early diagenesis. Although they were not able to identify precisely which gas might be responsible for MTS, Furniss et al. (1998) pointed out that methane (CH_4), hydrogen sulfide (H_2S), and carbon dioxide (CO_2) are all common products of microbial activity during early diagenesis in marine sediments.

1.4.3 Sulfate Reduction, Methanogenesis, and Organic Matter Decay

Frank et al. (1998) applied carbon isotope geochemistry to investigate the potential roles of different gas sources in the formation of MTS. If microbial sulfate reduction played a role, the bicarbonate generated by oxidation of methane would inherit its very low $\delta^{13}\text{C}$ values, which would be reflected in the MTS. Microbial sulfate reduction (MSR) of methane produces hydrogen sulfide and bicarbonate, increasing pore water alkalinity, and therefore promoting calcite precipitation:



The authors noted that if reduced sulfur was present in a carbonate-buffered system, it would exist as dissolved, pore water bisulfide (HS^-) rather than as gaseous hydrogen sulfide. Production of carbon dioxide by methanogenesis or oxidation of organic matter could have also served as a gas source to create voids, and would result in $\delta^{13}\text{C}$ enrichment and depletion, respectively.

Given that $\delta^{13}\text{C}$ analyses indicate molar tooth structures and their host matrix have virtually indistinguishable isotope compositions, any mechanism entailing MSR seems to be unviable. Frank et al. (1998) noted that a large pool of dissolved inorganic carbon (DIC) would suppress any isotopic signal resulting from remineralization of methane or organic

carbon. Hence, while the inconclusive isotopic data do not support these mechanisms, they cannot be definitely ruled out.

Shen et al. (2016) revisited the possible role of MSR and methanogenesis in triggering the formation of MTS, through sulfur isotope analyses of carbonate-associated sulfate in five molar tooth structure samples from the Neoproterozoic Wanlong Formation, China. They found $\delta^{34}\text{S}$ values of 31.9-42.8‰ in five molar tooth structures, compared to $\delta^{34}\text{S}$ values of 19.1-27.5‰ in the host rock. They also measured an enrichment of 0.5-1.0‰ in $\delta^{13}\text{C}$ of molar tooth structures relative to the host matrix. The authors hypothesized that near the top of the sediment column, methanogenesis and MSR co-occurred, with the release of methane fracturing sediments, and MSR increasing alkalinity, promoting the precipitation of calcite. Using the measured enrichment of 0.5-1.0‰ in $\delta^{13}\text{C}$ of the MTS relative to the host sediment, they constructed a binary mixing model that implies the contribution of carbon from methanogenesis must be very small ($\sim 0.7\%$). Shen et al. (2016) further postulated that an increase in ocean oxygenation during the purported mid-Neoproterozoic oxygenation event pushed methanogenesis deeper in the sediment column, eliminating the overlap of MSR and methanogenesis. This hypothesis successfully accounts for both the mechanism of formation of MTS and its disappearance from the stratigraphic record.

We note that this model is based on only a few data points, and these showing a slight relative $\delta^{13}\text{C}$ enrichment in the MTS. Most studies have shown no statistically significant difference in $\delta^{13}\text{C}$ between MTS and the matrix (Frank et al., 1998; Bishop et al., 2006a, this study). This question will be explored in detail in Chapter 3 of this thesis.

1.4.4 Seismites

A hypothesis proposed by Pratt (1998) invoked seismic activity as a mechanism for forming molar tooth structures. Propagating Love waves in the 20 to 1 Hz frequency band could trigger the deflocculation of clay structures in the uppermost metre of sediment, increasing pore pressure. This newly released pore water would have coalesced, producing fissures within the sediment that were closed to the sediment-water interface due to the tensile strength of clay-rich sediments. The water filling these fissures would have carried lime mud, in addition to rare silt and clay, and subsequently crystallized to form molar tooth structures. Additional seismic events would have resulted in plastic deformation or brittle fracturing of pre-existing molar tooth structures. Pratt also noted that compression of sediments around molar tooth structures, up to approximately 80%, is consistent with that of modern, clay-rich sediments. Furthermore, stratigraphic sections measured in the Mesoproterozoic Helena Formation, Montana, indicated the occurrence of a seismic event approximately every 0.5-3 metres of stratigraphy, roughly half of which are associated with molar tooth structures (Pratt, 1998). For comparison, Quaternary lacustrine sediments in Washington state, U.S.A, record the occurrence of seismic events approximately every 1.3 metres of stratigraphy (Sims, 1975). Clearly, seismic activity and mixed carbonate-siliciclastic facies continued to occur after the disappearance of molar tooth structures. Pratt (1998) therefore attributes their disappearance to increased bioturbation of sediments by metazoa.

Contrary to this hypothesis, there is no evidence for metazoan bioturbation prior to ~550 Ma (Shields, 2002). Coupled with the continued occurrence of seismicity and mixed carbonate-siliciclastic environments into the Phanerozoic, a seismic/tsunamigenic mechanism alone cannot explain their formation and disappearance.

1.4.5 Wave-pumping

Bishop et al. (2006b) hypothesized that molar tooth structures may be caused by wave-induced fluid pumping. A series of interconnected cracks may have formed as the result of cyclic sediment loading by the movement of waves overhead. The rhythmic loading of waves produces heaving and contraction of muddy sediments, a process that has been observed to produce centimetre-scale cracks in modern sediments (Forristall et al., 1985). Bishop et al. (2006b) proposed that storm waves then pumped water through the crack network, mixing seawater and pore water. Calcite nuclei formed, and grew through Ostwald ripening to approximately 7-10 μm in size. Sediment compaction eventually filled any remaining voids, while plastically deforming the molar tooth structures. Subsequent overgrowth and cementation solidified molar tooth structures, resulting in brittle deformation.

1.4.6 Changing Ocean Chemistry

Whereas changing ocean chemistry in the Proterozoic is not a specific mechanism in the formation of MTS, it is frequently invoked to explain the cessation of molar tooth structures (e.g. Bishop et al., 2006b). Shields (2002) noted that early microspar cements have been observed in organic-walled fossils and stromatolite layers, suggesting that very early microspar cement is not exclusive to molar tooth structures. Shields (2002) also pointed out that molar tooth structures and stromatolites both “peak” and “collapse” in the Mesoproterozoic and Neoproterozoic, respectively, suggesting that the two share a controlling factor. Grotzinger (1990) previously suggested that a decrease in the concentration of dissolved inorganic carbon in the ocean may account for the Neoproterozoic decline of stromatolites; the same mechanism may therefore play a role in the disappearance of MTS (Shields, 2002). Alternatively, it has been suggested that the decline of MTS may be the result of an increase in the concentration of calcite precipitation inhibitors, such as Fe^{2+} , Mg^{2+} , or SO_4^{2-} (Shields, 2002).

1.4.7 Evaporite Replacement

Eby (1977) interpreted the Helena Fm. to have been deposited in a hypersaline lake and suggested that MTS form by the precipitation of evaporite minerals which were subsequently replaced by fine-grained calcite. In this hypothesis, molar tooth structure blobs were nodular evaporites, and horizontal ribbons were evaporite crusts. Similarly, vertical ribbons represent shrinkage cracks which were subsequently infilled by evaporite minerals, and then replaced by microcrystalline calcite. The absence of evaporite casts in the smooth walls of molar tooth structures, combined with the absence of evaporite pseudomorphs, makes this scenario highly unlikely (Furniss et al., 1998).

1.5 Research Objectives

Despite the occurrence of molar tooth structures in numerous carbonate environments across a broad swath of time and space, they remain enigmatic. Proposed mechanisms of formation range from the ordinary to the eccentric, but have yet to produce a theory which comprehensively explains both their formation and disappearance in the sedimentary record. Rather than an esoteric Proterozoic phenomenon, we view molar tooth structures as an important environmental indicator, the formation of which is indicative of the co-occurrence of a variety of environmental conditions.

James et al. (1998), Bartley et al. (2004), and Higgins et al. (2009) have noted that throughout Earth history, there has been a first order shift in carbonate precipitation toward increasingly shallow depositional environments, evidenced by the shift from Paleoproterozoic seafloor aragonite fans, to Mesoproterozoic micrites and stromatolites, to Phanerozoic skeletal carbonates. The occurrence of molar tooth structures is consistent with these observations, and may record an intermediary mode of carbonate production spanning from deep to shallow depositional environments. Furthermore, James et al. (1998) noted that molar tooth structures can comprise approximately 5-25% of sediment by volume, comparable to that of seafloor

aragonite fans and crusts from the Paleoproterozoic, and invertebrate carbonate fossils in the Phanerozoic, making them a significant contributor to the Proterozoic carbonate record.

Many theories for molar tooth structures invoke separate mechanisms for the formation of cracks and the rapid precipitation of microspar (e.g. Bishop et al., 2006b; Shen et al., 2016). Here, we present and test the hypothesis that molar tooth structures are the result of a specific pathway of microbial iron reduction, in which Fe-rich smectite is converted to illite in the uppermost sediment column. Although this mechanism was suggested by Bishop et al. (2006b), these authors discounted it under the assumption that the reaction is typically K^+ limited, and therefore could not significantly change alkalinity. Nonetheless, this process offers a single mechanism to locally increase porewater alkalinity while simultaneously creating void spaces for molar tooth structures to form in, and merits greater investigation. Microbial illitisation has been shown to occur rapidly, converting up to 40% of smectite to illite at room temperature and pressure, within less than two weeks (Kim et al., 2004). Furthermore, microbial illitisation results in the release of alkaline pore water, providing a single mechanism to explain both the formation of the fissures which MTS fill, in addition to the nucleation of calcite. It follows from this hypothesis that the disappearance of molar tooth structures might be linked, at least in part, to variations in the production of smectite due to changing weathering conditions.

Bibliography

- Bartley, J. K. and Kah, L. C. (2004). "Marine carbon reservoir, Corg-Ccarb coupling, and the evolution of the Proterozoic carbon cycle." *Geology* 32.2, pp. 129–132.
- Bauerman, H. (1884). *Report on the Geology of the Country Near the Forty-ninth Parallel of North Latitude West of the Rocky Mountains: From Observations Made 1859-1861*. Dawson.
- Bishop, J. W. and Sumner, D. Y. (2006a). "Molar tooth structures of the Neoarchean Monteville Formation, Transvaal Supergroup, South Africa. I: Constraints on microcrystalline CaCO₃ precipitation." *Sedimentology* 53.5, pp. 1049–1068.
- Bishop, J. W., Sumner, D. Y., and Huerta, N. J. (2006b). "Molar tooth structures of the Neoarchean Monteville Formation, Transvaal Supergroup, South Africa. II: A wave-induced fluid flow model." *Sedimentology* 53.5, pp. 1069–1082.
- Campbell, F. and Cecile, M. (1981). "Evolution of the Early Proterozoic Kilohigok Basin, Bathurst Inlet–Victoria Island, Northwest Territories." *Proterozoic basins of Canada*. Vol. 81, pp. 103–131.
- Eby, D. E. (1977). *Sedimentation and Early Diagenesis Within Eastern Portions of the "Middle Belt Carbonate Interval" (Helena Formation) Belt Supergroup (Precambrian)*,

- Western Montana*. [unpublished Ph.D Thesis]: State University of New York, Stony Brook. 712p.
- Forristall, G. Z. and Reece, A. M. (1985). "Measurements of wave attenuation due to a soft bottom: the SWAMP experiment." *Journal of Geophysical Research: Oceans (1978–2012)* 90.C2, pp. 3367–3380.
- Frank, T. D. and Lyons, T. W. (1998). "'Molar-tooth' structures: A geochemical perspective on a Proterozoic enigma." *Geology* 26.8, pp. 683–686.
- Furniss, G., Rittel, J. F., and Winston, D. (1998). "Gas bubble and expansion crack origin of 'molar-tooth' calcite structures in the middle Proterozoic Belt Supergroup, western Montana." *Journal of Sedimentary Research* 68.1, pp. 104–114.
- Grotzinger, J. P. (1990). "Geochemical model for Proterozoic stromatolite decline." *American Journal of Science* 290, pp. 80–103.
- Higgins, J., Fischer, W., and Schrag, D. (2009). "Oxygenation of the ocean and sediments: consequences for the seafloor carbonate factory." *Earth and Planetary Science Letters* 284.1, pp. 25–33.
- Hofmann, H. (1976). "Precambrian microflora, Belcher Islands, Canada: significance and systematics." *Journal of Paleontology*, pp. 1040–1073.
- James, N. P., Narbonne, G. M., and Sherman, A. G. (1998). "Molar-tooth carbonates: shallow subtidal facies of the Mid-to Late Proterozoic." *Journal of Sedimentary Research* 68.5, pp. 716–722.
- Kim, J., Dong, H., Seabaugh, J., Newell, S. W., and Eberl, D. D. (2004). "Role of microbes in the smectite-to-illite reaction." *Science* 303.5659, pp. 830–832.
- Kuang, H.-W. (2014). "Review of molar tooth structure research." *Journal of Palaeogeography* 3.4, pp. 359–383.
- Macdonald, F. A., Schmitz, M. D., Crowley, J. L., Roots, C. F., Jones, D. S., Maloof, A. C., Strauss, J. V., Cohen, P. A., Johnston, D. T., and Schrag, D. P. (2010). "Calibrating the cryogenian." *Science* 327.5970, pp. 1241–1243.

- McCormick, D. S. and Grotzinger, J. (1992). "Evolution and significance of an overfilled alluvial foreland basin: Burnside Formation (1.9 Ga), Kilohigok Basin, NWT, Canada." *Basin research* 4.3-4, pp. 253–278.
- O'Connor, M. P. (1972). "Classification and environmental interpretation of the cryptalgal organosedimentary" molar-tooth" structure from the Late Precambrian Belt-Purcell Supergroup." *The Journal of Geology*, pp. 592–610.
- Pratt, B. R. (1998). "Molar-tooth structure in Proterozoic carbonate rocks: Origin from synsedimentary earthquakes, and implications for the nature and evolution of basins and marine sediment." *Geological Society of America Bulletin* 110.8, pp. 1028–1045.
- Ricketts, B. and Donaldson, J. (1981). "Sedimentary history of the Belcher Group of Hudson Bay." *Proterozoic Basins of Canada*. Vol. 81, pp. 235–254.
- Shen, B., Dong, L., Xiao, S., Lang, X., Huang, K., Peng, Y., Zhou, C., Ke, S., and Liu, P. (2016). "Molar tooth carbonates and benthic methane fluxes in Proterozoic oceans." *Nature communications* 7. DOI: 10.1038/ncomms10317.
- Shields, G. A. (2002). "Molar-tooth microspar': a chemical explanation for its disappearance 750 Ma." *Terra Nova* 14.2, pp. 108–113.
- Sims, J. D. (1975). "Determining earthquake recurrence intervals from deformational structures in young lacustrine sediments." *Tectonophysics* 29.1, pp. 141–152.
- Smith, A. G. (1968). "The origin and deformation of some" molar-tooth" structures in the Precambrian Belt-Purcell Supergroup." *The Journal of Geology*, pp. 426–443.

CHAPTER 2

Molar Tooth Structures in the Sedimentary Environment

2.1 Introduction

To develop a model applicable to all occurrences of molar tooth structures, we have studied examples from many different parts of the world, representing different intervals of the Proterozoic time scale and varying depositional facies. Here, we present stratigraphic columns and depositional environment interpretations for three different localities of molar tooth structures: the early Mesoproterozoic Helena Formation, Montana, U.S.A, the latest Mesoproterozoic Victor Bay Formation, Baffin Island, Nunavut, Canada, and the mid-Neoproterozoic Annijokka Member of the Båtsfjord Formation, Arctic Norway. In addition, the depositional environments of four other molar tooth structure bearing units which were sampled for this study will be discussed. These successions span an approximately 700 Ma time interval, and cover a broad range of depositional environments, from below storm wave base, to the intertidal zone.

2.2 Localities Studied

2.2.1 Helena Formation, Belt Basin, Montana, U.S.A

The ~ 1.45 Ga Helena Formation (Evans et al., 2000) is the effective type locality of molar tooth structures, and has been the focus of numerous molar tooth structure studies (e.g. Furniss et al., 1998; Frank et al., 1998; Pratt, 1998). The studied section near Roger's Pass (~ 100 km NW of Helena, Montana) is approximately 230 metres thick, and was deposited across a broad range of water depths, from near storm wave base to shoreface (Figure 2.2). Much of the lower half of the section is interpreted as being deposited below storm wave base. In the lowermost 105 metres of section, the Helena Formation is predominantly composed of dolomitized siltstone and black shale, with rare beds of limestone micrite, dolomicrite, or stromatolitic limestone. Molar tooth structures occur most often in dolomitic siltstone, but also in limestone micrite. There are minor amounts of molar tooth structures and intraclast breccias, wave ripples, and channelization. Between 105 to 140 metres, the section shallows, transitioning from siliciclastic-dominated to carbonate-dominated. Thick packages of limestone micrite are interbedded with siltstones (in places dolomitic), minor black shale, and rare sandstone and dolomicrite. Both stromatolites and molar tooth structures are common, and there are minor amounts of brecciation, hummocky cross stratification, and wave ripples. The uppermost 100 metres of section are dominated by limestone, primarily stromatolitic but also micritic, with very minor amounts of black shale, siltstone (sometimes dolomitic), and dolomicrite. Molar tooth structures are abundant, and breccias consisting of both molar tooth structures and intraclasts occur. Ooids occur in several horizons, and there are two instances of channelization.

This section is interpreted as a shallowing upward succession, from a silty-shaley environment below storm wave base to a carbonate-dominated, near shoreface environment. The shale and dolomitic siltstone comprising the Lower Helena Formation exhibit little indication of forming in a high energy environment. In contrast, the Upper Helena Formation, which

is primarily composed of micrite, contains rare hummocky cross stratification, indicating formation above storm wave base. Furthermore, the relative increase in carbonate lithologies suggests shallower deposition. The increased brecciation, in addition to ooid horizons, supports deposition in a relatively shallow environment.

2.2.2 Victor Bay Formation, Borden Basin, Nunavut, Canada

The ~ 1.0 Ga Victor Bay Formation, Bylot Supergroup, contains a very well preserved, mixed carbonate-siliciclastic sequence hundreds of meters thick, with abundant molar tooth structures and molar tooth “tempestites”. One partial section, measuring 510 metres, was logged from the contact with the underlying Angmaat Formation at Pingo Valley N (Figure 2.4). Several samples were also collected from a section located at Mala River, ~ 10 km to the northeast of the Pingo Valley N location (Figure 2.3).

The section measured at Pingo Valley N records a shallowing upward sequence. The lowermost 150 metres of the section are predominantly siltstone and dolomitic siltstone, with minor amounts of organic-rich shale, molar tooth structures, and limestone nodules. It then sharply transitions into 200 metres of silty limestone, with minor dolomicrite and limestone beds which are internally fining upwards, while dolomicrite and silty dolomicrite become more common. Molar tooth structures occur intermittently. Dolomite lithofacies become increasingly common upsection, with the uppermost 150 metres comprising dolomite microbialaminite, in addition to dolomitized “tempestites” with abundant clasts of MTS microspar (Figure 2.12a). These are interpreted to be molar tooth structures which formed, and were subsequently eroded, fractured, and redeposited. There are also minor amounts of dolomicrite and silty dolomicrite, often containing a significant volume of molar tooth structures, which may comprise up to 80% of the rock. Molar tooth structures also occur in microbialaminite beds, where they crosscut laminations.

This section is interpreted as a shallowing upward succession. The dolomitic siltstones and shales of the Lower Victor Bay Formation were deposited in a low energy environment, which then shallows upward into carbonate-dominated lithofacies, such as silt and clay-rich micrite. The uppermost 150 metres are composed primarily of microbialaminites and storm deposits (tempestites), which were subject to a much higher energy environment than that of the Lower Victor Bay Formation.

2.2.3 Båtsfjord Formation, Timan Basin, Finnmark, Norway

When the Annijokka Member of the Båtsfjord Formation was first studied in detail by Siedlecka (1978), molar tooth structures were misinterpreted as synaeresis cracks. Given that there is an abundance of molar tooth structures, synaeresis cracks, and desiccation cracks, the mistake is understandable. It has since been recognized (e.g. James et al., 1998) that some of the synaeresis cracks in the Annijokka Member are molar tooth structures, although no detailed study has taken place since the work of Siedlecka (1978) until now.

Four partial sections of the Annijokka Member of the Båtsfjord Formation, totalling approximately 600 metres, were measured on a 60 kilometre northwest-southeast transect (Figure 2.5). This transect shows significant, systematic variation in the lithologies of the Annijokka Member (Figure 2.6). Siliciclastic content decreases from northwest to southeast, with the northwesternmost Båtsfjord E section containing the largest proportion of coarse siliciclastics. The clastic content markedly decreases both in amount and coarseness towards the southeast, while carbonate sediments become more abundant. The unit as a whole also shows increasing carbonate content upsection. Throughout the Annijokka Member, in all stratigraphic sections, there are abundant sedimentary structures, such as bimodal cross bedding, teepees, desiccation cracks, sand lenses, and flaser bedding, which indicate deposition in intertidal to intermittently exposed environments.

Given the shallow-water, tidally influenced sedimentary structures, and rapid but systematic changes along the northwest-southeast transect in the Annijokka Member, we interpret it to

represent deposition on a mixed carbonate-siliciclastic tidal flat. The large proportion of clastic sediments in the northwestern sections indicate a proximal environment, whereas the more carbonate-rich, southeastern sections were deposited in slightly deeper, marine-dominated setting. The presence of desiccation cracks and teepees throughout all stratigraphic sections indicates that all areas were subject to intermittent subaerial exposure. Molar tooth structures form throughout the stratigraphic sections, but are most concentrated in carbonate-dominated facies. Interestingly, molar tooth structures were often found near structures indicating subaerial exposure, such as desiccation cracks and teepees, as well as brecciated surfaces and bimodal cross bedding, indicating that they are able to form in very shallow environments subject to intermittent subaerial exposure and traction currents.

Molar tooth structure “blobs” (Figure 2.10a) and horizontal ribbons (Figure 2.8a) are unusually common in the Annijokka Mb., in contrast to all other formations in this study, where they are rare to non-existent. One possible explanation for the unusual abundance of these morphologies is their occurrence in a tidal flat environment where cementation occurred early. Evidence for early cementation comes from the absence of tidal channels, and the presence of edgewise breccias and intraclast brecciation. We therefore hypothesize that the horizontal ribbons and blobs are the result of voids forming by lifting sheets of partially cemented sediment, rather than the coalescence of gases or fluids into vertical ribbons. This is conceivable in a muddy, partially cemented tidal flat.

2.2.4 Other Basins

The other molar tooth localities presented in this study comprise relatively few samples, ten in total, compared to the 67 from the Helena, Victor Bay, and Båtsfjord Formations.

The Boot Inlet Formation, Shaler Supergroup, is interpreted as a prograding, storm-dominated, carbonate ramp (Rainbird et al., 1994). It is up to ~500 m thick, composed of alternating packages of ooid grainstones, stromatolitic dolostone, and dolosiltite, with intermittent black shale intervals (van Acken et al., 2013).

The Reefal Assemblage, in the Ogilvie Mountains, Fifteenmile Group, is a thick (up to 1.4 km) mixed shale/siltstone-carbonate succession which records the progradation of a stromatolitic reef system into grey-black shales of a deep, basinal setting (Halverson et al., 2011). Proximal parts of the Reefal Assemblage commonly contain microbialaminites, teepees, and exposure surfaces, indicative of back-reef, intertidal to supratidal environments. Molar tooth structures occur in micrite facies.

The Draken Formation, Svalbard, is a predominantly dolomitic carbonate succession which spans from subtidal, coated grain shoals and bioherms, to intertidal stromatolitic mats and desiccated shales, to high-intertidal to supratidal microbialaminites (Fairchild et al., 1991). Molar tooth structures occur in micrite in both the upper and lower Draken Formation, and are interpreted to have been deposited in a lagoonal environment.

The final sample set in this study is of questionable origin, and should be treated with caution. Field studies of the “cap carbonate” to the Marinoan Snowball Earth glaciation in northwestern Namibia found what appear to be molar tooth structures. These potential MTS were found along a single stratigraphic horizon in the Maieberg Formation, near the town of Khorixas. They bear remarkable similarity to molar tooth structures, namely, they occurred in all three morphologies, vertical and horizontal ribbons, in addition to “blobs”, which crosscut laminations of the host sediment and are filled with homogenous, microcrystalline calcite. These same structures were also observed in a separate outcrop of the Maieberg Formation near the town of Vrede, approximately 40 kilometres west (P.F. Hoffman, personal communications). If they are indeed molar tooth structures, they appear at least 100 Ma after the last “significant” deposition of MTS. The authors are aware of only one other report of post-Cryogenian molar tooth structures, in the Wonoka Formation, Australia, deposited sometime in the Ediacaran Period (James et al., 1998; Husson et al., 2015). To the extent that these highly isolated occurrences of MTS are correct, they post-date the commonly accepted disappearance of widespread MTS by approximately 100 Ma., and hence imply the rare recurrence of the unique conditions under which they formed.

2.3 Variations in Depositional Environments

The successions described above contain molar tooth structures formed in the full range of depositional environments documented in the literature, from below storm wave base to the intertidal zone. In the Helena Formation, molar tooth structures frequently formed in calm, dolomitic siltstone environments, but also in limestone micrite beds with ooids and breccias, indicating fairly energetic environments. MTS in the Victor Bay Formation variably formed below storm wave base, near silty shales, and in shallower, micritic and microbialaminite environments where they were subjected to extensive scouring and reworking prior to redeposition. The Annijokka Member of the Båtsfjord Formation represents the upper range of depositional environments, with evidence for a dominantly intertidal to supratidal environment, such as an abundance of teepees, desiccation cracks, brecciation, and bimodal cross bedding. Molar tooth structures are a common occurrence in four stratigraphic sections measured over a 60 kilometre transect of a tidal flat, in which siliciclastic input changes markedly from the proximal to distal environments, indicating that they were able to form over a large range of siliciclastic influx.

Despite the broad range of environments in which molar tooth structures formed, it is important to note that within a particular sedimentary succession, molar tooth structures will predominantly occur in one particular facies, even if there are others which seem suitable for their formation (i.e. mixed carbonate-siliciclastics). Even in cases where they occur in more than one facies, they rarely occur in all facies in between. For example, in the Victor Bay Formation, molar tooth structures form in what is interpreted as below storm wave base, and in shallower environments of micrite and microbialaminite, but only very rarely in the facies in between. This indicates that although molar tooth structures can form in a broad range of environments, the range of conditions required for their formation is quite narrow.

2.4 Microspar Outside of Molar Tooth Structures

Despite the propensity for Proterozoic microspar to form in molar tooth structures, it is not exclusive to such occurrences. For example, in the Båtsfjord Formation, microspar calcite fills large, polygonally interconnected networks of cracks interpreted as mud cracks (Figure 2.9). In the ~900 Ma Black Canyon Creek Formation, Yukon Territory, Canada, microspar has been observed filling pore spaces and voids between conglomerate clasts, adjacent to molar tooth structures (Figure 2.12). A similar occurrence of MTS and microspar cements has also been observed in the Neoarchean Monteville Formation (Bishop et al., 2006). Hofmann (1985) similarly described microspar infilling of three dimensionally preserved fossils in the Basinal assemblage and Rusty shale formation of the early Neoproterozoic Little Dal Group, and noted that these microspar infills occurred alongside molar tooth structures.

These field observations, while consistent with an early diagenetic origin, could suggest that either the mechanism(s) which result in calcite precipitation and generation of void spaces for the formation of molar tooth structures are separate. Alternatively, if one mechanism is responsible for the creation of void spaces and precipitation of calcite, it does not always result in the formation of void spaces for molar tooth structure formation. Given that microspar infill typically happens alongside molar tooth structures, the latter explanation is preferred.

2.5 Conclusion

Observations from field studies presented here indicate that molar tooth structures are not restricted to a particular sedimentary environment. Rather, they form across a broad range of water depths, from below storm wave base to the intertidal zone, in a range of siliciclastic inputs, from siliciclastic dominated to carbonate dominated (Figure 2.6). Despite the wide range of environments which MTS may form in, within a given succession, they will typically only occur in one facies. Finally, the microspar which comprises molar tooth structures is

not unique; it has been observed to infill organic-walled fossils, voids in sediments between grains or clasts, and mud cracks (Personal observations; Hofmann, 1985), suggesting that the mechanism that triggers the precipitation of microspar in molar tooth structures does not necessitate the formation of large voids within the sediment column.




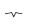








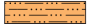

















LITHOFACIES	SEDIMENTARY STRUCTURES
 limestone tempestite/intraclast	 brecciation
 dolomite tempestite/intraclast	 dessication cracks
 dolomite microbialaminite	 wave ripples
 limestone micrite	 sand lenses
 silty limestone micrite	 channelisation
 dolomicrite	 molar tooth structures
 silty dolomicrite	 bimodal cross bedding
 limestone flakestone	 tabular cross bedding
 dolomite flakestone	 tangential cross bedding
 sandstone	 teepees
 siltstone	 syneresis cracks
 dolomitic siltstone	 stromatolite
 black shale	 limestone nodule
 dolerite dyke	 hummocky cross stratification
 covered interval	 ooids

Figure 2.1 Legend for all stratigraphic columns.

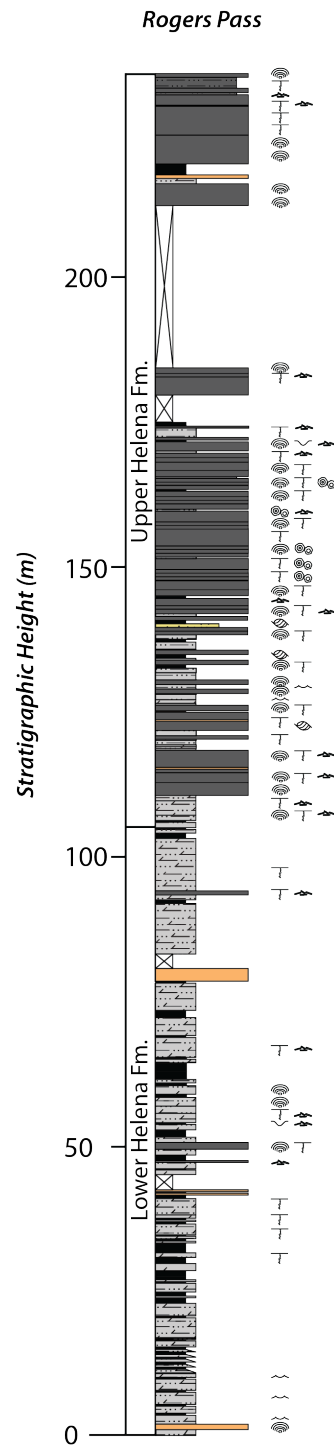
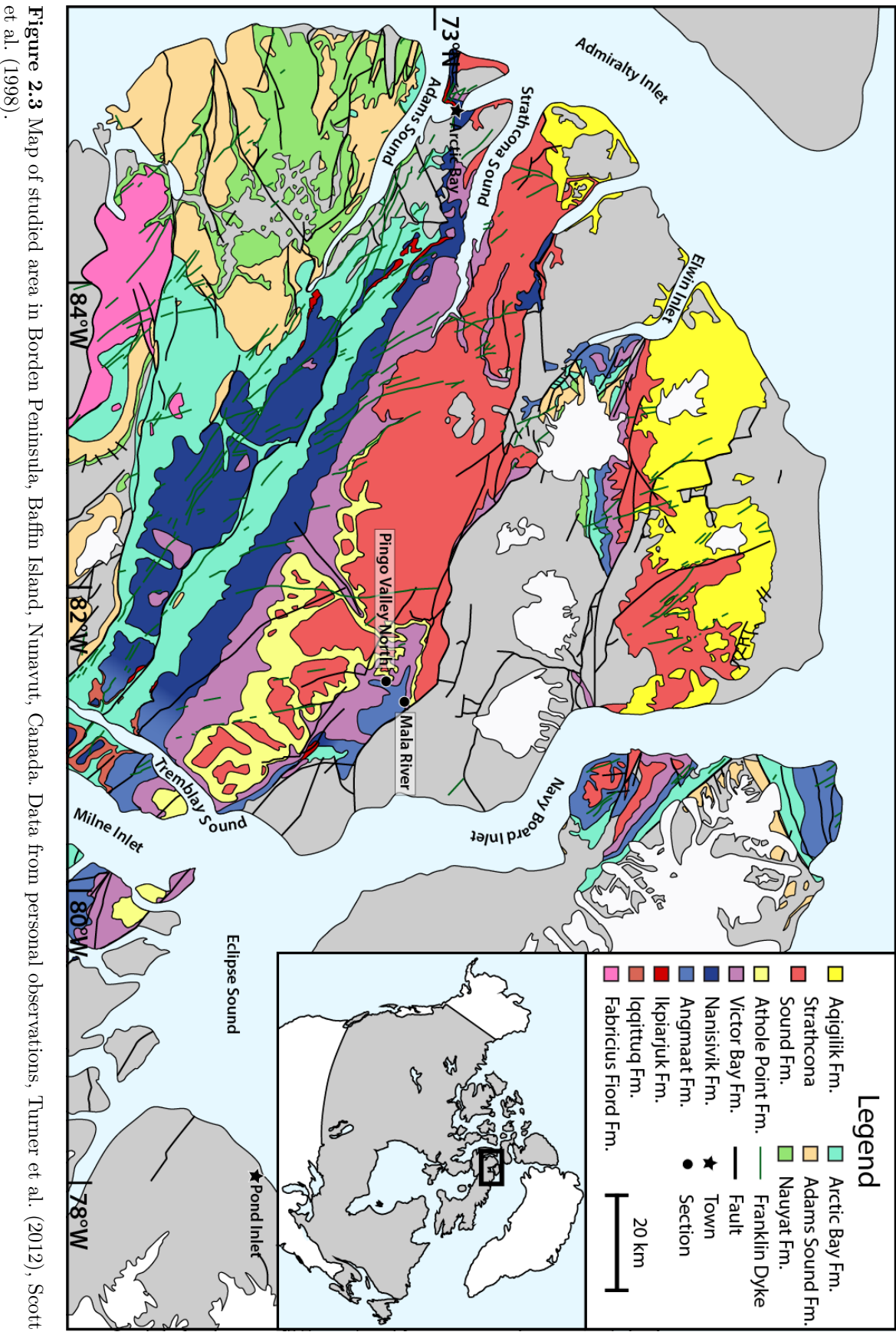


Figure 2.2 Complete stratigraphic section of the Helena Formation. Lower contact is with the Empire Formation, upper contact is with the Wallace Formation.



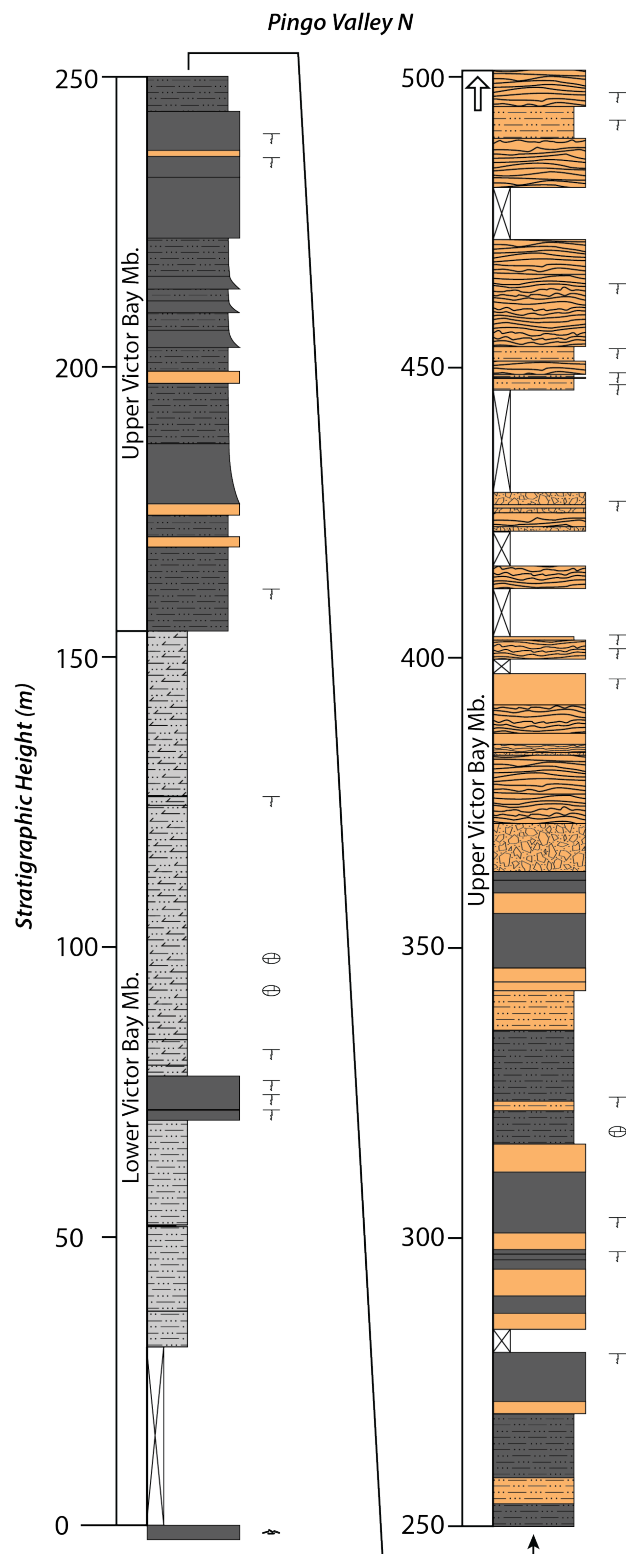


Figure 2.4 Partial stratigraphic section of the Victor Bay Formation. Lower contact with brecciated limestone is the Angmaat Formation. Arrow at top of section indicates that the Victor Bay Formation continues, but is covered by scree.

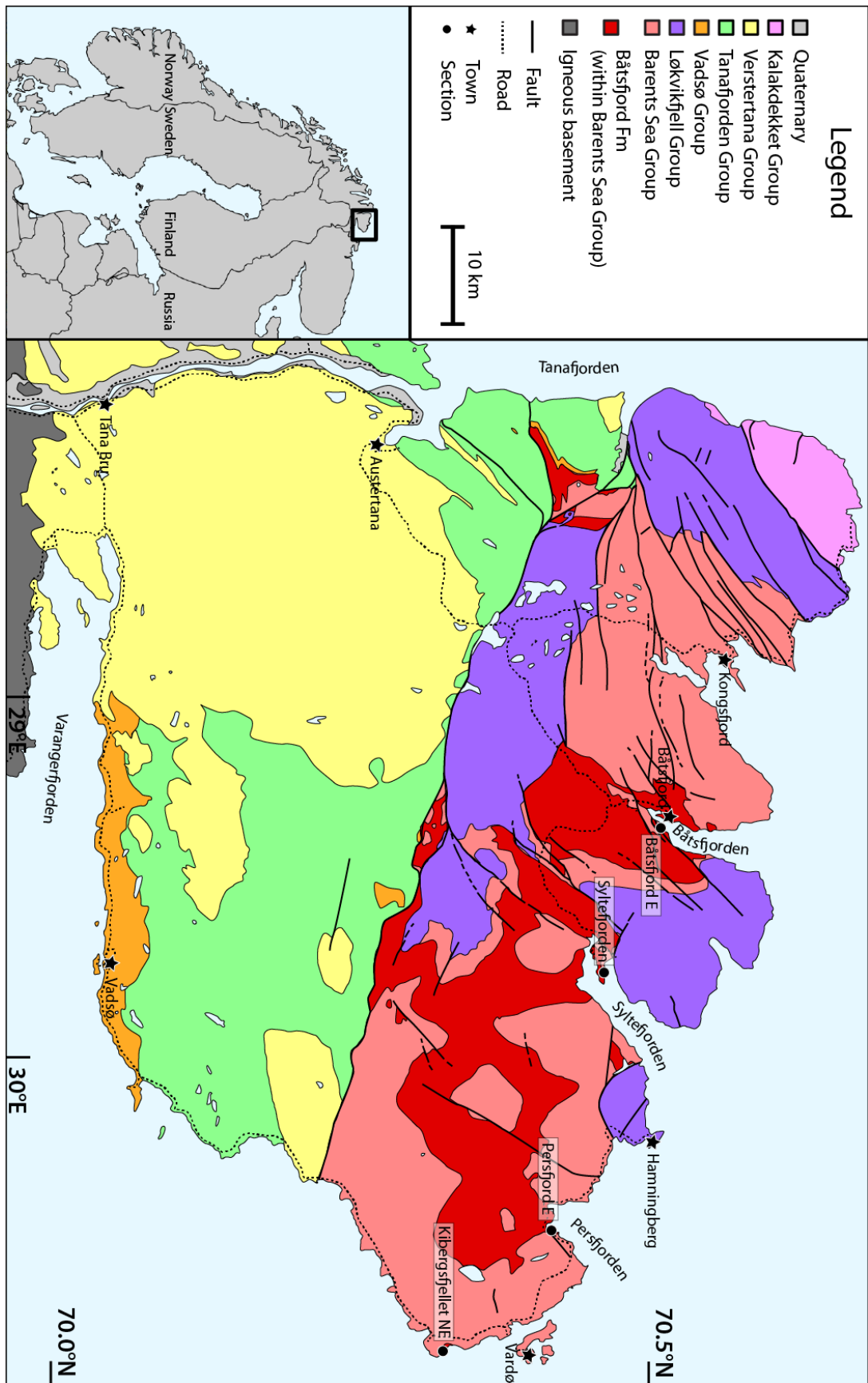


Figure 2.5 Map of studied area in Finnmark, northern Norway. Data from personal observations, Siedlecki (1980).

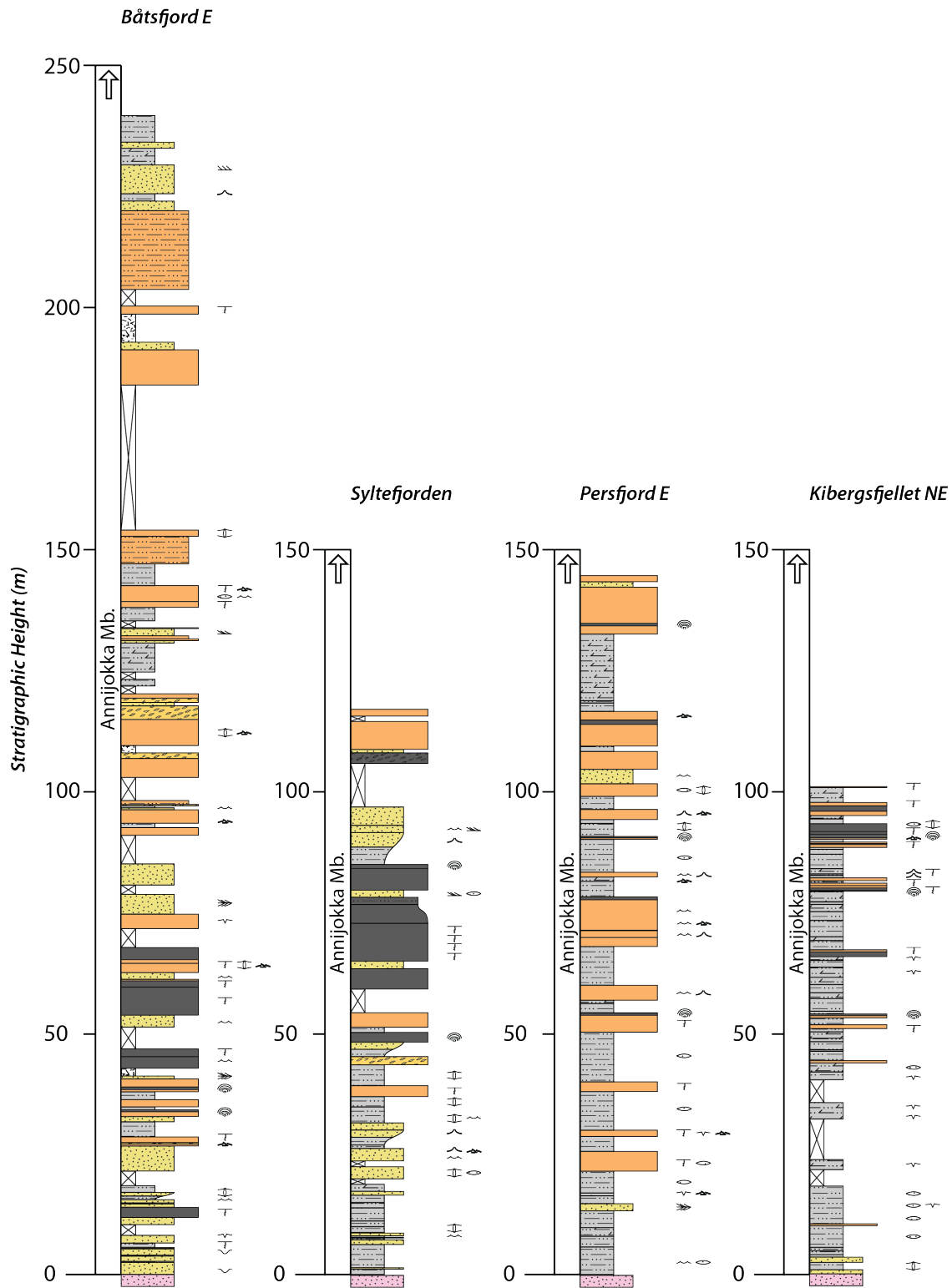


Figure 2.6 Partial stratigraphic sections of the Annijokka Member, lower Båtsfjord Formation. Pink sandstone at base indicates contact with underlying Båsnæring Formation. Arrow at top of sections indicates that the Annijokka Member continues, but was not measured due to lack of exposure.



(a)



(b)



(c)

Figure 2.7 Molar tooth structures in micrite with laminations to thin beds of sandy carbonate, in the Båtsfjord Fm. at Syltefjorden, northernmost Norway. 10 Kroner coin for scale, 24 mm in diameter: (a) Molar tooth structures shows a clear preference for formation in dark, fine grained, clay-rich limestone mud rather than the sandier, buff weathering beds; (b) Some areas exhibit obvious compaction of the host matrix around molar tooth structures; (c) Molar tooth structures may, in some instances, comprise a large portion of the outcrop, obfuscating the original bedding.



(a)



(b)

Figure 2.8 (a) A molar tooth structure “blob” at Syltefjorden, northernmost Norway. While typically rare, MTS blobs are unusually common in the Båtsfjord Fm.; (b) Outcrop containing a substantial amount of large MTS at Båtsfjord E.



(a)



(b)

Figure 2.9 (a) Small, highly interconnected microspar cement replacement of desiccation cracks at Syltefjorden. Plan view; (b) Large, polygonal, interconnected cracks at Kibergsfjellet NE filled with microspar.



(a)



(b)

Figure 2.10 (a) Horizontal ribbon at Syltefjorden; (b) Looking down-section (NE) at Persfjord E. The Båtsfjord Fm. is best exposed along the coast, during low tide.

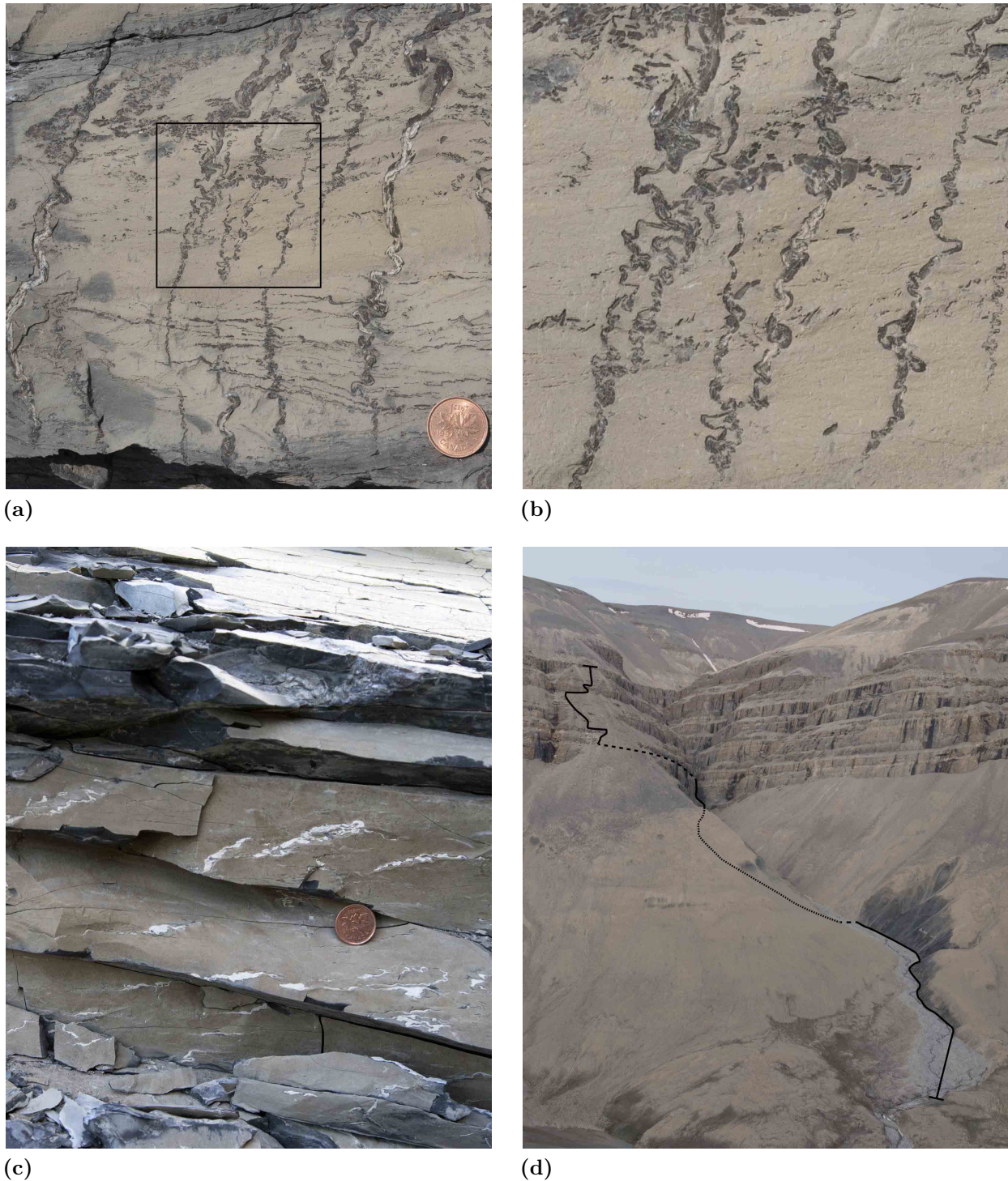
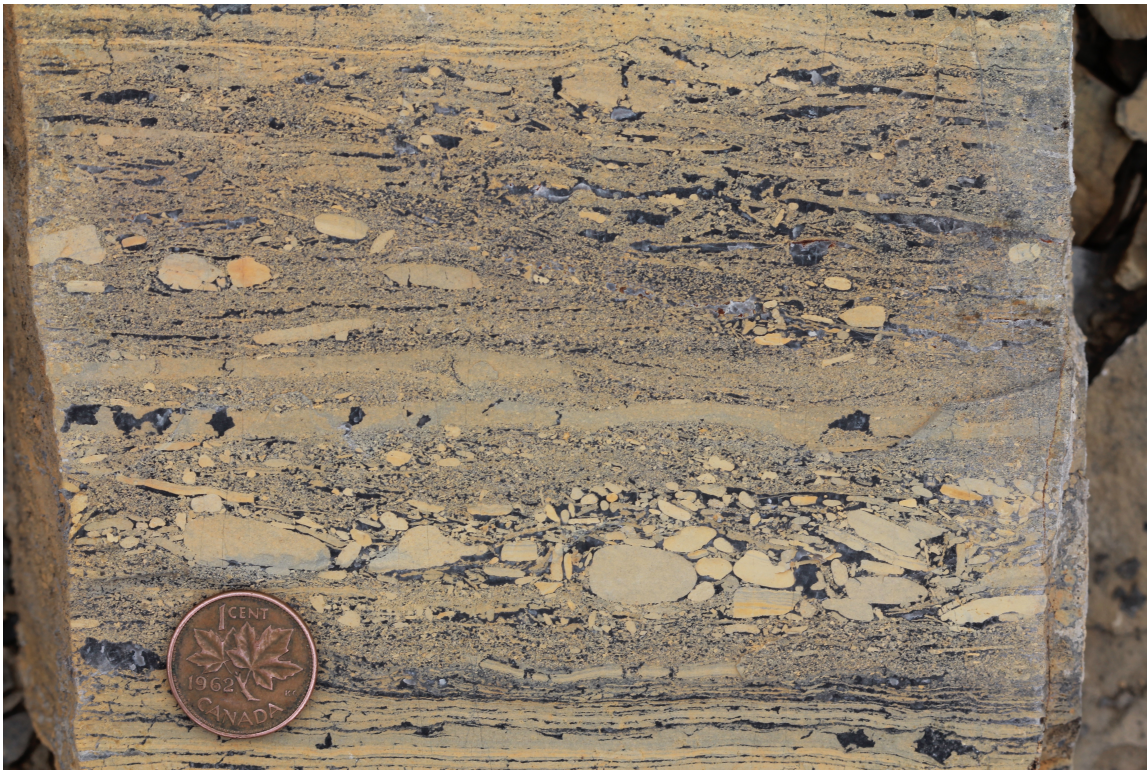


Figure 2.11 (a) Ptygmatic molar tooth structures in the lower Victor Bay Fm. Canadian penny for scale (19 mm in diameter); (b) Enlarged area of black box from 2.11a; (c) Horizontal ribbons in fissile limestone, lower Victor Bay Fm.; (d) Victor Bay Fm. section measured at Pingo Valley N. Solid black line indicates where the section was measured, tightly dashed line indicates where the section was measured but is obscured from view, spaced dashed line indicates along strike correlations made during the measuring of the section.



(a)



(b)

Figure 2.12 (a) Molar tooth structure “tempestite” in the upper Victor Bay Formation; (b) Dark grey microspar infilling voids in an intraformational conglomerate in the Black Canyon Creek Formation.

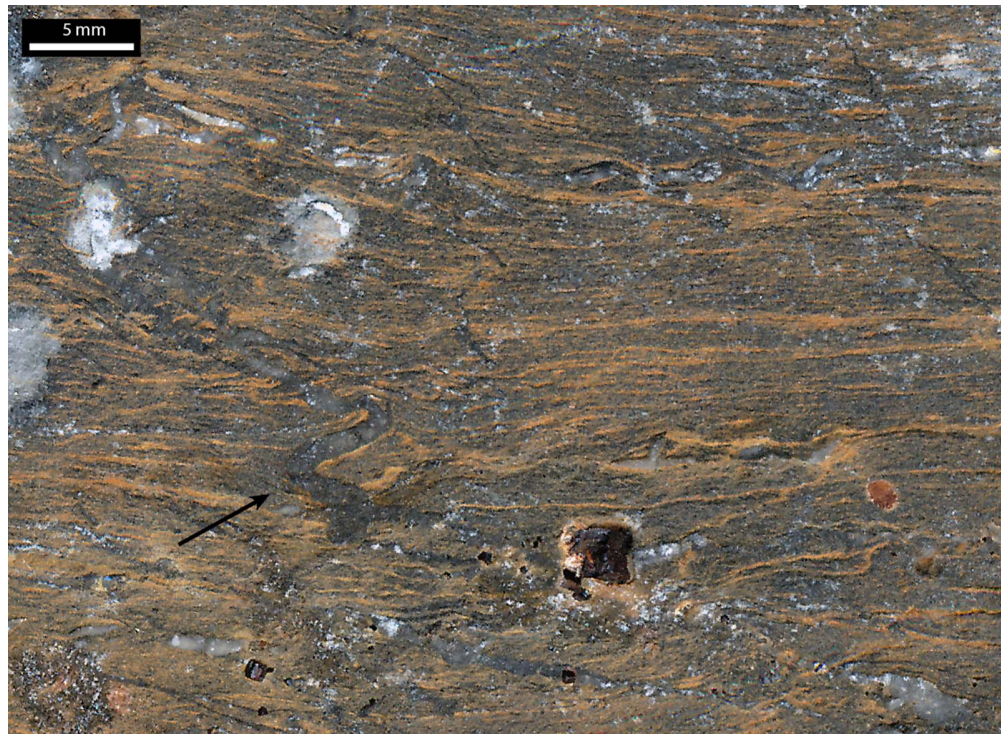


(a)

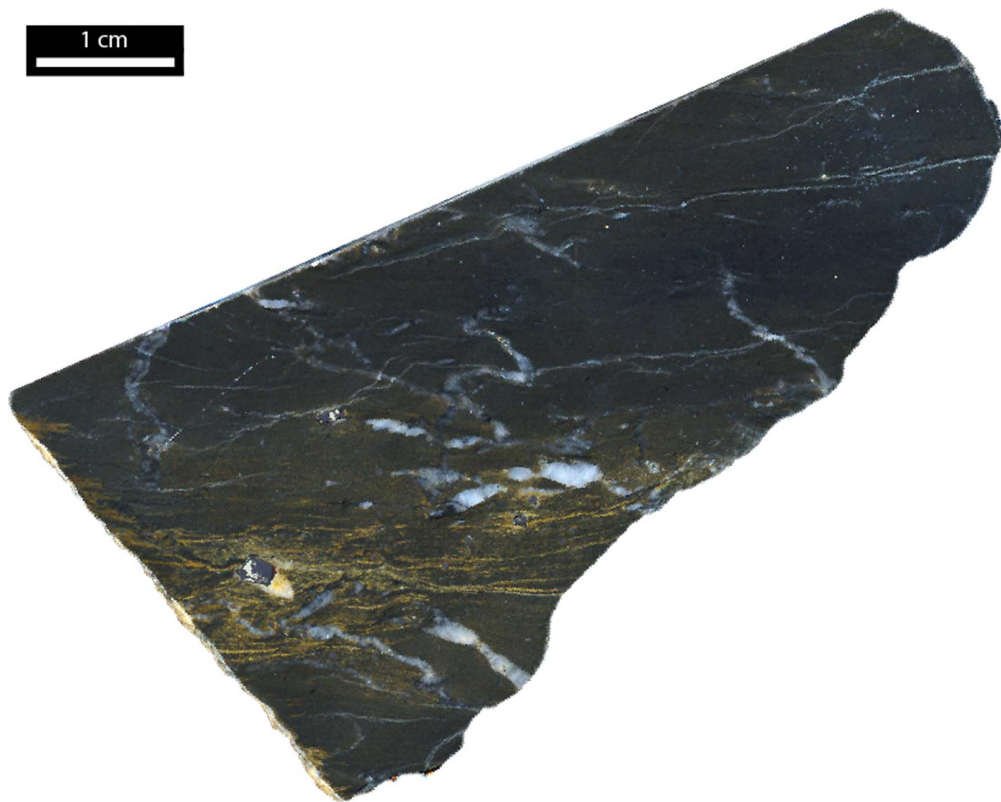


(b)

Figure 2.13 (a) Dark grey microspar infilling intergranular voids in ripple cross-laminated grainstone and filling desiccation cracks in the Black Canyon Creek Formation. Reactivation surface and smooth transition from rippled grainstone to mud-cracked dololomite imply formation in a tidally-influenced, intermittently exposed environment; (b) Molar tooth structures in Black Canyon Creek Formation filled with a dark grey microspar similar to void filling microspar in intraformational conglomerates and between grains.



(a)



(b)

Figure 2.14 Ediacaran molar tooth structures in sample MN1500B from the Maieberg Formation, Namibia. (a) Molar tooth structures cross cutting laminations, weathered surface; (b) Molar tooth structures viewed on a fresh, polished surface. Sedimentary laminations oriented horizontally.

Bibliography

- Bishop, J. W. and Sumner, D. Y. (2006). "Molar tooth structures of the Neoproterozoic Monteville Formation, Transvaal Supergroup, South Africa. I: Constraints on microcrystalline CaCO₃ precipitation." *Sedimentology* 53.5, pp. 1049–1068.
- Evans, K. V., Aleinikoff, J. N., Obradovich, J. D., and Fanning, C. M. (2000). "SHRIMP U-Pb geochronology of volcanic rocks, Belt Supergroup, western Montana: evidence for rapid deposition of sedimentary strata." *Canadian Journal of Earth Sciences* 37.9, pp. 1287–1300.
- Fairchild, I. J., Knoll, A. H., and Swett, K. (1991). "Coastal lithofacies and biofacies associated with syndepositional dolomitization and silicification (Draken Formation, Upper Riphean, Svalbard)." *Precambrian research* 53.3, pp. 165–197.
- Frank, T. D. and Lyons, T. W. (1998). "'Molar-tooth' structures: A geochemical perspective on a Proterozoic enigma." *Geology* 26.8, pp. 683–686.
- Furniss, G., Rittel, J. F., and Winston, D. (1998). "Gas bubble and expansion crack origin of 'molar-tooth' calcite structures in the middle Proterozoic Belt Supergroup, western Montana." *Journal of Sedimentary Research* 68.1, pp. 104–114.

- Halverson, G. P., Macdonald, F. A., Strauss, J. V., Smith, E. F., Cox, G. M., and Hubert-Théou, L. (2011). “Updated definition and correlation of the lower Fifteenmile Group in the central and eastern Ogilvie Mountains.” *Yukon Exploration and Geology*, pp. 75–90.
- Hofmann, H. (1985). “The mid-Proterozoic Little Dal macrobiota, Mackenzie Mountains, north-west Canada.” *Palaeontology* 28.2, pp. 331–354.
- Husson, J. M., Maloof, A. C., Schoene, B., Chen, C. Y., and Higgins, J. A. (2015). “Stratigraphic expression of Earth’s deepest $\delta^{13}\text{C}$ excursion in the Wonoka Formation of South Australia.” *American Journal of Science* 315.1, pp. 1–45.
- James, N. P., Narbonne, G. M., and Sherman, A. G. (1998). “Molar-tooth carbonates: shallow subtidal facies of the Mid-to Late Proterozoic.” *Journal of Sedimentary Research* 68.5, pp. 716–722.
- Pratt, B. R. (1998). “Molar-tooth structure in Proterozoic carbonate rocks: Origin from synsedimentary earthquakes, and implications for the nature and evolution of basins and marine sediment.” *Geological Society of America Bulletin* 110.8, pp. 1028–1045.
- Rainbird, R., Jefferson, C., Hildebrand, R., and Worth, J. (1994). “The shaler supergroup and revision of Neoproterozoic stratigraphy in Amundsen Basin, Northwest Territories.” *Geological Survey of Canada, Paper*.
- Scott, D. and De Kemp, E. (1998). *Bedrock Geology Compilation Northern Baffin Island and Northern Melville Peninsula, Northwest Territories*. Geological Survey of Canada, Natural Resources Canada.
- Siedlecka, A. (1978). “Late Precambrian tidal-flat deposits and algal stromatolites in the Båtsfjord Formation, East Finnmark, North Norway.” *Sedimentary Geology* 21.4, pp. 277–310.
- Siedlecki, S. (1980). *Geologisk Kart over Norge, Berggrunnskart Vadsø: Trondheim, Norway, Norges Geologiske Undersøkelse*, scale 1:250,000, 1 sheet.

- Turner, E. C. and Kamber, B. S. (2012). “Arctic Bay Formation, Borden Basin, Nunavut (Canada): Basin evolution, black shale, and dissolved metal systematics in the Mesoproterozoic ocean.” *Precambrian Research* 208, pp. 1–18.
- Van Acken, D., Thomson, D., Rainbird, R. H., and Creaser, R. A. (2013). “Constraining the depositional history of the Neoproterozoic Shaler Supergroup, Amundsen Basin, NW Canada: Rhenium-osmium dating of black shales from the Wynniatt and Boot Inlet Formations.” *Precambrian Research* 236, pp. 124–131.

Geochemistry of Molar Tooth Structures: Testing the Role of Dissimilatory Iron Reduction

3.1 Abstract

In an effort to address the enigmatic formation of molar tooth structures, we test the potential role of microbial dissimilatory iron reduction of Fe-rich smectite, a mechanism which could generate voids in sediment while promoting calcite precipitation by locally increasing porewater alkalinity. We present major and minor element concentrations, in addition to stable carbon and oxygen isotope measurements, for 77 molar tooth structure samples. A subset of 28 samples was analyzed for iron isotopes. The sample set analyzed is the most comprehensive of any molar tooth structure study to date, collected from eight different geographical locations, spanning from ~ 1450 -635 Ma. $\delta^{56}\text{Fe}$ values in molar tooth structures are generally lighter than those of the matrix carbonate, indicating that they formed by distinct processes. Furthermore, in ten samples for which the $\delta^{56}\text{Fe}$ of the siliciclastic component of the matrix was analyzed,

the $\delta^{56}\text{Fe}$ of the molar tooth structure was almost always isotopically lighter. If iron in molar tooth structures is sourced from Fe-rich clay in the matrix siliciclastics, and fractionated by dissimilatory iron reduction, the measured $\delta^{56}\text{Fe}$ values are consistent with a dissimilatory iron reduction origin for molar tooth structures. $\delta^{56}\text{Fe}$ values of molar tooth structure, matrix, and detrital material within a single sample differ by up to 3.57‰, more than half the range of all natural materials.

3.2 Introduction

Molar tooth structures have long been a mystery. These curious structures, while exclusive to the Precambrian, have been found in numerous sedimentary basins around the world. Although many hypotheses have been put forth to explain their formation and disappearance in the sedimentary record, including bacterial sulphate reduction, seismicity, and wave-induced fluid pumping, they typically fail to explain both phenomena. Furthermore, many invoke separate mechanisms for the creation of void spaces and subsequent calcite precipitation.

A valid explanation for molar tooth structures must resolve three questions: How are the voids in which molar tooth structures form generated? What causes the precipitation of microcrystalline calcite in these void spaces? Why are the mechanism(s) proposed for the creation of void spaces and precipitation of calcite restricted to 2600 to 720 Ma? Although numerous hypotheses have previously been put forth to explain the formation of molar tooth structures, they typically fail to explain all three of these requirements.

An important constraint on the origin of MTS is that the mechanism(s) responsible for calcite precipitation must be relatively rapid. If they were not, the void spaces would either collapse during sediment compaction, or, if they were open to the water column, the calcite infill would contain significant amounts of detrital material. Furthermore, the very fine-grained nature of the calcite in molar tooth structures indicates rapid precipitation.

3.3 Microbial Reduction of Smectite

In their study of Neoproterozoic molar tooth structures, Bishop et al. (2006) proposed microbial reduction of Fe-rich smectite to illite as a potential mechanism for increasing alkalinity, but concluded that because illitisation is often K^+ limited, it was unlikely to significantly affect alkalinity. However, seawater potassium concentrations are thought to be at least 10 mM throughout the Phanerozoic (Demicco et al., 2005), which would provide a large pool of K^+ for smectite reduction. Furthermore, the reaction of smectite to illite depends greatly on the initial clay composition, and it is possible for the so-called “cannibalisation” of smectite to partially or completely provide the necessary reactants for illite formation (Pollastro, 1985). The possibility that microbial illitisation could potentially create void spaces was not addressed by Bishop et al. (2006).

Microbial reduction of structural Fe(III) in smectite, and the subsequent conversion to illite is a reaction with consequences that make it a potential mechanism to consider for the formation of molar tooth structures. Microbial reduction of smectite occurs rapidly, reaching up to 40% reduction within 14 days at room temperature and pressure (Kim et al., 2004). Furthermore, this process results in shrinkage of clay sediments by up to 40%, and the release of water, bicarbonate (HCO_3^-), Ca^{2+} , Fe^{2+} , and silica (Stucki et al., 2006; Vorhies et al., 2009). Through the shrinkage of clay sediments, expulsion of water, and a local increase in porewater alkalinity caused by the release of silica and bicarbonate, microbial reduction of smectite to illite could conceivably create void spaces and cause the rapid precipitation of calcite. The process of microbial reduction of smectite occurs by means of dissimilatory iron reduction, which fractionates iron by approximately -3‰ (Crosby et al., 2007). If microbial dissimilatory iron reduction plays a role in the formation of molar tooth structures, the iron isotope composition of molar tooth structures should be isotopically depleted in $\delta^{56}Fe$ relative to both the carbonate component of the matrix, which presumably formed directly from seawater, and the siliciclastic component of the matrix.

3.4 Iron Isotopes

Iron has four stable isotopes, ^{54}Fe (5.845%), ^{56}Fe (91.75%), ^{57}Fe (2.119%), and ^{58}Fe (0.2819%) (Dauphas et al., 2006). Iron isotope values are typically reported as $\delta^{56}\text{Fe}$ and $\delta^{57}\text{Fe}$ using the permil notation (‰):

$$\delta^{56}\text{Fe} = \left(\frac{\left(\frac{^{56}\text{Fe}}{^{54}\text{Fe}} \right)_{\text{sample}}}{\left(\frac{^{56}\text{Fe}}{^{54}\text{Fe}} \right)_{\text{standard}}} - 1 \right) * 1000$$

$$\delta^{57}\text{Fe} = \left(\frac{\left(\frac{^{57}\text{Fe}}{^{54}\text{Fe}} \right)_{\text{sample}}}{\left(\frac{^{57}\text{Fe}}{^{54}\text{Fe}} \right)_{\text{standard}}} - 1 \right) * 1000$$

Iron isotopes are fractionated by mass dependent processes, such that $\delta^{56}\text{Fe}$ can be related to $\delta^{57}\text{Fe}$ by a factor of 1.47 (Beard et al., 2004). $\delta^{56}\text{Fe}$ values are typically reported against the standard reference material IRMM-014.

Iron exhibits relatively small isotopic fractionations, when compared to light isotope systems. The entire range of $\delta^{56}\text{Fe}$ values in nature, including plants, animals, and rocks, spans from approximately -3.5 to +3.0‰ (Dauphas et al., 2006). Geologic samples span this entire range, and bulk silicate Earth has a $\delta^{56}\text{Fe}$ composition of approximately 0.1‰ relative to IRMM-014 (Dauphas et al., 2006).

3.5 Sample Set

All samples were collected from outcrops while measuring stratigraphic sections. The samples collected for this study span much of the world, from Tasmania to southern Africa, to the high Arctic, to western North America; from the early Mesoproterozoic to the earliest Ediacaran; from below storm wave base to the intertidal zone. To the author's knowledge,

Table 3.1 Sample set details.

Region	Stratigraphic Unit	Coordinates	Number of Samples	Age (Ma)	Age Reference
Belt Mountains, Montana, U.S.A	Helena Formation	N47.09354 W112.35905	23	1454 \pm 9	Furniss et al. (1998) Evans et al. (2000)
Southern Tasmania, Australia	Humboldt Formation	—	1	1200	Black et al. (2004) Halpin et al. (2014) Calver (personal communications)
Borden Peninsula, Baffin Island, Nunavut, Canada	Victor Bay Formation	N72.89733 W081.41192 N72.94994 W081.26838	22	1033 \pm 22	Gibson (personal communications)
Northern Northwest Territories, Canada	Boot Inlet Formation	N69.01123 W122.67110 N69.94448 W121.60923	2	892 \pm 13	van Acken et al. (2013)
Ogilvie Mountains, Yukon Territory, Canada	Reefal Assemblage	—	1	>811.5	Macdonald et al. (2010)
Northern Finnmark, Norway	Annijokka Member, Batsfjord Formation	N70.53613 E030.13258 N70.62790 E029.74576 N70.42614 E030.80095 N70.29190 E031.05384	22	~810	Rice et al. (2012), personal observations
Svalbard	Draken Formation	N78.69733 E018.41302	3	~770	Halverson (personal communications)
Northwestern Namibia	Maiberg Formation	S20.38524 E014.43349	3	<635.5	Hoffmann et al. (2004)

this comprises the most comprehensive suite of molar tooth structures presented in a single geochemical study.

In the Victor Bay Formation, and Annijokka Member, Båtsfjord Formation, several samples were collected laterally along a single stratigraphic horizon, or in very close vertical proximity, to determine geochemical variability over small scales.

3.6 Methods

3.6.1 Sample Preparation

Samples were cleaned of any surface contaminants and weathered surfaces, and cut perpendicular to the molar tooth structures. These cut surfaces were then cleaned using 18.2 M Ω water, dried, and subsequently drilled to depths of less than 3 mm to extract rock powder. Special care was taken to avoid contamination by accidentally drilling into the molar tooth structure when drilling the matrix and vice versa. Wherever possible, powder was drilled



Figure 3.1 Distribution of molar tooth structures in this study.

from a single molar tooth structure or stratigraphic horizon within the matrix, although the generally thin, sinuous nature of MTS made this impossible in most cases. When not possible, powder was drilled from several molar tooth structures and homogenized. Aliquots of this powder were then used for stable carbon, oxygen, and iron isotope analyses, and to measure major/minor element abundances. For analyses of total organic carbon and total sulfur, 15-50 g of bulk sample (i.e. containing both molar tooth structure and matrix) was crushed in a shatter box, using a hardened steel grinding container.

3.6.2 Total Organic Carbon and Total Sulfur

Approximately 400 mL of 6N HCl was added to 15-50 g of each sample, and placed on a shaker for several hours to dissolve the carbonate fraction of the sample. Supernatant was poured off, and the residues were rinsed in approximately 0.5 L of distilled water. Samples were dried in an oven for several days at 60°C, then crushed using an agate mortar and pestle. Approximately 150 mg of each sample was weighed into ceramic crucibles, and 1 g each of tungsten pellets and iron chips were added to catalyze combustion. Samples were analyzed in

triplicate using an Eltra CS 800 Carbon Sulfur Determinator. Standard deviations on carbon and sulfur measurements are 0.03 wt% and 0.01 wt%, respectively.

3.6.3 Carbon and Oxygen Isotopes

Stable carbon and oxygen isotope measurements were made using a Nu Instruments Perspective dual inlet isotope ratio mass spectrometer at McGill University. Samples were reacted in 70°C phosphoric acid (H_3PO_4), and the evolved CO_2 was cryogenically purified and analyzed against an in-house reference gas. $\delta^{13}\text{C}$ and $\delta^{18}\text{O}$ measurements had uncertainties of 0.04‰ and 0.14‰, based on long-term reproducibility of measurements of internal standards.

3.6.4 Sample Dissolution for Elemental Concentrations and Iron Isotopes

Due to the mixed carbonate-siliclastic nature of the matrix in which MTS form, special care was taken to avoid contamination by partial dissolution of siliclastic minerals when dissolving the carbonate fraction of the sample, which could alter the element concentrations and iron isotope values. Rongemaille et al. (2011) tested a variety of acids for carbonate dissolution, including 2-20% acetic acid, 18.5% hydrochloric acid, and 5% nitric acid. Ultimately, a 5% acetic acid (CH_3COOH) leach for 24 hours at room temperature fully dissolved the carbonate portion of the rock, while incorporating minimal amounts of siliclastic material. Furthermore, Pichat et al. (2003) showed that the use of weak acetic acid to dissolve carbonate samples induces minimal isotopic fractionation of the solute and is stable over a range of temperatures (up to $\sim 125^\circ\text{C}$).

Three distinct components of each sample were analyzed: the molar tooth structure, the carbonate fraction of the matrix, and the siliclastic fraction of the matrix, defined by the portion of a sample which is not soluble in 5% acetic acid. A modified version of the procedure from Rongemaille et al. (2011) was used. All acids used were “ultra-pure”, and all work was carried out in a class 100 clean lab at GEOTOP (Montréal, Québec, Canada). Approximately 30 mg of powder was weighed into Teflon beakers, rinsed with 18.2 M Ω water, then dried

on a hotplate. Samples were taken up in 5 mL of 5% acetic acid, and agitated several times over a duration of 24 hours at room temperature. After 24 hours, the acetic acid supernatant was transferred into Teflon beakers and dried on a hotplate. Prior to analyses, 2.5 mL of 2% nitric acid was added, and the samples were placed on a hotplate for several hours to ensure full dissolution.

The insoluble residue that remained after the acetic acid leach was rinsed three times with 5 mL of 18.2 M Ω water to prevent the formation of carboxylates, and dried on a hotplate. Once dry, 5 mL of 50% hydrofluoric acid was added, and the samples were left on a hotplate at 125°C for 72 hours. The samples were then dried, treated with a mixture of 2.5 mL 16N nitric acid and 2.5 mL 6N hydrochloric acid, dried, and treated with 5 mL of 16N nitric acid at 125°C for 24 hours. Finally, the samples were dried and taken up in 2.5 mL of 2% nitric acid, and put on a hotplate for several hours to ensure full dissolution.

3.6.5 Major/minor elements

All element concentrations for the molar tooth structure and carbonate portion of the matrix were calculated relative to the sample mass that was soluble in 5% acetic acid, whereas insoluble residue concentrations are calculated relative to the mass that was not dissolved after exposure to 5% acetic acid. Aliquots of each dissolution were used for measurement of major and minor element concentrations using a Thermo Scientific iCap 6500 inductively coupled plasma optical emission spectrometer (ICP-OES) at McGill University. Samples were diluted by a factor of approximately 10 in a 2% nitric acid matrix. The ICP-OES was calibrated using multi-element solutions prepared from PlasmaCAL single element standards. Repeat analyses of the standard reference material USGS COQ-1 carbonatite yielded an external error of $\leq 7\%$ for all elements (Al, Ba, Ca, Fe, Mg, Mn, Rb, Sr, Ti), with best precision achieved for Ca, Mg, Mn, and Sr (2-4%).

3.6.6 Iron Isotopes

In order to separate iron from other dissolved elements in the sample dissolutions, dissolved iron was isolated using anion-exchange chromatography. First, an aliquot of 1.75 mL of each sample solution in a 2% nitric acid matrix was dried in Teflon beakers and taken up in 1 mL of 6N HCl. BioRad AG 1-X4, 200-400 mesh resin was cleaned using 5 mL of 0.05N HCl, followed by 5 mL of 6N HCl, and subsequently 5 mL of 0.05N HCl. The columns were then conditioned with 0.5 mL of 6N HCl to remove most cations. The sample was then introduced and allowed to drip through, followed by seven separate additions of 0.5 mL of 6N HCl. In order to all of the iron from the column while not releasing any zinc, 0.5 mL of 2N HCl was added eight times, with the elutant collected in precleaned Teflon beakers. This fraction was dried at approximately 125°C, and taken up in 1.0 mL of 2% nitric acid.

Iron isotopes were measured on a Nu Instruments Plasma II ES MC ICP-MS at GEOTOP/Université du Québec à Montréal, operating in high resolution mode. Samples were introduced using a CETAC Technologies ASX-112FR AutoSampler, connected to a CETAC Technologies Aridus II desolvating nebulizer. An argon flow rate of between 2.6-3.9 L/minute was used as the sweep gas, optimized prior to each set of analyses in order to maximize instrument sensitivity. No nitrogen gas flow was used. The MC ICP-MS was fitted with ES Dry Plasma nickel coated cones to improve sensitivity. Most samples (N=52) were measured in triplicate using standard-sample bracketing, against the international standard NIST 3126a, in addition to two internal standards. For samples which had too little iron to allow for triplicate analyses, samples were measured either twice (N=12) or once (N=1). For comparison against previous $\delta^{56}\text{Fe}$ data, values are reported relative to both NIST 3126a and IRMM-014 (Table S3, S4), although all further discussion and figures are relative to IRMM-014, where $\delta^{56}\text{Fe}_{\text{NIST 3126a}} = 0.39 \pm 0.13$ (2σ) relative to IRMM-014 (Rouxel et al., 2010).

Analyses of three separate acetic acid leaches of the standard reference material USGS COQ-1 carbonatite yielded $\delta^{56}\text{Fe}$ values in excellent agreement, with $\delta^{56}\text{Fe}$ values of $0.65 \pm 0.07\text{‰}$, $0.71 \pm 0.11\text{‰}$, and $0.78 \pm 0.05\text{‰}$ ($\pm 1\sigma$). Due to low concentrations of iron in molar tooth structures, $\delta^{56}\text{Fe}$ was measured at one of two voltages depending on the concentration. Concentrated samples, usually the matrix carbonate and matrix siliciclastics, were analyzed at a signal intensity of ~ 7 V, whereas molar tooth structures were usually analyzed at a signal intensity of ~ 0.7 V. Comparison of two internal standards shows that measurements of $\delta^{56}\text{Fe}$ are consistent at this range of intensities, although the precision is slightly lower at lower intensities. Mean $\delta^{57}\text{Fe}$ values at 0.7V are offset relative to higher intensities, and have lower precision, but are still within analytical error (Figure 3.2). Given that ^{57}Fe comprises 2% of Fe, compared to 92% for ^{56}Fe , and 6% for ^{54}Fe , the imprecise measurements of $\delta^{57}\text{Fe}$ at 0.7V are attributed to sufficiently low concentrations of ^{57}Fe that background noise becomes non-negligible.

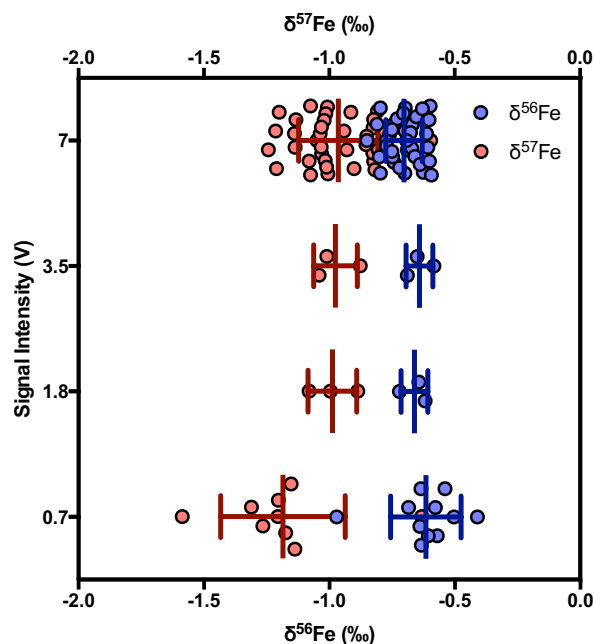


Figure 3.2 Comparison of $\delta^{56}\text{Fe}$ and $\delta^{57}\text{Fe}$ measurements on an internal standard “SCP” against NIST 3126a, at mass 56 intensities ranging from 7 volts (~ 0.5 ppm) to 0.7 volts (~ 50 ppb). Large centre bar corresponds to mean, small bars correspond to $\pm 1\sigma$.

3.6.7 Scanning Electron Microscopy

Polished thin sections ($\sim 30\ \mu\text{m}$ thick) and thick sections ($\sim 200\ \mu\text{m}$ thick) were coated with 4 nm of platinum to improve conductivity, using a Leica EM ACE600 sputter coater. Samples were subsequently analyzed using an FEI Inspect F50 scanning electron microscope (SEM) at McGill University's Facility for Electron Microscopy Research (FEMR). Element mapping was conducted using an EDAX Octane Super Silicon Drift Detector, operating at 14.0 kV, with a spot size of $3.0\ \mu\text{m}$. "Pseudo line scans" were reconstructed using element mapping data, using a moving average of 60 pixels.

3.7 Results

3.7.1 Total Organic Carbon and Total Sulfur

Total organic carbon (TOC) and sulfur content were measured on decarbonated residue, but values are reported relative to the original mass of the bulk rock. TOC measurements are low, ranging from 0.01-0.24 wt%, with an average of 0.08 wt%. All sulfur is assumed to come from pyrite. Pyrite contents are low, ranging from 0.00 to 0.89 wt%, with a mode of ~ 0.01 wt% and a mean of 0.08 wt%.

3.7.2 Carbon Isotopes

Both the matrix and molar tooth structure span a large range of $\delta^{13}\text{C}$ values, from -5.8‰ to 7.0‰ (VPDB; Figure 3.3a). These variations are stratigraphic in nature, reflecting the large secular variation in marine carbonate during the Proterozoic (Shields et al., 2002). Indeed, $\delta^{13}\text{C}$ of the molar tooth structure and matrix are essentially indistinguishable, with the mean difference of $\delta^{13}\text{C}_{\text{MTS-MX}}$ of -0.03 , -0.08 , -0.08 , and -0.22‰ for the Victor Bay, Helena, Båtsfjord, and other successions (Humboldt, Draken, Boot Inlet, Reefal Assemblage, Maieberg Formations), respectively. There is no significant difference between the $\delta^{13}\text{C}$ values

of a molar tooth structure and the corresponding matrix (Figure 3.3c).

3.7.3 Oxygen Isotopes

Similar to $\delta^{13}\text{C}$ measurements, there is large variation in $\delta^{18}\text{O}$ between different sedimentary successions, with a range of -2.1 to -15.4‰ relative to VPDB (Figure 3.4b). Unlike carbon isotopes, oxygen isotopes show a comparatively systematic difference between the molar tooth structure and matrix carbonate. Molar tooth structures are generally depleted in $\delta^{18}\text{O}$ relative to the matrix carbonate, with a modal difference of approximately -1.0‰, and a range from -7.4 to +2.6‰ (Figure 3.3d).

3.7.4 Element Abundances

Element abundances are significantly different between the molar tooth structures and matrix carbonate. Most notably, there is a large difference in the Ca and Mg content of the molar tooth structures and corresponding matrix carbonate. In molar tooth structures, Mg/Ca values are 0.01 on average, with a maximum of 0.05, whereas the matrix has an average value of approximately 0.25, and ranges from 0.01 to 0.58. Similarly, Fe contents in the molar tooth structure are low compared to the matrix carbonate (average of approximately 0.1 and 1.0 wt%, respectively). Mn/Sr is typically much lower in the molar tooth structure than the matrix carbonate (averages of 1.8 and 4.3, respectively), and exhibits much less variability (Figure 3.8).

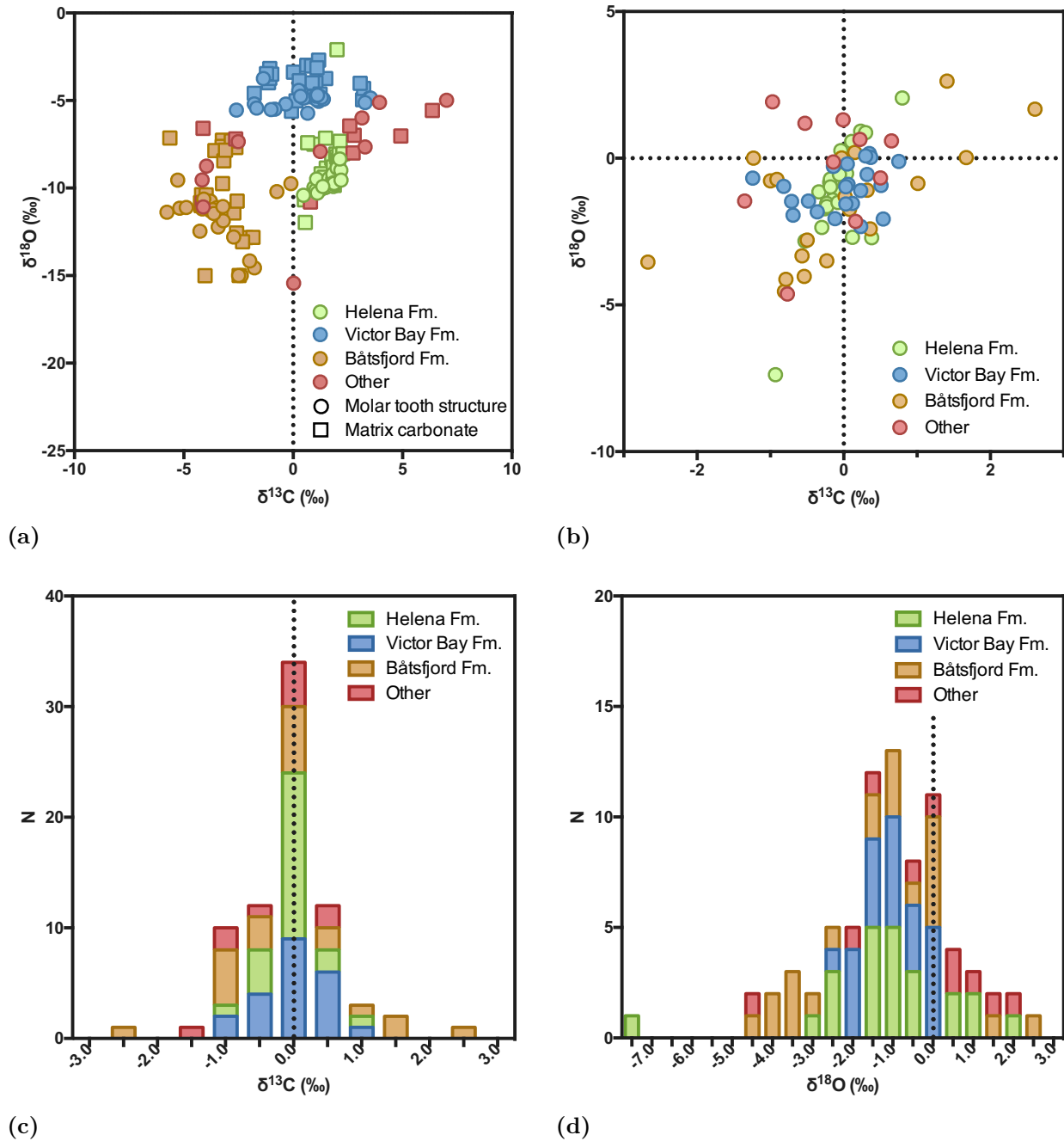


Figure 3.3 $\delta^{13}\text{C}$ and $\delta^{18}\text{O}$. “Other” category includes samples from the Boot Inlet, Reefal Assemblage, Maieberg, Humboldt, and Draken Formations. (a) Cross plot of $\delta^{13}\text{C}$ and $\delta^{18}\text{O}$ for molar tooth structures and matrix; (b) Cross plot of the difference in $\delta^{13}\text{C}$ and $\delta^{18}\text{O}$ between molar tooth structure and matrix for a given sample; (c) Histogram of the difference in $\delta^{13}\text{C}$ between molar tooth structure and matrix for a given sample; (d) Histogram of the difference in $\delta^{18}\text{O}$ between molar tooth structure and matrix for a given sample.

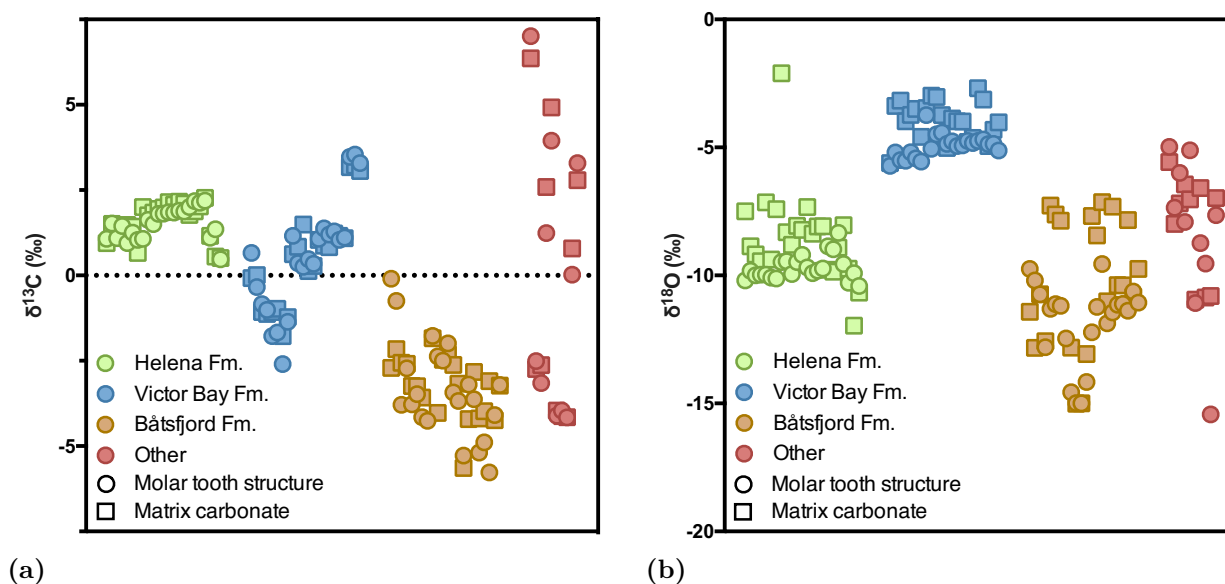


Figure 3.4 $\delta^{13}\text{C}$ and $\delta^{18}\text{O}$. “Other” category includes samples from the Boot Inlet, Reefal Assemblage, Maieberg, Humboldt, and Draken Formations. (a) $\delta^{13}\text{C}$ of molar tooth structure and the corresponding matrix. Note that there is no systematic difference; (b) $\delta^{18}\text{O}$ of molar tooth structure and the corresponding matrix. Note that the matrix is typically isotopically heavy relative to the molar tooth structure.

3.7.5 Iron Isotopes

Iron isotopes were measured on a subset of 28 samples considered to be representative of the whole sample suite, with samples from all studied successions with the exception of the Humboldt Formation. In molar tooth structures, $\delta^{56}\text{Fe}$ values range from -2.39 to 1.96‰, although half (N=14) measure between -1 to 0‰ (Figure 3.5). In the matrix carbonate, $\delta^{56}\text{Fe}$ values range from -0.69 to +2.20‰, with most values (N=15) falling between 0.5-1.5‰. The molar tooth structure is typically depleted in $\delta^{56}\text{Fe}$ relative to the associated matrix carbonate (N=23), with most being depleted by -1.0 to -2.0‰ (Figure 3.6b). Rare molar tooth structure samples (N=5) exhibit an enrichment in $\delta^{56}\text{Fe}$ relative to the matrix carbonate. Iron isotopes measured on the matrix siliciclastics were consistently isotopically heavy, with $\delta^{56}\text{Fe}$ values ranging from 0.13-2.12‰. For nine of ten samples in which the $\delta^{56}\text{Fe}$ of matrix siliciclastics was measured, it was isotopically heavy compared to the corresponding molar tooth structure, although it was variably heavy or light relative to the matrix carbonate (Figure 3.6c).

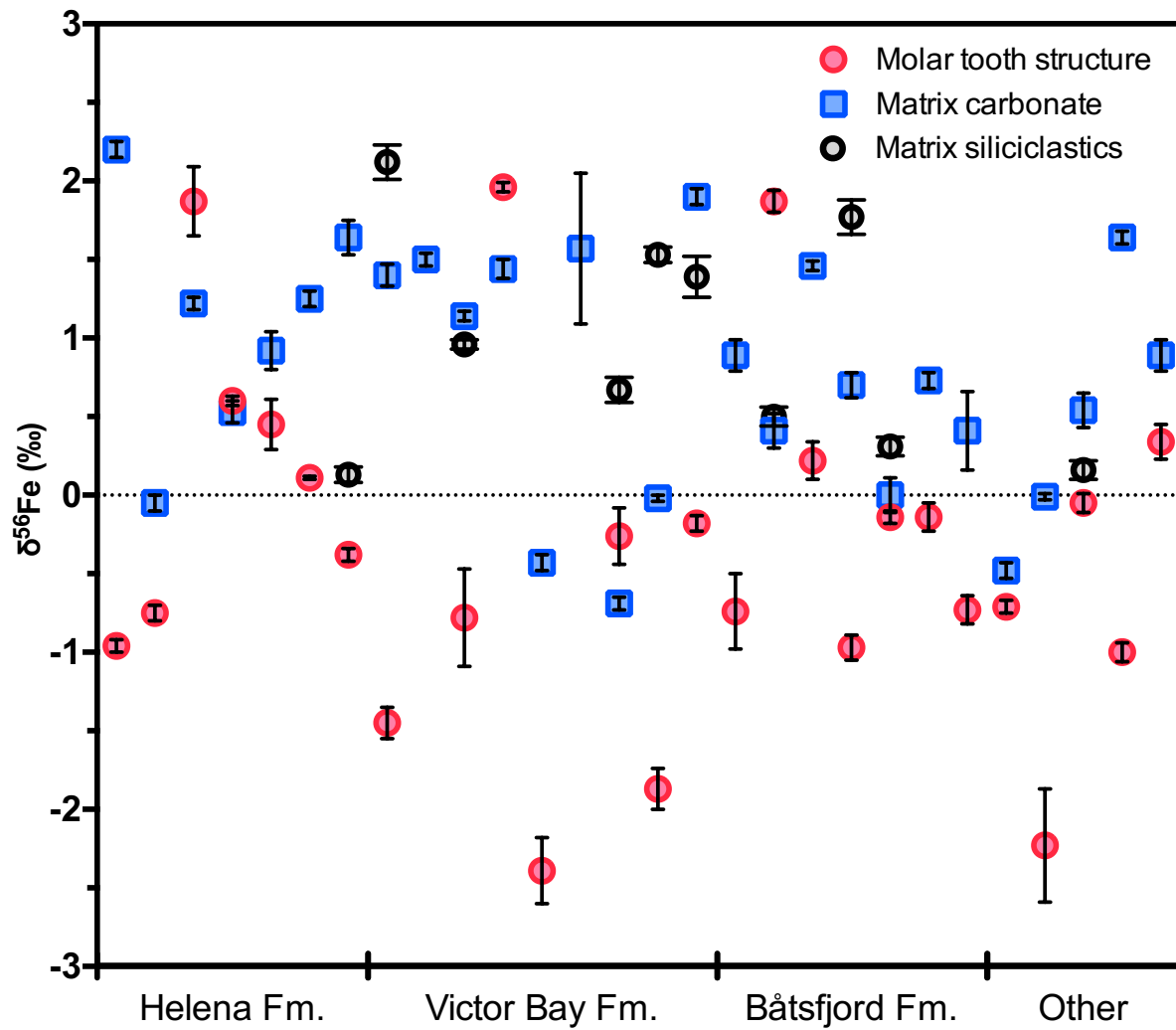


Figure 3.5 $\delta^{56}\text{Fe}$ for molar tooth structures, matrix carbonate, and the matrix siliciclastics. “Other” includes the Reefal Assemblage, Draken, Boot Inlet, and Maieberg Formations. Error bars are $\pm 1\sigma$.

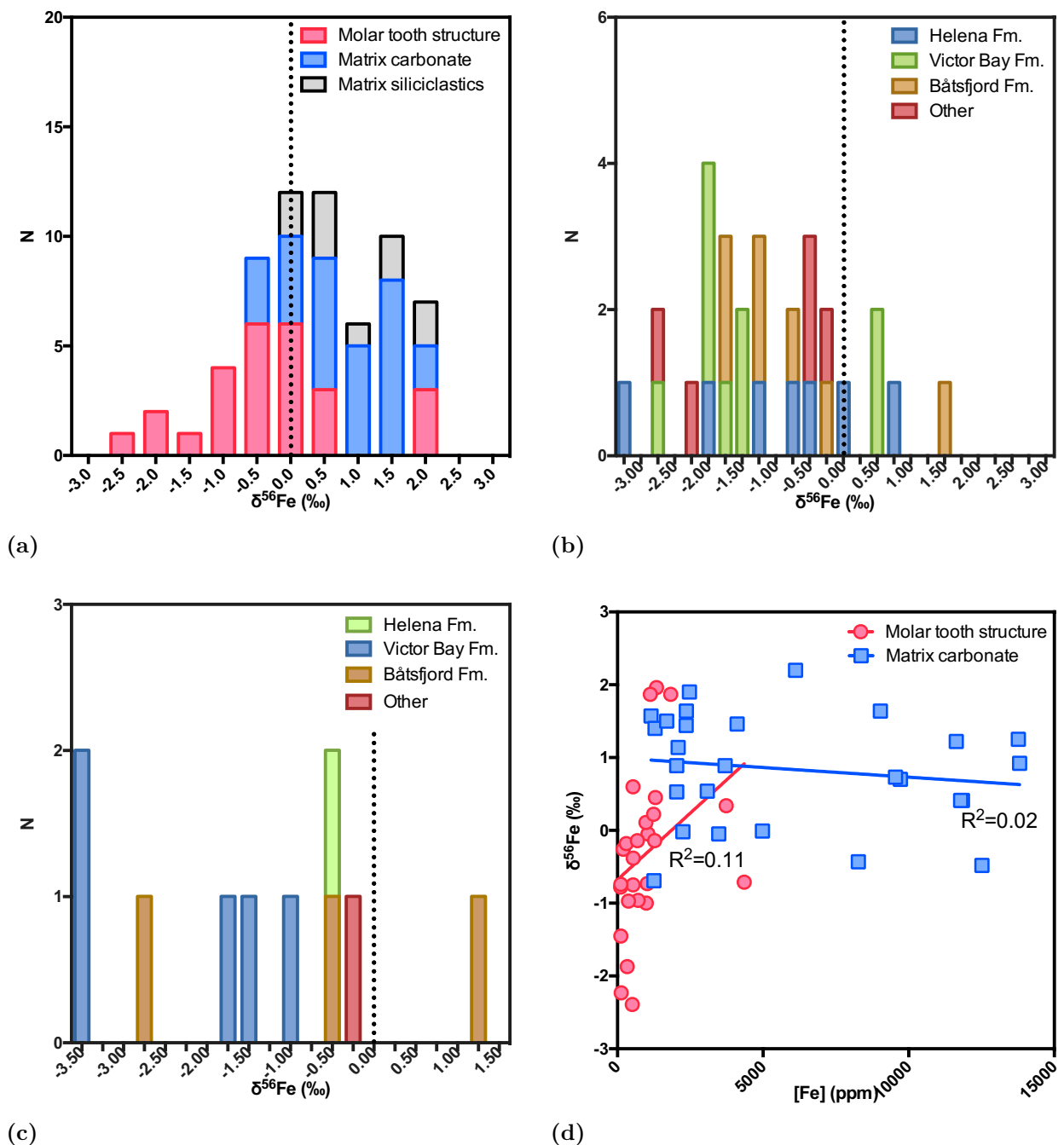


Figure 3.6 (a) Histogram of $\delta^{56}\text{Fe}$ for molar tooth structure, matrix carbonate, and matrix siliciclastics; (b) Histogram of the difference in $\delta^{56}\text{Fe}$ between molar tooth structure and matrix carbonate. “Other” includes Reefal Assemblage, Boot Inlet, Draken, and Maieberg Formations; (c) Histogram of the difference in $\delta^{56}\text{Fe}$ between molar tooth structure and matrix siliciclastics. “Other” includes the Draken Formation; (d) $\delta^{56}\text{Fe}$ of molar tooth structures and matrix carbonate against $[\text{Fe}]$ reveals a strong trend in molar tooth structures, attributed to microbial dissimilatory iron reduction. A similar trend is absent in the matrix carbonate.

3.7.6 Scanning Electron Microscope

One sample from the Draken Formation, Svalbard (GS2) and one sample from the Helena Formation, Montana (RP452) were analyzed by scanning electron microscopy in order to qualitatively verify that the matrix and molar tooth structure were each of relatively homogenous composition, and that there had been no significant diffusion of elements across the matrix-molar tooth structure contact. Back-scatter electron element mapping qualitatively showed that both the molar tooth structure and matrix are relatively homogenous in composition within a given sample, and that there had been little to no diffusion of elements across the matrix-molar tooth structure contact relative to the natural concentrations of elements within the molar tooth structure and matrix.

3.8 Discussion

3.8.1 Preservation of Primary Signatures

It is important to assess the extent of diagenetic changes to the sample composition. We use the elemental ratios Mn/Sr and Mg/Ca to explore for the effect of meteoric diagenesis and dolomitisation on the chemistry of both molar tooth structures and the matrix carbonate. During precipitation, carbonate will inherit a trace element and isotopic composition that reflects the composition of the seawater from which it formed. Seawater generally contains less Mn, more Sr, and heavier $\delta^{18}\text{O}$ than meteoric water; when carbonate minerals interact with meteoric water, dissolution and reprecipitation will result in a meteoric influence in the trace element and isotopic composition (Brand et al., 1980). The relatively high concentration of Mn in meteoric water, combined with the leachability of Sr, means that with increasing meteoric alteration, the Mn content should increase while the Sr content decreases, and $\delta^{18}\text{O}$ will shift toward lighter values (Brand et al., 1980; Brand et al., 1981). Mg/Ca acts as a measure of dolomitisation, as Mg substitutes into the crystal lattice to form dolomite. The process of dolomitisation will result in heavier $\delta^{18}\text{O}$ by 2-4‰ (Land, 1980; Halverson et al.,

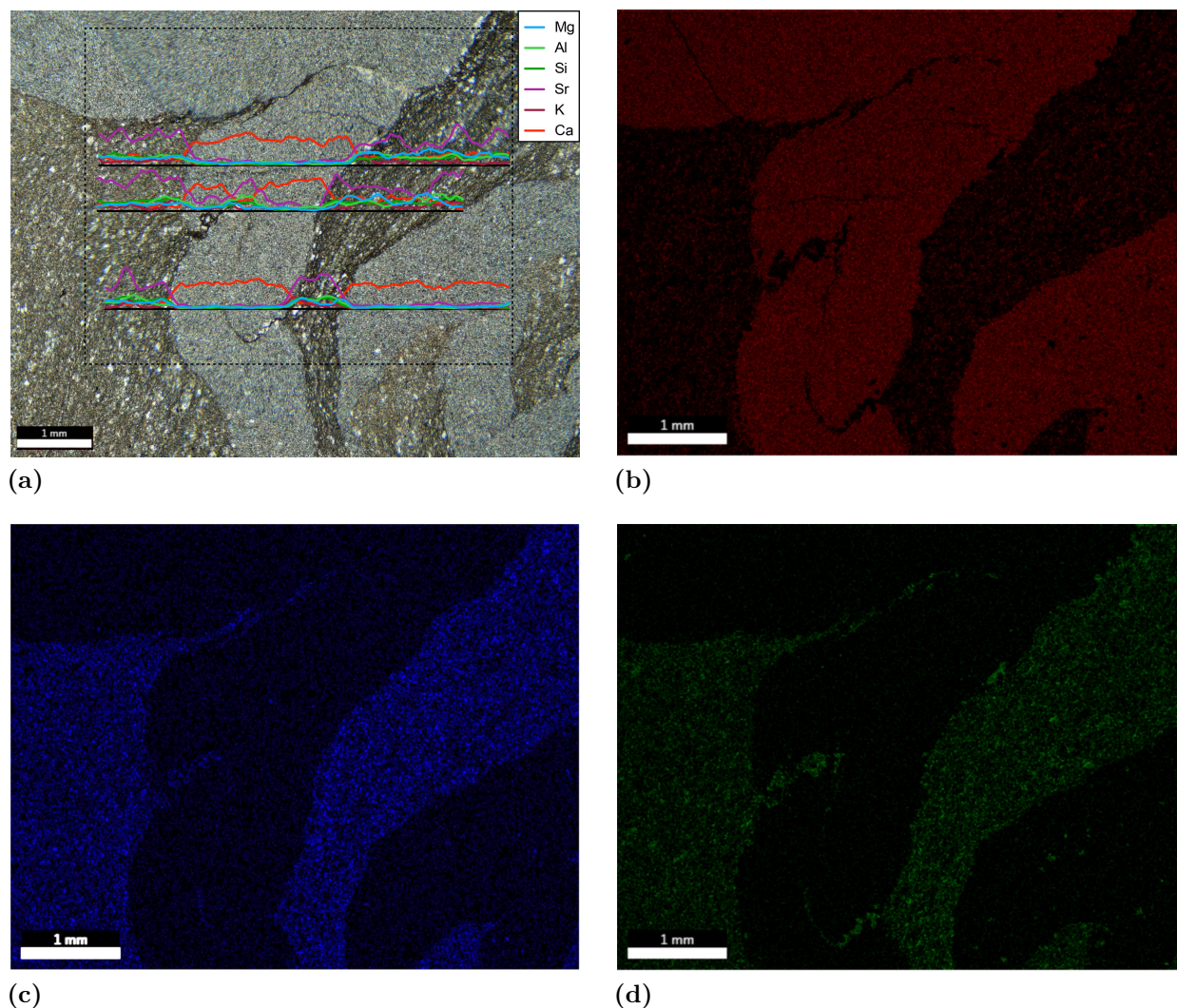


Figure 3.7 Sample RP452 from the Helena Formation under BSE SEM. (a) Sample under plane-polarized light with line scans super imposed. Black, dashed box indicates area studied under SEM; (b) Map of Ca; (c) Map of Mg; (d) Map of Al.

2007). It follows that a “pristine” carbonate which was precipitated from seawater, and not influenced by meteoric alteration or dolomitisation will have low Mn/Sr (<1) and low Mg/Ca (<0.05) (Jacobsen et al., 1999; Halverson et al., 2007).

Comparing the matrix carbonate values for each sedimentary succession, it is apparent that each has its own "alteration pathway" with varying influences of meteoric alteration and dolomitisation (Figure 3.8). Interestingly, however, molar tooth structures typically have very low Mn/Sr and Mg/Ca, indicating minimal meteoric alteration and dolomitisation. This

suggests that the calcite within molar tooth structures is better preserved than the host rock within which it formed.

These data can also be used to constrain the relative timing of meteoric alteration and dolomitisation of the matrix carbonate. Extrapolating the lines of fit to where there has been no dolomitisation (i.e. $\text{Mg}/\text{Ca} \approx 0$) corresponds to elevated Mn/Sr ranging from approximately 2-5 for the Helena and Båtsfjord Formations (Figure 3.8). The Victor Bay Formation exhibits

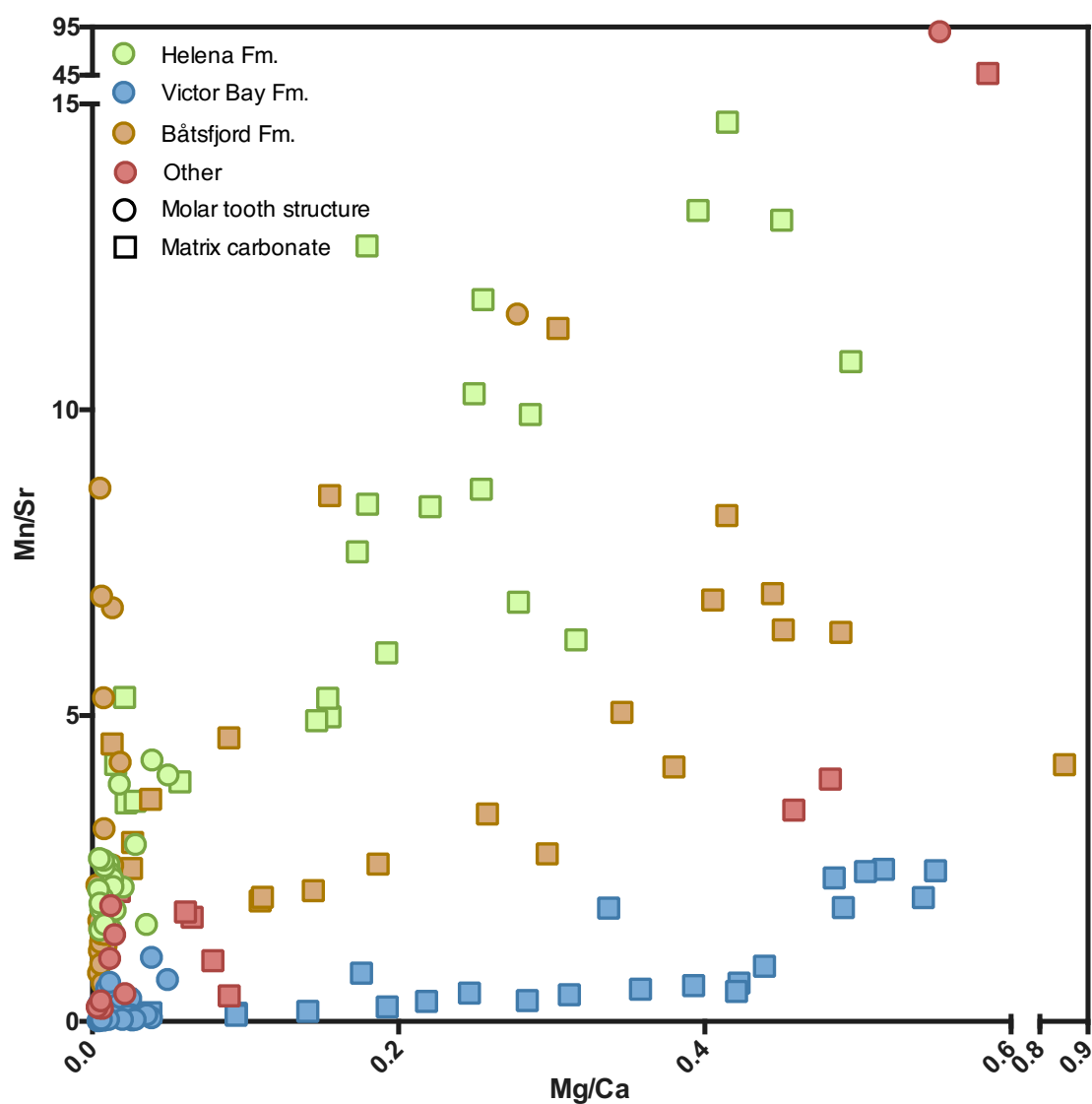


Figure 3.8 Comparison of Mn/Sr vs Mg/Ca for both molar tooth structure and matrix carbonate. Molar tooth structures consistently have low Mn/Sr and Mg/Ca , unlike the matrix carbonate.

little to no evidence for meteoric alteration, suggesting that dolomitisation occurred prior to meteoric alteration. Given that dolomitisation would drive $\delta^{18}\text{O}$ towards heavier values, this would suggest that the Victor Bay Formation records a $\delta^{18}\text{O}$ of seawater of approximately -5‰, although the interpretation of this is beyond the scope of this study.

Comparison of $\delta^{18}\text{O}$ with Mg/Ca in the matrix carbonate of the Victory Bay, Båtsfjord, and Helena Formations shows a strong relationship, with increasing dolomitisation correlating to heavier $\delta^{18}\text{O}$ values (R^2 of 0.60, 0.57, 0.60, respectively; Figure 3.9a). Given the susceptibility of oxygen isotopes to being “reset” (Veizer et al., 1976; Land, 1980), this relationship is unsurprising. Further, it explains the observed depletion in $\delta^{18}\text{O}$ between molar tooth structures and matrix, specifically that the $\delta^{18}\text{O}$ of the matrix carbonate has been increased by dolomitisation. There is no relationship between $\delta^{13}\text{C}$ and either Mg/Ca or Mn/Sr, so it is assumed that $\delta^{13}\text{C}$ values reflect primary isotopic compositions.

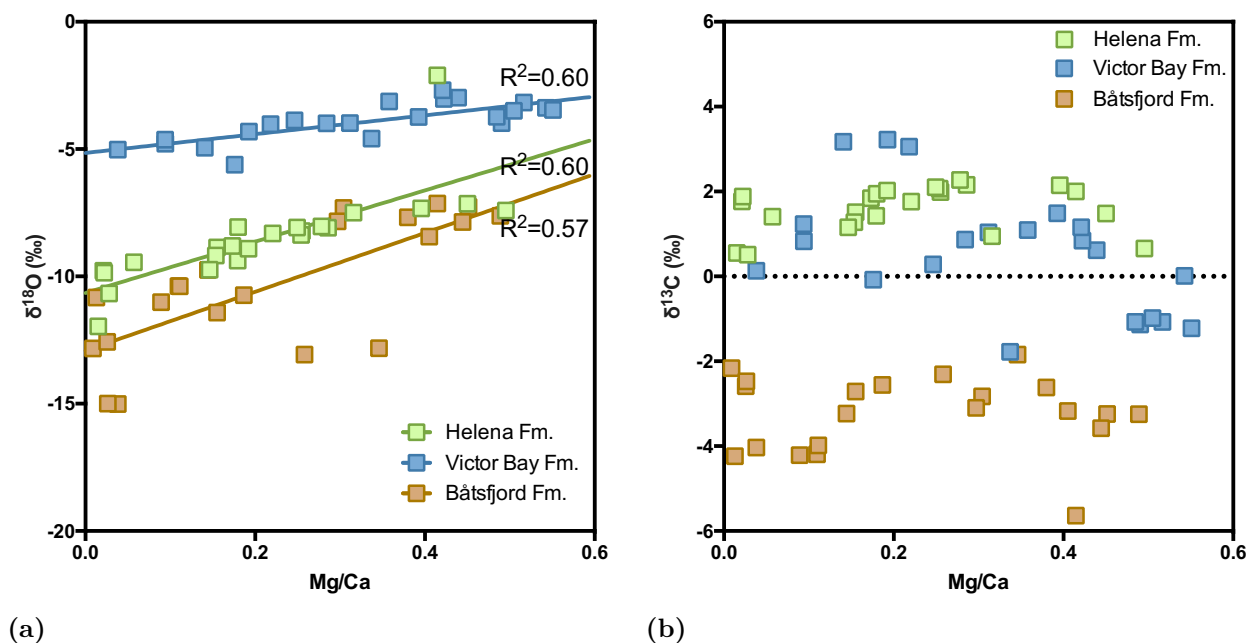


Figure 3.9 (a) Increasing dolomitisation of the matrix carbonate is correlated to heavier $\delta^{18}\text{O}$. Equations for Helena, Victor Bay, and Båtsfjord Formations, respectively, are: $\delta^{18}\text{O} = 10.07 \cdot \text{Mg/Ca} - 10.65$, $\delta^{18}\text{O} = 3.687 \cdot \text{Mg/Ca} - 5.150$, $\delta^{18}\text{O} = 11.55 \cdot \text{Mg/Ca} - 12.92$; (b) Increasing dolomitisation of the matrix carbonate has no impact on $\delta^{13}\text{C}$.

There is considerable variation in $\delta^{56}\text{Fe}$ of the samples, even over small changes in stratigraphic height. For example, two samples from the Victor Bay Formation, MB1501.489.0 and MB1501.489.8 were collected only 80 centimetres apart, but exhibit variation in $\delta^{56}\text{Fe}$ of matrix carbonate of almost 2‰. Similar variation in $\delta^{56}\text{Fe}$ is observed in the Båtsfjord Formation, where $\delta^{56}\text{Fe}$ of the matrix carbonate spans from 0.0‰ to 1.46‰, and in the Helena Formation, where it spans from -0.05 to +2.2‰. This variation is not inconsistent with measurements made by others. Johnson et al. (2008a) measured $\delta^{56}\text{Fe}$ variations up to ~ 1.8 ‰ in banded iron formations over the scale of centimetres. There is no relationship between $\delta^{56}\text{Fe}$ measurements with either Mn/Sr or Mn content, suggesting that meteoric alteration has little influence on the preservation of iron isotope signatures in carbonates.

The Effects of Dolomitisation on $\delta^{56}\text{Fe}$

The relationship between dolomitisation and $\delta^{56}\text{Fe}$ in carbonates has, to date, not been constrained. Here, we present $\delta^{56}\text{Fe}$ and Mg/Ca measurements for 28 matrix carbonate samples of varying degrees of dolomitisation, in an attempt to constrain the relationship between increasing Mg/Ca and $\delta^{56}\text{Fe}$. When the $\delta^{56}\text{Fe}$ of samples from all the studied sedimentary successions is plotted against Mg/Ca, there does not appear to be a relationship ($R^2=0.08$), although comparison of $\delta^{56}\text{Fe}$ and Mg/Ca for individual sedimentary successions exhibits relationships of varying strength. Samples from the Helena Formation exhibit no relationship between $\delta^{56}\text{Fe}$ and Mg/Ca ($R^2=0.06$). The Victor Bay Formation, which exhibits minimal meteoric alteration (Mn/Sr typically less than 0.5), but Mg/Ca ranging from 0.04-0.55, exhibits very little relationship between $\delta^{56}\text{Fe}$ and Mg/Ca ($R^2=0.13$), with increasing dolomitisation corresponding to slightly lighter $\delta^{56}\text{Fe}$ values. The Båtsfjord Formation exhibits the strongest relationship between Mg/Ca and $\delta^{56}\text{Fe}$ ($R^2=0.42$), with increasing dolomitisation corresponding to slightly lighter $\delta^{56}\text{Fe}$. The relationship is therefore ambiguous, and it is concluded that dolomitisation has little to no effect on $\delta^{56}\text{Fe}$ (Figure 3.10). Nonetheless, given

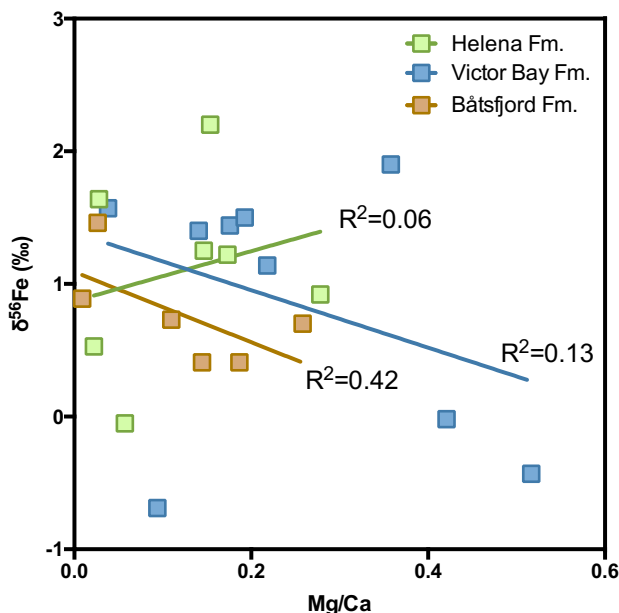


Figure 3.10 $\delta^{56}\text{Fe}$ compared to Mg/Ca for matrix carbonate from the Helena, Victor Bay, and Båtsfjord Formations. Whereas the Victor Bay and Båtsfjord Formations exhibit decreasing $\delta^{56}\text{Fe}$ with increasing dolomitisation, the Helena Formation does not exhibit any trend.

that samples from both the Victor Bay and Båtsfjord Formations are in general agreement, whereas there is no relationship in samples from the Helena Formation, it seems that if dolomitisation does have an effect on the $\delta^{56}\text{Fe}$ of carbonate, it will result in the substitution of a small amount of isotopically light iron into the calcite/dolomite lattice. This is further supported by the correlation of iron content within the matrix and Mg/Ca of the matrix carbonate, which is exhibited in the Helena, Victor Bay, and Båtsfjord Formations (R^2 of 0.67, 0.59, and 0.45 respectively).

A scanning electron microscope equipped with a backscatter electron detector was used to create elemental maps of several polished thick sections, to determine if there had been diffusion of elements between the molar tooth structure and matrix. Qualitatively, this does not seem to have been the case, even where very thin “wisps” of matrix are encased by the molar tooth structure.

In light of the above discussion, $\delta^{13}\text{C}$ and $\delta^{56}\text{Fe}$ values for both the matrix carbonates and molar tooth structures are interpreted as largely unchanged from their original compositions. Dolomitisation does not seem to significantly affect the $\delta^{56}\text{Fe}$ of carbonate minerals, but if it does, it would appear to result in a slight shift toward isotopically lighter values. The low Mg/Ca of molar tooth structures, especially compared to that of the matrix carbonate, suggests that if anything, the present difference in $\delta^{56}\text{Fe}$ between molar tooth structures and associated matrix carbonates is smaller than it would have been prior to dolomitisation of the matrix carbonate. Given that molar tooth structures consistently have lower Mn/Sr and Mg/Ca, and display no relationship between $\delta^{18}\text{O}$ and Mg/Ca, it would appear that they are better preserved than their host matrix. We speculate that this is due to the homogenous, early cemented, tightly packed microcrystalline calcite that MTS are composed of, in contrast to the mineralogically heterogeneous, uncemented matrix sediments which are inherently more susceptible to fluid flow and subsequent diagenesis.

3.8.2 Microbial Illitisation and the Formation of Molar Tooth Structures

The microbial smectite-illite reaction has been shown to occur very quickly. In a laboratory experiment, Kim et al. (2004) incubated *Shewanella oneidensis* strain MR-1 with formate as the electron donor, and an Fe-rich smectite as the electron acceptor. At room temperature and pressure, 43% of the smectite was converted to illite within 14 days. The smectite-illite reaction may also occur by burial diagenesis, at temperatures of 300-350°C, pressures of 100 MPa, and time spans of several months (Kim et al., 2004). These conditions are obviously not encountered during the formation of molar tooth structures, given the extensive field observations that support a very early diagenetic formation in the uppermost sediment column (Personal observations, Furniss et al., 1998; Pratt, 1998).

The illitisation of Fe-rich smectite could conceivably create the void spaces within which MTS form. Kostka et al. (1999) conducted experiments to determine how the surface chemistry

of smectite minerals changes upon reduction to illite. Importantly, they found that the process causes the clay mineral structure to collapse, with expulsion of 40-44% of the water within the parental clay, while the surface area of the clay minerals decreased by 26-46%, depending on the smectite mineralogy. The expulsion of water during deflocculation, and reduction in clay volume, could therefore generate the void spaces in which molar tooth structures form.

Finally, the process of illitisation results in a change in local pore water chemistry which favours the precipitation of calcite. Although the stoichiometry of the chemical reaction will vary depending on the mineralogy of the smectite, the process of illitisation will release Ca^{2+} , Fe^{2+} , bicarbonate, silica, and water (Stucki et al., 2006; Vorhies et al., 2009). The smectite to illite transformation pathway requires K^{+} ions, which in the uppermost sediment column may have been sourced from the overlying seawater, providing a near-infinite source of K^{+} (Demicco et al., 2005). Furthermore, studies of mixed-layer illite/smectite have shown that illitisation may occur without an external source of K^{+} , by the cannibalisation of smectite layers (Pollastro, 1985). It is therefore conceivable that microbial illitisation may not be K^{+} limited.

The microbial reduction of Fe-rich smectite to illite may therefore address how molar tooth structures are created. The deflocculation of clay minerals simultaneously increases the alkalinity and calcium concentration of the local pore water while clay minerals shrink, and may allow for the generation of voids within the sediment. Hence, the conversion of smectite to illite should also locally increase porewater alkalinity, promoting the precipitation of fine-grained calcite within the void spaces.

The microbial reduction of smectite to illite has previously been used to explain the growth of quartz, pyrite, and calcite intergrowths in Cambrian mudstones. Vorhies et al. (2009) found the intergrowth of these minerals in void spaces within mudrocks of the Wheeler Formation, Utah, and suggested that these voids could not have stayed open during overburden pressure, meaning that the intergrowths must have formed prior to compaction of the sediment. $\delta^{18}\text{O}$ analyses of the quartz intergrowths were used for paleothermometry calculations, and yielded

temperatures consistent with microbial processes (26-69°C). Ultimately, Vorhies et al. (2009) concluded that the calcite, quartz, and pyrite intergrowths resulted from the release of Fe^{2+} , Ca^{2+} , SiO_2 , and HCO_3^- due to microbial reduction of smectite to illite. It is therefore seemingly possible for the microbial conversion of smectite to illite to facilitate the growth of other minerals on a meaningful scale.

Carbon and Oxygen Isotopes

Comparison of $\delta^{13}\text{C}$ between the molar tooth structure and matrix carbonate is essential for understanding the source of carbon in molar tooth structure microspar. Frank et al. (1998) reasoned that if carbon in molar tooth structures was partly sourced from the decay of organic matter, or methanogenesis, this should be reflected in the $\delta^{13}\text{C}$ composition. However, analyses of the molar tooth structures and matrix carbonate of 77 samples reveals that there is no systematic difference in $\delta^{13}\text{C}$ (Figure 3.3c). This contrasts with the findings of Shen et al. (2016), who observed a 0.5-1.0‰ difference, but agrees with other studies, for example, Frank et al. (1998) and Bishop et al. (2006), where $\delta^{13}\text{C}$ values of the molar tooth structure and associated matrix carbonate are indistinguishable. The process of DIR oxidizes organic matter, generating $\delta^{13}\text{C}$ depleted bicarbonate. Given that organic matter typically has a $\delta^{13}\text{C}$ of approximately -30 to -25‰, a negative $\delta^{13}\text{C}$ signal should be recorded in molar tooth structures.

The indistinguishable $\delta^{13}\text{C}$ of molar tooth structures and associated matrix carbonate does not preclude the importance of dissimilatory iron reduction, or other mechanisms which result in carbon isotope fractionation. The bicarbonate which results from dissimilatory iron reduction is not of fixed isotopic composition; rather, it varies depending on the size of available pools of organic carbon and dissolved inorganic carbon, and as little as 1/4 of the resulting alkalinity may be in the form of isotopically depleted bicarbonate (Heimann et al., 2010). Furthermore, Frank et al. (1998) noted that if there was a large pool of dissolved inorganic carbon, this would buffer the $\delta^{13}\text{C}$ of the molar tooth carbonate, potentially obscuring the

isotopic signature of the remineralized organic carbon. This would be consistent with a very early diagenetic origin, in which alkalinity for microspar precipitation may be sourced in large part from pore waters or diffusion of seawater.

Microbial Iron Reduction and Iron Isotopes

The largest natural fractionations of iron isotopes occur as the result of redox reactions, for example, the reduction of Fe(III) to Fe(II), and the oxidation of Fe(II) to Fe(III). Although both reduction and oxidation of iron may occur with or without microbial pathways, Johnson et al. (2008b) showed that the isotopic fractionation of iron resulting from microbial iron reduction and oxidation is several orders of magnitude larger than for abiological processes, and microbial reduction and oxidation therefore play a major role in iron isotope variations.

In the reduction of iron from a ferric substrate, there are three main pools of iron: reactive ferric iron in the substrate ($\text{Fe(III)}_{\text{reac}}$), ferrous iron sorbed onto the surface of the ferric substrate ($\text{Fe(II)}_{\text{sorb}}$), and aqueous ferrous iron ($\text{Fe(II)}_{\text{aq}}$). The isotopic fractionation associated with dissimilatory iron reduction (DIR) is not the result of a single process, but rather several processes occurring simultaneously (Crosby et al., 2007). Bioavailable iron from a ferric substrate, $\text{Fe(III)}_{\text{reac}}$, is metabolized by DIR bacteria, which couple Fe(III) reduction to organic matter oxidation, generating $\text{Fe(II)}_{\text{aq}}$. Crosby et al. (2007) showed that a portion of this $\text{Fe(II)}_{\text{aq}}$ is sorbed back onto $\text{Fe(III)}_{\text{reac}}$, where it undergoes electron exchange and atom exchange, resulting in a layer of $\text{Fe(III)}_{\text{reac}}$ on the surface of the ferric substrate (Figure 3.11). The net fractionation between $\text{Fe(III)}_{\text{reac}}$ and $\text{Fe(II)}_{\text{aq}}$ is $\simeq -2.95\text{‰}$ (Crosby et al., 2007).

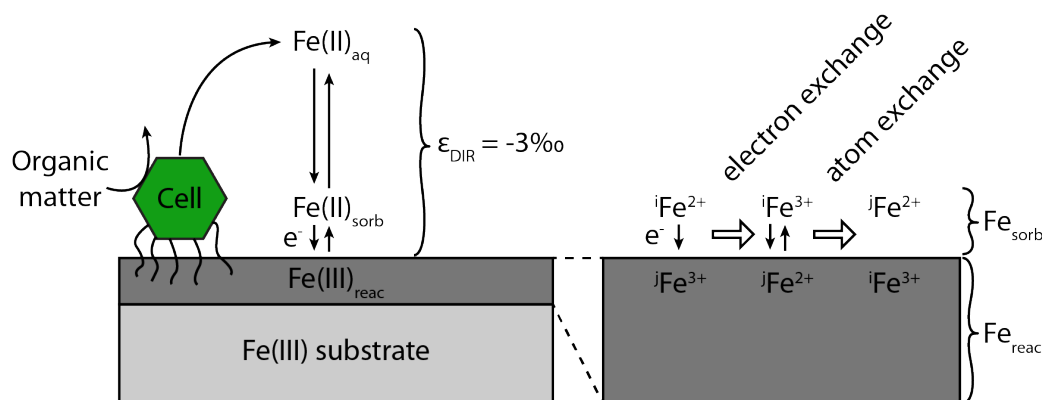


Figure 3.11 Mechanisms behind microbial dissimilatory iron reduction. Model from Crosby et al. (2007).

Crosby et al. (2007) demonstrated that DIR does not induce a unique fractionation factor; rather, it catalyses equilibrium isotope fractionations by promoting electron exchange. For example, *Shewanella oneidensis* strain MR1 can produce highly conductive “nano-wires” which penetrate the substrate surface, greatly increasing the amount of $\text{Fe(III)}_{\text{reac}}$ beyond that of the reactive surface area (Gorby et al., 2006). To date, the fractionation caused by microbial dissimilatory iron reduction of Fe-rich clay minerals has not been measured. Nevertheless, Crosby et al. (2007) measured $\delta^{56}\text{Fe}$ fractionations caused by *Geobacter sulfurreducens* strain PCA and *Shewanella putrefaciens* strain CN32 on both hematite and goethite, and found that the fractionation induced is independent of the reducing bacteria and ferric substrate. It is therefore reasonable to expect that reduction of Fe-rich clays will also fractionate $\delta^{56}\text{Fe}$ by approximately -3‰.

$\delta^{56}\text{Fe}$ in Molar Tooth Structures

The vast majority of molar tooth structures have $\delta^{56}\text{Fe}$ values less than 0‰, and reach values as light as -2.39‰. The $\delta^{56}\text{Fe}$ of the matrix carbonates, however, is distinctly heavier, with most samples between approximately 0.5-1.5‰. There is considerable variability in the $\delta^{56}\text{Fe}$ of the matrix siliciclastics (i.e. the matrix insoluble residue component), with values ranging from 0.13-2.12‰. It is therefore clear that, with few exceptions, the $\delta^{56}\text{Fe}$ of molar tooth structures is both lighter than that of the associated matrix carbonate and matrix siliciclastics. Furthermore, in the ten samples in which the $\delta^{56}\text{Fe}$ of the matrix siliciclastics was measured, nine were heavier than that of the corresponding molar tooth structure. This difference in $\delta^{56}\text{Fe}$ between the molar tooth structure and matrix carbonate and siliciclastics is consistent with the dissimilatory iron reduction hypothesis for the genesis of molar tooth structures in which iron in molar tooth structures is sourced from the reduction of smectite to illite in the matrix siliciclastics. Furthermore, the $\delta^{56}\text{Fe}$ values of molar tooth structures are broadly consistent with dissimilatory iron reduction (Severmann et al., 2006; Crosby et al., 2007).

There is a weak relationship between the concentration of Fe in molar tooth structures and $\delta^{56}\text{Fe}$ (Figure 3.6d), where higher Fe concentrations correspond to heavier $\delta^{56}\text{Fe}$ ($R^2=0.11$). This could be interpreted as the result of alteration, in which isotopically heavy iron is added to the molar tooth structure by fluid flow, dolomitisation, or other means. However, the consistently low Mn/Sr and Mg/Ca exhibited by molar tooth structures, in addition to the lack of evidence for alteration when samples are observed under SEM, refutes iron addition by processes which postdate molar tooth structure formation. An alternate, preferred explanation is that this relationship is due to isotopic mass balance relationships between $\text{Fe(II)}_{\text{aq}}$ and $\text{Fe(III)}_{\text{reac}}$. During DIR, a small amount of dissimilatory iron reduction will result in a small pool of $\text{Fe(II)}_{\text{aq}}$ which is highly depleted in $\delta^{56}\text{Fe}$, but as DIR proceeds to greater degrees, the pool of $\text{Fe(II)}_{\text{aq}}$ will increase in size while $\delta^{56}\text{Fe}$ shifts to heavier values (Crosby et al., 2007). The dataset presented here broadly agrees with this relationship and

studies of modern sediments (e.g. Severmann et al., 2006; Bergquist et al., 2006), supporting the interpretation that this trend is reflective of processes which were occurring during molar tooth structure formation.

Reduction of Ferric Non-clay Minerals

The reduction of clay minerals has been of particular focus in this study due to the near-exclusive occurrence of molar tooth structures in argillaceous carbonate sediments. Further, the pool of reducible iron in clay minerals may constitute a sizeable portion of redox active iron, and has been shown to be comparable in size to that of iron oxides in some marine environments (Thamdrup, 2000). For example, in the Elbe Estuary in the North Sea, 26% of iron was in the form of reducible Fe(III) in clay minerals, and 20% of iron was in the form of fine grained iron oxides such as hematite and goethite (König et al., 1997; Drodt et al., 1997). Whereas this study has thus far focussed on dissimilatory iron reduction of clay minerals as a source of alkalinity, the reduction of iron-bearing non-clay minerals in the host sediment may also play an important role. The reduction of ferric hydroxide occurs according to:



The reduction of ferric hydroxides in the host sediment may therefore promote the formation of molar tooth structures by the release of hydroxide, bicarbonate, and water, locally boosting pore water alkalinity and creating fissures in the sediment.

3.8.3 Effect of Clay Minerals

Aside from providing a ferric substrate for dissimilatory iron reduction, the presence of clay minerals within sediment has implications which may favour the formation of molar tooth structures. The presence of organic matter in sediment which contain clay results in a decrease of permeability, due to sorption of organic matter onto the clay mineral surface and the occupation of pore space by organic matter (Curry et al., 2007; Tosca et al., 2010). The decrease in permeability may aid in the coalescence of pore waters into ribbons and blobs, creating the voids in which molar tooth structures form (Pratt, 1998). Clay minerals are also highly effective at burying organic matter, due to the sorption of organic carbon onto their surface (Kennedy et al., 2002; Wattel-Koekkoek et al., 2003). A corollary to this is that the supply of clays to carbonate sediments provides both an electron donor (organic matter) and an electron acceptor (Fe-rich smectites) for DIR.

3.8.4 A Dissimilatory Iron Reduction Model for Molar Tooth Structure Formation

From field observations of molar tooth structures, several crucial constraints may be placed on their formation: they form in argillaceous, carbonate environments, near the sediment-water interface, in environments ranging from the storm wave base to the intertidal zone. Further, because their occurrence is restricted to the Neoarchean to Neoproterozoic, constraints may be placed on the ocean chemistry which they formed in, namely a very large pool of dissolved inorganic carbon, and widespread ferruginous conditions (Higgins et al., 2009; Poulton et al., 2011; Sperling et al., 2015). Therefore, in addition to resolving the three aspects of MTS formation (i.e. void generation, calcite precipitation, temporal restriction), a model for MTS formation must consider these physical and chemical constraints.

We propose that molar tooth structure formation occurred as the direct consequence of the accumulation of clay-rich carbonates in dominantly anoxic oceans with a very large DIC pool.

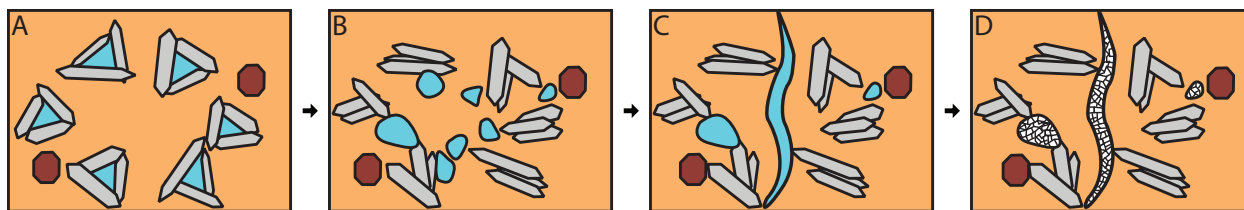


Figure 3.12 A dissimilatory iron reduction model for molar tooth structure formation. A) Carbonate sediments containing Fe-rich smectite and Fe oxides. B) DIR of Fe-rich smectites and oxides releases alkaline pore waters. C) Alkaline pore waters coalesce into ribbons and blobs. D) Calcite begins to precipitate, with additional alkalinity being provided by wave-pumping and pore waters.

Clay-rich carbonates accumulated in relatively shallow marine environments, ranging from below storm wave base to the intertidal zone, underneath an anoxic water column which was supersaturated with respect to calcite. Microbial dissimilatory reduction of Fe(III) to Fe(II) reduced Fe-rich smectites and oxides in the uppermost sediment column. K^+ for this reaction may have either been sourced from dissolved K^+ in the water column, the cannibalisation of clays, or siliciclastic minerals in the sediment column. These reduction reactions resulted in locally increased pore water alkalinity. The shrinking and deflocculation of clay minerals and water released during Fe(III) reduction coalesced in ribbons and blobs, instead of dewatering, due to decreased permeability as a result of clay content (Figure 3.12). While it seems unlikely that DIR of smectites and oxides created sufficient alkalinity to precipitate all of the calcite within molar tooth structures, it may have pushed alkalinity beyond a critical threshold, at which point calcite nucleation occurred. Once nucleation occurred, calcite precipitation may continue by supply of alkalinity from pore waters, or by replenishment of dissolved calcite by wave-pumping of ocean water supersaturated with respect to calcite, while obscuring the isotopically light carbon that results from remineralization of organic matter.

3.8.5 Abundance and Disappearance of Molar Tooth Structures

If dissimilatory iron reduction of Fe-rich clays and oxides did play a role in the formation of molar tooth structures, this introduces previously unexplored ways to explain the changes in abundance of MTS through time, in addition to their disappearance.

Clay minerals are produced through the chemical weathering of igneous rocks, and smectite is most efficiently produced when the chemical index of alteration (CIA) is between 70-85 (Nesbitt et al., 1989; Tosca et al., 2010). If weathering is too weak, the residual will be plagioclase-rich, and if it is too intense, it will be Al-rich (for example, kaolinite) (Nesbitt et al., 1989). The formation of smectites therefore occurs in a “sweet spot” of moderate chemical weathering conditions. Tosca et al. (2010) examined clay mineralogy throughout the Proterozoic, using X-Ray Diffraction to analyze clay bearing sediments, and construct a CIA curve from the Archean to Cambrian. The paleo-CIA curve indicates that weathering was most conducive for the formation of smectites from the Mesoproterozoic to the mid-Neoproterozoic, coincident with the peak of molar tooth structures. Prior to this, weathering was too intense to permit significant production of smectites, whereas after the mid-Neoproterozoic, weathering was too weak.

Alternatively, a rise in dissolved O_2 in the oceans would have decreased the extent of dissimilatory iron reduction, as anoxia is required for the reduction of Fe(III) to Fe(II). The reduction of iron under anoxic conditions is a mechanism to boost alkalinity and increase carbonate saturation in the surface ocean, promoting carbonate precipitation in shallow environments (Higgins et al., 2009). Higgins et al. (2009) noted that there is a first order relationship between the redox state of the ocean and atmosphere, and carbonate production in the ocean, as anoxic remineralization of organic carbon results in increased carbonate saturation compared to respiration of organic matter under oxic conditions. The redox state of the ocean therefore likely plays a critical role in the formation of molar tooth structures.

Glauconite offers an independent record which is also compatible with peak molar tooth structure formation in the Mesoproterozoic to mid-Neoproterozoic. Glauconite is thought to form from a precursor material that occurs near the sediment-water interface, in reducing conditions with low sedimentation rate and seawater K^+ diffusion into the sediment column (Rousset et al., 2004; Meunier et al., 2007; Tosca et al., 2010). The environment required for the formation of glauconite, namely reducing conditions and a source of K^+ , overlap with the

hypothesized conditions necessary for the formation of molar tooth structures. Similarly, the proportion of glauconite in shales peaked in the Mesoproterozoic and remained high into the Neoproterozoic, before dropping precipitously in the late Neoproterozoic (Tosca et al., 2010). This further supports that molar tooth structures disappeared from the sedimentary record at least in part due to changing sediment mineralogy and ocean redox conditions.

Finally, the demise of molar tooth structures could be the result of a decrease in the saturation state of calcite in the ocean. Shields (2002) noted that the disappearance of MTS broadly cooccurs with a decrease in the abundance of stromatolites. Grotzinger (1990) suggested that the decrease in stromatolite abundance is the result of a decrease in the size of the DIC pool in the ocean, so this may similarly affect the formation of molar tooth structures.

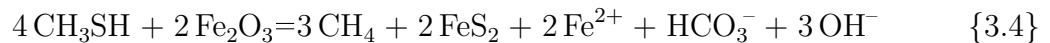
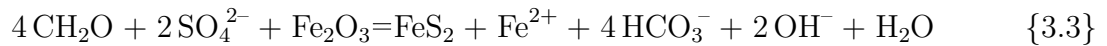
If the calcite veins observed in the Maieberg Formation, Namibia, are indeed molar tooth structures, this is consistent with the requirement of a large DIC pool in the ocean for MTS formation. Following the Marinoan Snowball Earth, the pool of DIC in the ocean would be very large due to intense silicate weathering (Higgins et al., 2003; Higgins et al., 2009). It is therefore conceivable that during this period of extremely high DIC concentration, molar tooth structures may have briefly reoccurred. This would be consistent with field observations of molar tooth structures in the Maieberg Formation, a Marinoan “cap carbonate”.

3.8.6 Implications for Molar Tooth Structure Formation by BSR and Methanogenesis

The results of this study have significant implications for other hypotheses of molar tooth structure formation. Shen et al. (2016) measured a difference in $\delta^{13}\text{C}$ between molar tooth structures and matrix carbonate, where the molar tooth structures were enriched in $\delta^{13}\text{C}$ by approximately 0.5-1.0‰ relative to the matrix carbonate. These limited results were used to infer a contribution of methanogenesis to molar tooth structure formation. However, the $\delta^{13}\text{C}$

measurements presented here on 77 samples from eight basins spanning ~ 810 Ma indicate that the $\delta^{13}\text{C}$ of molar tooth structure and matrix are indistinguishable.

The model put forth by Shen et al. (2016) invokes the following reactions for the formation of molar tooth structures:



In addition to the formation of hydroxide and bicarbonate, this model predicts the formation of pyrite. Whereas Shen et al. (2016) measured bulk rock pyrite contents of 0.05 to 1.37 wt%, with an average of 0.42 wt% in the Wanlong Formation (N=17), analyses conducted on the Helena, Victor Bay, Båtsfjord, Boot Inlet, Reefal Assemblage, Maieberg, and Draken Formations (N=36) found a much lower modal content of ~ 0.01 wt% (average of 0.08 wt%). It would therefore seem that the reactions put forth by Shen et al. (2016) do not occur in a significant amount in molar tooth structure bearing sediments. Perhaps the abnormally high pyrite contents documented by Shen et al. (2016) in the Wanlong Formation could be attributed to pyritization by fluid flow or other means, following lithification of the sediment.

Finally, work by Severmann et al. (2006) indicates that bacterial sulfate reduction results in $\delta^{56}\text{Fe}$ values of $\sim 0.5\text{‰}$. This value is heavier than the vast majority of molar tooth structures studied, further refuting a role for bacterial sulfate reduction and methanogenesis in the formation of molar tooth structures.

3.9 Conclusion

Until now, there has been no detailed study of the geochemical implications of clay minerals for the formation of molar tooth structures, despite their near-exclusive occurrence in argillaceous carbonate sediments. The implications for this are numerous, in particular for a source of bioavailable iron for reduction, and consequently an increase in pore water alkalinity.

We envisage a model for molar tooth structure formation in which dissimilatory iron reduction of Fe-rich smectites and Fe oxides in the uppermost sediment column plays a major role. The shrinking of clay minerals and release of water from deflocculation during reduction would coalesce to create the voids in which molar tooth structures form. A localized increase in pore water alkalinity would push the calcite saturation above a critical threshold, at which point calcite precipitation initiates. Alkalinity for continued calcite precipitation is sourced either from pore waters or by wave-induced pumping of ocean water into the uppermost sediment column.

A dissimilatory iron reduction origin for molar tooth structures is evidenced by a significant depletion in $\delta^{56}\text{Fe}$ of molar tooth structures relative to that of coeval matrix carbonate (modal difference of $\sim 2\%$). Furthermore, molar tooth structures are almost always depleted in $\delta^{56}\text{Fe}$ relative to corresponding matrix siliciclastics. Dissimilatory iron reduction should result in isotopically light carbon isotope values in the resulting carbonate minerals due to the partial sourcing of carbon from organic matter (Heimann et al., 2010). However, $\delta^{13}\text{C}$ values of molar tooth structures and the corresponding matrix carbonate are indistinguishable. This is consistent with a model in which alkalinity for molar tooth structure formation is supplied in part by ocean waters with a very large pool of dissolved inorganic carbon, which would obscure the isotopic signature of remineralized organic matter.

The proposed model for molar tooth structure formation is also consistent with the environmental conditions of the Proterozoic, a period characterized by ferruginous oceans and a large pool of dissolved inorganic carbon (Poulton et al., 2011; Higgins et al., 2009).

Furthermore, weathering conditions were most favourable for the production of smectite in the Mesoproterozoic and early Neoproterozoic, broadly coincident with the peak in molar tooth structure formation. Given the apparently narrow range of conditions required for molar tooth structure formation, subtle variations in these parameters could conceivably put an end to the formation of molar tooth structures. This is also consistent with an isolated reoccurrence of molar tooth structures in the wake of the Marinoan Snowball Earth, a time which would have had an extremely large DIC pool (Higgins et al., 2009).

Through Earth history, there has been a trend toward increasingly shallow carbonate depositional environments, from seafloor cements in the Paleoproterozoic, to stromatolites and micrites in the Mesoproterozoic and Neoproterozoic, to shell organisms in the Phanerozoic (James et al., 1998). Rather than an inconsequential Proterozoic carbonate structure, we view molar tooth structures as an important mechanism for carbonate production, the occurrence of which signifies the occurrence of a narrow “window” of conditions during which MTS may form. The appearance and disappearance of molar tooth structures is therefore reflective of an Earth system in transition.

Bibliography

- Beard, B. L. and Johnson, C. M. (2004). “Fe isotope variations in the modern and ancient earth and other planetary bodies.” *Reviews in Mineralogy and Geochemistry* 55.1, pp. 319–357.
- Bergquist, B. and Boyle, E. (2006). “Iron isotopes in the Amazon River system: Weathering and transport signatures.” *Earth and Planetary Science Letters* 248.1, pp. 54–68.
- Bishop, J. W., Sumner, D. Y., and Huerta, N. J. (2006). “Molar tooth structures of the Neoproterozoic Monteville Formation, Transvaal Supergroup, South Africa. II: A wave-induced fluid flow model.” *Sedimentology* 53.5, pp. 1069–1082.
- Black, L., Calver, C., Seymour, D. B., and Reed, A. (2004). “SHRIMP U–Pb detrital zircon ages from Proterozoic and Early Palaeozoic sandstones and their bearing on the early geological evolution of Tasmania.” *Australian Journal of Earth Sciences* 51.6, pp. 885–900.
- Brand, U. and Veizer, J. (1980). “Chemical diagenesis of a multicomponent carbonate system-1: Trace elements.” *Journal of Sedimentary Research* 50.4, pp. 1219–1236.
- Brand, U. and Veizer, J. (1981). “Chemical diagenesis of a multicomponent carbonate system-2: stable isotopes.” *Journal of Sedimentary Research* 51.3, pp. 987–997.

- Crosby, H. A., Roden, E. E., Johnson, C. M., and Beard, B. L. (2007). "The mechanisms of iron isotope fractionation produced during dissimilatory Fe (III) reduction by *Shewanella putrefaciens* and *Geobacter sulfurreducens*." *Geobiology* 5.2, pp. 169–189.
- Curry, K. J., Bennett, R. H., Mayer, L. M., Curry, A., Abril, M., Biesiot, P. M., and Hulbert, M. H. (2007). "Direct visualization of clay microfabric signatures driving organic matter preservation in fine-grained sediment." *Geochimica et Cosmochimica Acta* 71.7, pp. 1709–1720.
- Dauphas, N. and Rouxel, O. (2006). "Mass spectrometry and natural variations of iron isotopes." *Mass Spectrometry Reviews* 25.4, pp. 515–550.
- Demicco, R. V., Lowenstein, T. K., Hardie, L. A., and Spencer, R. J. (2005). "Model of seawater composition for the Phanerozoic." *Geology* 33.11, pp. 877–880.
- Drodt, M., Trautwein, A., König, I., Suess, E., and Koch, C. B. (1997). "Mössbauer spectroscopic studies on the iron forms of deep-sea sediments." *Physics and Chemistry of Minerals* 24.4, pp. 281–293.
- Evans, K. V., Aleinikoff, J. N., Obradovich, J. D., and Fanning, C. M. (2000). "SHRIMP U-Pb geochronology of volcanic rocks, Belt Supergroup, western Montana: evidence for rapid deposition of sedimentary strata." *Canadian Journal of Earth Sciences* 37.9, pp. 1287–1300.
- Frank, T. D. and Lyons, T. W. (1998). "'Molar-tooth' structures: A geochemical perspective on a Proterozoic enigma." *Geology* 26.8, pp. 683–686.
- Furniss, G., Rittel, J. F., and Winston, D. (1998). "Gas bubble and expansion crack origin of 'molar-tooth' calcite structures in the middle Proterozoic Belt Supergroup, western Montana." *Journal of Sedimentary Research* 68.1, pp. 104–114.
- Gorby, Y. A., Yanina, S., McLean, J. S., Rosso, K. M., Moyles, D., Dohnalkova, A., Beveridge, T. J., Chang, I. S., Kim, B. H., Kim, K. S., et al. (2006). "Electrically conductive bacterial nanowires produced by *Shewanella oneidensis* strain MR-1 and other microorganisms." *Proceedings of the National Academy of Sciences* 103.30, pp. 11358–11363.

- Grotzinger, J. P. (1990). "Geochemical model for Proterozoic stromatolite decline." *American Journal of Science* 290, pp. 80–103.
- Halpin, J. A., Jensen, T., McGoldrick, P., Meffre, S., Berry, R. F., Everard, J. L., Calver, C. R., Thompson, J., Goemann, K., and Whittaker, J. M. (2014). "Authigenic monazite and detrital zircon dating from the Proterozoic Rocky Cape Group, Tasmania: Links to the Belt-Purcell Supergroup, North America." *Precambrian Research* 250, pp. 50–67.
- Halverson, G. P., Dudás, F. Ö., Maloof, A. C., and Bowring, S. A. (2007). "Evolution of the $^{87}\text{Sr}/^{86}\text{Sr}$ composition of Neoproterozoic seawater." *Palaeogeography, Palaeoclimatology, Palaeoecology* 256.3, pp. 103–129.
- Heimann, A., Johnson, C. M., Beard, B. L., Valley, J. W., Roden, E. E., Spicuzza, M. J., and Beukes, N. J. (2010). "Fe, C, and O isotope compositions of banded iron formation carbonates demonstrate a major role for dissimilatory iron reduction in ~ 2.5 Ga marine environments." *Earth and Planetary Science Letters* 294.1, pp. 8–18.
- Higgins, J., Fischer, W., and Schrag, D. (2009). "Oxygenation of the ocean and sediments: consequences for the seafloor carbonate factory." *Earth and Planetary Science Letters* 284.1, pp. 25–33.
- Higgins, J. A. and Schrag, D. P. (2003). "Aftermath of a snowball Earth." *Geochemistry, Geophysics, Geosystems* 4.3, p. 1028.
- Hoffmann, K.-H., Condon, D., Bowring, S., and Crowley, J. (2004). "U-Pb zircon date from the Neoproterozoic Ghaub Formation, Namibia: constraints on Marinoan glaciation." *Geology* 32.9, pp. 817–820.
- Jacobsen, S. B. and Kaufman, A. J. (1999). "The Sr, C and O isotopic evolution of Neoproterozoic seawater." *Chemical Geology* 161.1, pp. 37–57.
- James, N. P., Narbonne, G. M., and Sherman, A. G. (1998). "Molar-tooth carbonates: shallow subtidal facies of the Mid-to Late Proterozoic." *Journal of Sedimentary Research* 68.5, pp. 716–722.

- Johnson, C. M., Beard, B. L., Klein, C., Beukes, N. J., and Roden, E. E. (2008a). “Iron isotopes constrain biologic and abiologic processes in banded iron formation genesis.” *Geochimica et Cosmochimica Acta* 72.1, pp. 151–169.
- Johnson, C. M., Beard, B. L., and Roden, E. E. (2008b). “The iron isotope fingerprints of redox and biogeochemical cycling in modern and ancient Earth.” *Annu. Rev. Earth Planet. Sci.* 36, pp. 457–493.
- Kennedy, M. J., Pevear, D. R., and Hill, R. J. (2002). “Mineral surface control of organic carbon in black shale.” *Science* 295.5555, pp. 657–660.
- Kim, J., Dong, H., Seabaugh, J., Newell, S. W., and Eberl, D. D. (2004). “Role of microbes in the smectite-to-illite reaction.” *Science* 303.5659, pp. 830–832.
- König, I., Drodt, M., Suess, E., and Trautwein, A. (1997). “Iron reduction through the tan-green color transition in deep-sea sediments.” *Geochimica et Cosmochimica Acta* 61.8, pp. 1679–1683.
- Kostka, J. E., Wu, J., Nealson, K. H., and Stucki, J. W. (1999). “The impact of structural Fe (III) reduction by bacteria on the surface chemistry of smectite clay minerals.” *Geochimica et Cosmochimica Acta* 63.22, pp. 3705–3713.
- Land, L. S. (1980). “The isotopic and trace element geochemistry of dolomite: the state of the art.” 28, pp. 87–110.
- Macdonald, F. A., Schmitz, M. D., Crowley, J. L., Roots, C. F., Jones, D. S., Maloof, A. C., Strauss, J. V., Cohen, P. A., Johnston, D. T., and Schrag, D. P. (2010). “Calibrating the cryogenian.” *Science* 327.5970, pp. 1241–1243.
- Meunier, A. and El Albani, A. (2007). “The glauconite–Fe-illite–Fe-smectite problem: a critical review.” *Terra Nova* 19.2, pp. 95–104.
- Nesbitt, H. and Young, G. M. (1989). “Formation and diagenesis of weathering profiles.” *The Journal of Geology*, pp. 129–147.

- Pichat, S., Douchet, C., and Albarède, F. (2003). “Zinc isotope variations in deep-sea carbonates from the eastern equatorial Pacific over the last 175 ka.” *Earth and Planetary Science Letters* 210.1, pp. 167–178.
- Pollastro, R. M. (1985). “Mineralogical and morphological evidence for the formation of illite at the expense of illite/smectite.” *Clays and Clay Minerals* 33.4, pp. 265–274.
- Poulton, S. W. and Canfield, D. E. (2011). “Ferruginous conditions: a dominant feature of the ocean through Earth’s history.” *Elements* 7.2, pp. 107–112.
- Pratt, B. R. (1998). “Molar-tooth structure in Proterozoic carbonate rocks: Origin from synsedimentary earthquakes, and implications for the nature and evolution of basins and marine sediment.” *Geological Society of America Bulletin* 110.8, pp. 1028–1045.
- Rice, A. H. N., Edwards, M. B., and Hansen, T. A. (2012). “Neoproterozoic glacial and associated facies in the Tanafjord-Varangerfjord area, Finnmark, North Norway.” *Field Guides* 26, pp. 1–83.
- Rongemaille, E., Bayon, G., Pierre, C., Bollinger, C., Chu, N., Fouquet, Y., Riboulot, V., and Voisset, M. (2011). “Rare earth elements in cold seep carbonates from the Niger delta.” *Chemical Geology* 286.3, pp. 196–206.
- Rousset, D., Leclerc, S., Clauer, N., Lancelot, J., Cathelineau, M., and Aranyossy, J.-F. (2004). “Age and origin of Albian glauconites and associated clay minerals inferred from a detailed geochemical analysis.” *Journal of Sedimentary research* 74.5, pp. 631–642.
- Rouxel, O. J. and Auro, M. (2010). “Iron Isotope Variations in Coastal Seawater Determined by Multicollector ICP-MS.” *Geostandards and Geoanalytical Research* 34.2, pp. 135–144.
- Severmann, S., Johnson, C. M., Beard, B. L., and McManus, J. (2006). “The effect of early diagenesis on the Fe isotope compositions of porewaters and authigenic minerals in continental margin sediments.” *Geochimica et Cosmochimica Acta* 70.8.
- Shen, B., Dong, L., Xiao, S., Lang, X., Huang, K., Peng, Y., Zhou, C., Ke, S., and Liu, P. (2016). “Molar tooth carbonates and benthic methane fluxes in Proterozoic oceans.” *Nature communications* 7. DOI: 10.1038/ncomms10317.

- Shields, G. A. (2002). “Molar-tooth microspar’: a chemical explanation for its disappearance 750 Ma.” *Terra Nova* 14.2, pp. 108–113.
- Shields, G. and Veizer, J. (2002). “Precambrian marine carbonate isotope database: Version 1.1.” *Geochemistry, Geophysics, Geosystems* 3.6, pp. 1–12.
- Sperling, E. A., Wolock, C. J., Morgan, A. S., Gill, B. C., Kunzmann, M., Halverson, G. P., Macdonald, F. A., Knoll, A. H., and Johnston, D. T. (2015). “Statistical analysis of iron geochemical data suggests limited late Proterozoic oxygenation.” *Nature* 523.7561, pp. 451–454.
- Stucki, J. W. and Kostka, J. E. (2006). “Microbial reduction of iron in smectite.” *Comptes Rendus Geoscience* 338.6, pp. 468–475.
- Thamdrup, B. (2000). “Bacterial manganese and iron reduction in aquatic sediments.” *Advances in microbial ecology*. Springer, pp. 41–84.
- Tosca, N. J., Johnston, D. T., Mushegian, A., Rothman, D. H., Summons, R. E., and Knoll, A. H. (2010). “Clay mineralogy, organic carbon burial, and redox evolution in Proterozoic oceans.” *Geochimica et Cosmochimica Acta* 74.5, pp. 1579–1592.
- Van Acken, D., Thomson, D., Rainbird, R. H., and Creaser, R. A. (2013). “Constraining the depositional history of the Neoproterozoic Shaler Supergroup, Amundsen Basin, NW Canada: Rhenium-osmium dating of black shales from the Wynniatt and Boot Inlet Formations.” *Precambrian Research* 236, pp. 124–131.
- Veizer, J. and Hoefs, J. (1976). “The nature of O 18/O 16 and C 13/C 12 secular trends in sedimentary carbonate rocks.” *Geochimica et Cosmochimica Acta* 40.11, pp. 1387–1395.
- Vorhies, J. S. and Gaines, R. R. (2009). “Microbial dissolution of clay minerals as a source of iron and silica in marine sediments.” *Nature Geoscience* 2.3, pp. 221–225.
- Wattel-Koekkoek, E., Buurman, P., Van Der Plicht, J., Wattel, E., and Van Breemen, N. (2003). “Mean residence time of soil organic matter associated with kaolinite and smectite.” *European Journal of Soil Science* 54.2, pp. 269–278.

CHAPTER 4

Concluding Thoughts and Future Work

A previously dismissed hypothesis for the formation of molar tooth structures was tested using a comprehensive sample suite and stable isotope geochemistry. Although the results are promising, and support a role for dissimilatory iron reduction in the formation of molar tooth structures, further field studies and geochemical analyses could be done to better elucidate the genesis of these enigmatic Proterozoic structures.

To date, the morphologies of molar tooth structures do not have any apparent significance, with the possible exception of “blobs” in the Annijokka Member of the Båtsfjord Formation. A highly detailed field study which systematically documents the morphologies of molar tooth structures through time and space may help to determine if there is any significance to the morphologies in which molar tooth structures occur. For future geochemical studies, it would be more informative to have a sample set in which the matrix is composed of limestone, rather than dolostone, in order to better constrain the effects of dolomitisation and alteration.

Other geochemical proxies may also be used to test the significance of the smectite-illite reaction in the formation of molar tooth structures. Clay minerals have unique geochemical

compositions in terms of calcium and lithium isotopes, and may therefore be used to understand the relationship between clay minerals and molar tooth structures. For example, smectite should contain isotopically light lithium, therefore if molar tooth structures form from illitisation of smectites and release of alkaline pore waters, they should also contain isotopically light lithium.

Molar tooth structures record differences only in some isotope systems, perhaps reflective of the relative size of each elemental pool in seawater. For example, $\delta^{13}\text{C}$ measurements are indistinguishable between molar tooth structures and their matrix carbonate, whereas $\delta^{56}\text{Fe}$ values in molar tooth structures are depleted relative to the matrix carbonate and siliciclastics. It also has interesting implications for the use of other geochemical proxies, and whether or not they will record systematically different values between the molar tooth structure, matrix carbonate, and matrix siliciclastics. The use of X-Ray diffraction would also be very helpful to constrain the mineralogy of the matrix, particularly of the clay minerals.

Aside from applying geochemical proxies to molar tooth structures to understand their formation, the dataset presented here has interesting implications for carbonate clumped isotope paleothermometry. The apparent resistance of the calcite in molar tooth structures to dolomitisation and meteoric alteration, especially compared to the matrix carbonate, makes them an interesting target for carbonate clumped isotope paleothermometry. Clumped isotopes in carbonate minerals are highly susceptible to being “reset” during burial due to recrystallization of the carbonate minerals. Given that the calcite in molar tooth structures is apparently resistant to post-depositional alteration, one may expect that they would record a more “pristine” isotopic signal than that of the matrix. They may therefore present a viable way to apply carbonate clumped isotope paleothermometry to the Proterozoic.

Supplementary Information

Table S1 Major/minor element abundances in molar tooth structures. Abbreviated formation names: Dra. = Draken Formation; B.In. = Boot Inlet Formation; Mai. = Maieberg Formation; Rf.A = Reefal Assemblage; Hel. = Helena Formation; V.By. = Victor Bay Formation; Båt. = Båtsfjord Formation.

Formation	Section	Sample Height	% IR	Al (ppm)	Ba (ppm)	Ca (ppm)	Fe (ppm)	Mg (ppm)	Mn (ppm)	Rb (ppm)	Sr (ppm)	Ti (ppm)	Mg/Ca	Mn/Sr
Dra.	—	A	0.0	44	1.6	400000	91	1700	63	98	290	5.6	0.00	0.2
	—	B	3.3	200	5.5	390000	1000	2500	340	100	1600	20	0.01	0.2
	—	C	0.0	67	7.3	400000	990	1300	270	100	1100	36	0.00	0.2
B.In.	T1516	16.2	0.0	43	2.9	210000	35000	120000	2900	55	32	16	0.55	90
	T1522	A	0.0	3.3	3.2	380000	130	2100	48	98	140	16	0.01	0.3
Mai.	MN1500	A	0.0	190	30	390000	4500	5600	580	96	410	68	0.01	1.4
	MN1500	B	0.0	33	15	410000	4200	4900	580	100	300	48	0.01	1.9
	MN1500	C	0.0	35	7.7	390000	3700	4400	460	99	440	18	0.01	1.0
	—	—	0.0	71	6.8	370000	4400	7900	260	95	580	23	0.02	0.5
Rf.A.	—	344.0	3.6	980	13	280000	1500	9700	140	67	91	20	0.04	1.6
Hel.	RP	383.0	0.2	40	9.8	410000	280	2200	220	100	120	5.8	0.01	1.8
	—	400.0	7.6	180	54	410000	710	4600	220	100	120	6.3	0.01	1.9
	—	434.5	0.0	270	8.1	330000	530	3500	230	82	89	4.9	0.01	2.6
	—	440.0	5.4	370	9.1	400000	820	5000	200	100	130	6.3	0.01	1.5
	—	452.0	0.0	320	10	350000	820	4100	270	88	110	11	0.01	2.4
	—	472.0	0.0	240	11	340000	720	2600	190	85	120	7.3	0.01	1.6
	—	492.5	0.0	500	10	200000	1500	9900	270	51	67	5.1	0.05	4.0
	—	500.0	21	900	110	400000	2900	15000	480	100	110	8.3	0.04	4.3
	—	510.0	14	1200	15	370000	1800	7500	230	95	100	11	0.02	2.2
	—	513.5	0.0	300	14	400000	1100	5400	280	99	120	22	0.01	2.3
	—	535.0	3.0	440	18	410000	1500	7100	460	97	120	44	0.02	3.9
	—	549.0	1.1	500	19	410000	1400	5500	250	99	110	40	0.01	2.2
	—	554.0	0.0	310	17	400000	1000	3100	290	96	120	38	0.01	2.5
	—	557.0	0.0	480	14	400000	1100	3000	320	98	120	21	0.01	2.6
	—	561.0	0.0	180	13	390000	810	2600	220	95	110	19	0.01	2.0
	—	568.0	0.0	47	12	400000	950	1700	230	98	110	19	0.00	2.2
	—	571.0	8.3	130	13	460000	540	2300	210	110	140	25	0.00	1.5
	—	584.0	19	1400	54	350000	3300	9900	380	87	130	23	0.03	2.9
	—	609.0	9.4	430	19	400000	1300	5900	230	99	130	21	0.01	1.8
	—	723.0	3.4	530	41	410000	980	2000	190	99	96	21	0.00	1.9

Formation	Section	Sample Height	% IR	Al (ppm)	Ba (ppm)	Ca (ppm)	Fe (ppm)	Mg (ppm)	Mn (ppm)	Rb (ppm)	Sr (ppm)	Ti (ppm)	Mg/Ca	Mn/Sr
V.By.	MB1501	730.0	6.5	380	30	400000	740	1900	280	98	100	22	0.00	2.7
		747.0	1.8	260	180	410000	540	3300	200	99	130	22	0.01	1.6
		72.6	4.0	180	6.2	390000	1300	4600	120	100	720	21	0.01	0.2
		157.5	0.0	630	9.6	390000	1100	7200	110	96	280	10	0.02	0.4
		235.3	13	180	1.6	440000	510	2000	120	110	410	6.9	0.00	0.3
		238.8	5.1	850	5.9	390000	1400	9800	150	96	390	11	0.03	0.4
		278.8	0.0	1700	19	360000	3200	18000	150	88	220	8.2	0.05	0.7
		279.0	0.0	250	6.3	400000	810	3700	110	100	200	11	0.01	0.5
		296.0	0.0	920	10	360000	1800	14000	190	89	180	10	0.04	1.0
		322.7	0.0	140	11	380000	560	4200	97	95	150	8.6	0.01	0.6
		402.0	0.0	230	74	340000	600	13000	56	85	900	8.5	0.04	0.1
		402.4	0.0	64	6.7	370000	380	9600	71	94	660	11	0.03	0.1
		426.0	0.0	74	3.7	370000	320	13000	24	95	220	9.8	0.04	0.1
		446.5	3.4	320	6.8	370000	480	9700	64	95	870	9.5	0.03	0.1
		448.0	0.0	210	8.9	390000	540	8800	62	98	680	11	0.02	0.1
Bât.	T1508	451.4	1.2	61	82	380000	390	10000	33	98	1200	9.1	0.03	0.0
		452.1	0.0	11	280	380000	120	1400	20	99	1600	9.1	0.00	0.0
		453.7	0.0	22	4.6	380000	200	1900	25	98	1200	5	0.00	0.0
		457.5	0.0	40	6.9	380000	190	2800	24	97	1100	9.4	0.01	0.0
		489.0	0.0	80	8.7	370000	340	10000	34	95	980	8.3	0.03	0.0
		489.8	0.0	100	7.4	380000	300	7500	32	97	990	10	0.02	0.0
		~190 A	0.0	24	6.7	390000	120	2500	26	100	940	9.5	0.01	0.0
		~190 B	0.0	53	9.7	390000	170	4100	37	100	1100	9.6	0.01	0.0
		~190 C	0.0	26	6.5	340000	110	2000	30	88	820	8.4	0.01	0.0
		67.6	4.8	0	4.5	410000	510	1900	800	110	530	5.9	0.00	1.5
		68.0	0.0	1.7	2.4	380000	120	1500	230	97	290	5	0.00	0.8
		72.5	0.0	90	7.8	400000	1100	3400	310	98	280	18	0.01	1.1
		83.1	0.0	780	24	350000	4600	4700	950	84	370	46	0.01	2.6
		A	1.6	130	6.1	400000	900	5200	2000	98	290	21	0.01	6.8
		B	0.0	2.5	3.3	380000	300	1900	2500	96	280	5.1	0.01	8.7
MF1507	C	28.7	55	4800	15	210000	27000	59000	3100	55	270	32	0.28	12
		46.5	0.0	33	6.6	380000	580	1700	270	99	240	17	0.00	1.2
		55.5	10	270	15	420000	1000	1800	540	110	330	53	0.00	1.7
		55.8	16	530	24	400000	1200	3600	820	100	330	46	0.01	2.5

Formation	Section	Sample Height	% IR	Al (ppm)	Ba (ppm)	Ca (ppm)	Fe (ppm)	Mg (ppm)	Mn (ppm)	Rb (ppm)	Sr (ppm)	Ti (ppm)	Mg/Ca	Mn/Sr
MF1509		138.0	0.0	0	13	400000	380	2500	330	100	540	32	0.01	0.6
		52.8	4.2	270	12	410000	1300	3700	490	110	390	51	0.01	1.2
		A	0.0	110	220	400000	1400	3000	640	96	400	40	0.01	1.6
		B	3.3	140	4.8	420000	1800	2500	2000	100	280	32	0.01	7.0
MF1510		53.7	86	86	5.2	270000	740	2100	600	65	190	21	0.01	3.2
		68.1	4.1	380	17	390000	1900	7100	1100	94	270	29	0.02	4.2
		81.1	5.8	84	4.3	420000	690	2200	400	100	310	27	0.01	1.3
		81.6	0.0	150	8	440000	750	2500	460	110	320	61	0.01	1.4
		81.7	0.0	64	4.2	410000	890	3400	410	99	290	25	0.01	1.4
		92.1	0.0	6.3	7.7	400000	1800	1200	1100	98	500	19	0.00	2.2
		98.2	2.3	130	9.4	400000	1000	2200	300	99	320	19	0.01	0.9

Table S2 Major/minor element abundances in matrix carbonate. Abbreviated formation names: Dra. = Draken Formation; B.In. = Boot Inlet Formation; Mai. = Maieberg Formation; Rf.A = Reefal Assemblage; Hel. = Helena Formation; V.By. = Victor Bay Formation; Båt. = Båtsfjord Formation.

Formation	Section	Sample Height	% IR	Al (ppm)	Ba (ppm)	Ca (ppm)	Fe (ppm)	Mg (ppm)	Mn (ppm)	Rb (ppm)	Sr (ppm)	Ti (ppm)	Mg/Ca	Mn/Sr	
Dra.	—	A	23	2800	19	250000	3900	110000	390	60	110	7.3	0.46	3.5	
	—	B	11	960	7.2	360000	3100	7900	500	94	1400	20	0.02	0.4	
	—	C	9.3	2300	13	320000	9000	29000	510	83	1200	22	0.09	0.4	
B.In.	T1516	16.2	0.6	150	4.1	200000	26000	120000	1900	54	40	15	0.58	47	
	T1522	A	6.0	460	5.5	230000	5000	110000	200	60	50	16	0.48	4.0	
Mai.	MN1500	A	100	820	25	350000	8800	23000	650	88	380	23	0.07	1.7	
	MN1500	B	11	740	24	340000	7900	21000	650	87	360	20	0.06	1.8	
	MN1500	C	14	840	80	360000	3700	6400	630	93	300	21	0.02	2.1	
Rf.A.	—	—	97	360	6.8	340000	13000	27000	440	87	440	19	0.08	1.0	
Hel.	RP	344.0	45	5600	42	220000	8800	70000	470	54	76	22	0.32	6.2	
		383.0	24	2400	27	270000	5300	42000	490	66	98	8.4	0.16	5.0	
		400.0	48	2200	28	360000	6100	55000	580	90	110	9.9	0.15	5.3	
		434.5	31	2400	21	380000	3500	22000	480	95	120	9.5	0.06	3.9	
		440.0	0.0	7900	57	230000	13000	100000	890	58	68	8.2	0.45	13	
		452.0	55	8800	71	260000	9800	47000	1100	66	85	8.5	12	0.18	13
		472.0	54	12000	130	210000	26000	110000	870	54	80	12	0.50	11	
		492.5	0.9	2900	19	190000	11000	80000	890	48	61	9.4	0.41	15	
		500.0	61	7500	84	420000	16000	93000	1200	110	150	12	0.22	8.4	
		510.0	47	9100	67	300000	12000	51000	660	70	86	50	0.17	7.7	
		513.5	45	4300	38	350000	11000	63000	880	85	100	32	0.18	8.5	
		535.0	41	4500	35	300000	14000	77000	1100	73	94	28	0.26	12	
		549.0	63	6800	84	210000	15000	85000	960	52	72	28	0.40	13	
		554.0	55	5900	61	280000	13000	71000	830	67	96	34	0.25	8.7	
		557.0	55	9900	120	240000	15000	68000	790	57	80	31	0.29	9.9	
		561.0	39	3400	29	290000	13000	73000	970	70	95	27	0.25	10	
		568.0	14	1100	22	370000	2000	7900	540	91	100	22	0.02	5.3	
		571.0	0.3	1600	16	320000	2000	7100	370	78	100	21	0.02	3.6	
		584.0	47	6300	100	150000	7200	29000	320	37	53	19	0.19	6.0	
		609.0	59	6100	89	240000	14000	66000	750	59	110	26	0.28	6.9	
723.0	47	16000	230	260000	14000	38000	380	62	78	41	0.15	4.9			

Formation	Section	Sample Height	% IR	Al (ppm)	Ba (ppm)	Ca (ppm)	Fe (ppm)	Mg (ppm)	Mn (ppm)	Rb (ppm)	Sr (ppm)	Ti (ppm)	Mg/Ca	Mn/Sr
V.By.	MB1501	730.0	57	4100	130	320000	2600	4900	320	76	77	37	0.02	4.2
		747.0	24	1800	850	370000	2400	10000	390	89	110	26	0.03	3.6
		72.6	32	1400	15	290000	2400	51000	300	74	390	25	0.18	0.8
		157.5	41	7000	31	220000	11000	120000	500	54	250	54	0.54	2.0
		235.3	43	2900	27	220000	8300	120000	530	57	210	7.8	0.52	2.5
		238.8	47	7600	44	220000	12000	110000	580	55	310	7.2	0.49	1.9
		278.8	45	8900	81	230000	13000	110000	540	57	230	7.7	0.48	2.3
		279.0	40	6700	38	220000	12000	110000	490	54	200	6.3	0.50	2.5
		296.0	30	5100	69	250000	8600	85000	410	63	220	8.3	0.34	1.9
		322.7	41	3300	21	200000	9200	110000	540	51	220	14	0.55	2.5
		402.0	16	1500	15	240000	3700	110000	200	62	220	8.6	0.44	0.9
		402.4	21	680	18	240000	3400	100000	220	62	360	8.1	0.42	0.6
		426.0	5.0	800	11	260000	2000	100000	78	66	130	8	0.39	0.6
		446.5	48	730	22	320000	1200	12000	91	80	640	11	0.04	0.1
		448.0	15	1200	15	290000	2900	70000	160	72	340	8.6	0.25	0.5
Bât.	T1508	451.4	13	300	17	280000	2800	86000	120	71	280	9.6	0.31	0.4
		452.1	15	330	30	280000	2000	81000	110	73	320	8.9	0.28	0.3
		453.7	14	210	7.9	360000	930	34000	66	92	490	7.5	0.09	0.1
		457.5	2.8	160	14	340000	1300	32000	64	88	610	8.7	0.09	0.1
		489.0	22	440	16	260000	2200	110000	140	66	280	8.9	0.42	0.5
		489.8	15	860	15	260000	2500	93000	120	67	230	8.6	0.36	0.5
		~190 A	6.1	300	13	330000	1300	47000	96	86	580	11	0.14	0.2
		~190 B	14	500	150	310000	1700	59000	130	79	530	10	0.19	0.2
		~190 C	20	680	16	320000	2100	69000	150	82	450	10	0.22	0.3
		67.6	40	3200	100	320000	26000	50000	2300	82	270	9.4	0.16	8.6
	MF1506	68.0	37	890	25	350000	2000	3100	560	90	370	8.2	0.01	1.5
		72.5	23	2300	38	290000	12000	55000	710	71	280	24	0.19	2.6
		83.1	34	2200	42	350000	7000	9000	1300	85	510	29	0.03	2.5
		A	30	1800	18	210000	13000	96000	1500	51	230	25	0.45	6.4
		B	54	4800	28	230000	16000	110000	1600	57	260	9.7	0.49	6.4
MF1507	C	25	3000	16	220000	15000	98000	1600	53	230	27	0.44	7.0	
	28.7	73	13000	81	10000	5700	8500	98	2.5	23	9.7	0.85	4.2	
	46.5	19	1900	23	240000	14000	85000	1300	64	260	20	0.35	5.1	
	55.5	58	6300	21	210000	5400	8000	760	53	210	45	0.04	3.6	
	55.8	40	3400	30	320000	4100	8300	1100	81	380	36	0.03	2.9	

Formation	Section	Sample Height	% IR	Al (ppm)	Ba (ppm)	Ca (ppm)	Fe (ppm)	Mg (ppm)	Mn (ppm)	Rb (ppm)	Sr (ppm)	Ti (ppm)	Mg/Ca	Mn/Sr
MF1509		138.0	18	1100	17	260000	9700	67000	890	67	260	42	0.26	3.4
		52.8	56	7200	40	200000	20000	78000	1300	53	320	28	0.38	4.2
		A	37	4000	730	230000	27000	94000	1900	56	270	24	0.41	6.9
		B	41	4200	29	230000	30000	94000	2900	54	350	33	0.41	8.3
MF1510		53.7	100	4300	31	270000	12000	24000	1500	63	330	56	0.09	4.6
		68.1	55	3600	22	260000	16000	78000	2600	62	230	30	0.30	11
		81.1	38	2800	12	330000	9500	37000	660	81	330	27	0.11	2.0
		81.6	40	3000	14	320000	10000	35000	690	77	340	29	0.11	2.0
		81.7	27	2600	12	270000	14000	79000	950	64	350	24	0.30	2.7
		92.1	26	1900	9.9	370000	5200	4800	1500	90	340	28	0.01	4.5
		98.2	68	8300	25	260000	12000	37000	610	61	280	41	0.14	2.1

Table S3 $\delta^{56}\text{Fe}$ in molar tooth structures. Abbreviated formation names: Dra. = Draken Formation; B.In. = Boot Inlet Formation; Mai. = Maieberg Formation; Rf.A = Reefal Assemblage; Hel. = Helena Formation; V.By. = Victor Bay Formation; Båt. = Båtsfjord Formation.

Formation	Section	Sample Height	$\delta^{56}\text{Fe}_{3126\text{a}}$	1σ	$\delta^{57}\text{Fe}_{3126\text{a}}$	1σ	$\delta^{56}\text{Fe}_{\text{IRMM-014}}$	1σ
Dra.	—	B	0.34	0.06	0.50	0.49	-0.05	0.06
	—	C	-0.61	0.06	-0.59	0.74	-1.00	0.06
B.In.	T1522	—	-1.84	0.36	-2.86	0.77	-2.23	0.36
Mai.	MN1500	C	0.73	0.11	1.16	0.19	0.34	0.11
Rf.A.	—	—	-0.32	0.04	-0.36	0.13	-0.71	0.04
Hel.	RP	400.0	-0.57	0.04	-0.63	0.37	-0.96	0.04
		434.5	-0.36	0.05	-0.92	0.84	-0.75	0.05
		510.0	2.26	0.22	3.62	0.57	1.87	0.22
		571.0	0.99	0.03	1.56	0.36	0.60	0.03
		609.0	0.84	0.16	1.29	0.37	0.45	0.16
		723.0	0.50	0.01	1.08	0.32	0.11	0.01
		747.0	0.01	0.04	0.49	0.41	-0.38	0.04
V.By.	MB1501	72.6	2.35	0.03	2.55	0.52	1.96	0.03
		235.3	-2.00	0.21	-3.12	0.44	-2.39	0.21
		457.5	0.13	0.18	0.44	0.45	-0.26	0.18
		489.0	-1.48	0.13	2.36	0.97	-1.87	0.13
		489.8	0.21	0.05	0.39	0.06	-0.18	0.05
	T1508	~190 A	-1.06	0.10	-1.82	0.08	-1.45	0.10
		~190 C	-0.39	0.31	-0.15	0.08	-0.78	0.31
Båt.	MF1506	68.0	-0.35	0.24	-0.42	0.44	-0.74	0.24
		72.5	2.26	0.07	3.49	0.94	1.87	0.07
	MF1507	55.8	0.61	0.12	1.21	0.44	0.22	0.12
		138.0	-0.58	0.08	-0.88	0.56	-0.97	0.08
	MF1509	52.8	0.25	0.04	0.58	0.60	-0.14	0.04
	MF1510	81.1	0.25	0.09	0.68	0.43	-0.14	0.09
		98.2	-0.34	0.09	-0.44	0.26	-0.73	0.09

Table S4 $\delta^{56}\text{Fe}$ in matrix carbonate. Abbreviated formation names: Dra. = Draken Formation; B.In. = Boot Inlet Formation; Mai. = Maieberg Formation; Rf.A = Reefal Assemblage; Hel. = Helena Formation; V.By. = Victor Bay Formation; Båt. = Båtsfjord Formation.

Formation	Section	Sample Height	$\delta^{56}\text{Fe}_{3126\text{a}}$	1σ	$\delta^{57}\text{Fe}_{3126\text{a}}$	1σ	$\delta^{56}\text{Fe}_{\text{IRMM-014}}$	1σ
Dra.	—	B	0.93	0.11	1.27	0.13	0.54	0.11
	—	C	2.03	0.04	2.99	0.07	1.64	0.04
B.In.	T1522	A	0.38	0.02	0.65	0.06	-0.01	0.02
Mai.	MN1500	C	1.28	0.1	1.82	0.12	0.89	0.10
Rf.A.	—	—	-0.09	0.05	0.03	0.04	-0.48	0.05
Hel.	RP	400.0	2.59	0.05	3.63	0.19	2.20	0.05
		434.5	0.34	0.05	0.50	0.06	-0.05	0.05
		510.0	1.61	0.04	2.35	0.08	1.22	0.04
		571.0	0.92	0.07	1.49	0.59	0.53	0.07
		609.0	1.31	0.12	1.92	0.14	0.92	0.12
		723.0	1.64	0.05	2.33	0.08	1.25	0.05
		747.0	2.03	0.11	3.05	0.18	1.64	0.11
V.By.	MB1501	72.6	1.83	0.06	2.80	0.06	1.44	0.06
		235.3	-0.04	0.05	-0.02	0.15	-0.43	0.05
		446.5	1.96	0.48	2.81	1.33	1.57	0.48
		457.5	-0.30	0.04	-0.47	0.11	-0.69	0.04
		489.0	0.37	0.02	0.59	0.03	-0.02	0.02
		489.8	2.29	0.05	3.44	0.02	1.90	0.05
	T1508	~190 A	1.79	0.07	2.93	0.55	1.40	0.07
		~190 B	1.89	0.04	2.82	0.07	1.50	0.04
		~190 C	1.53	0.03	2.26	0.04	1.14	0.03
Båt.	MF1506	68.0	1.28	0.10	1.89	0.15	0.89	0.10
		72.5	0.80	0.11	1.25	0.13	0.41	0.11
	MF1507	55.8	1.85	0.03	2.82	0.05	1.46	0.03
		138.0	1.09	0.08	1.68	0.18	0.70	0.08
	MF1509	52.8	0.39	0.11	0.56	0.17	0.00	0.11
	MF1510	81.1	1.12	0.05	1.57	0.02	0.73	0.05
		98.2	0.80	0.25	1.26	0.38	0.41	0.25

Table S5 $\delta^{56}\text{Fe}$ in matrix siliciclastics. Abbreviated formation names: Dra. = Draken Formation; B.In. = Boot Inlet Formation; Mai. = Maieberg Formation; Rf.A = Reefal Assemblage; Hel. = Helena Formation; V.By. = Victor Bay Formation; Båt. = Båtsfjord Formation.

Formation	Section	Sample Height	$\delta^{56}\text{Fe}_{3126\text{a}}$	1σ	$\delta^{57}\text{Fe}_{3126\text{a}}$	1σ	$\delta^{56}\text{Fe}_{\text{IRMM-014}}$	1σ
Dra.	—	B	0.55	0.06	0.82	0.11	0.16	0.06
Hel.	RP	747	0.52	0.05	0.85	0.17	0.13	0.05
V.By.	MB1501	457.5	1.06	0.08	1.60	0.07	0.67	0.08
		489.8	1.78	0.13	2.62	0.18	1.39	0.13
		489	1.92	0.05	2.87	0.15	1.53	0.05
	T1508	~190 A	2.51	0.11	3.68	0.23	2.12	0.11
		~190 C	1.35	0.03	2.08	0.12	0.96	0.03
Båt.	MF1506	72.5	0.89	0.06	1.26	0.03	0.50	0.06
	MF1507	138	2.16	0.11	3.17	0.19	1.77	0.11
	MF1509	52.8	0.70	0.06	1.01	0.09	0.31	0.06

Table S6 $\delta^{13}\text{C}$ in molar tooth structures. Abbreviated formation names: Dra. = Draken Formation; B.In. = Boot Inlet Formation; Mai. = Maieberg Formation; Rf.A. = Reefal Assemblage; Hum. = Humboldt Formation; Hel. = Helena Formation; V.By. = Victor Bay Formation; Båt. = Båtsfjord Formation.

Formation	Section	Sample Height	$\delta^{13}\text{C}_{\text{VPDB}}$	$\delta^{18}\text{O}_{\text{VPDB}}$
Dra.	—	A	7.01	-4.98
	—	B	-2.51	-7.35
	—	C	-3.15	-6.00
B.In.	T1516	16.2	1.20	-4.98
	T1522	A	3.91	-5.18
Mai.	MN1500	A	-4.14	-11.14
	MN1500	B	-3.99	-8.79
	MN1500	C	-4.18	-9.59
Rf.A.	—	—	3.29	-7.65
Hum.	—	—	0.00	-15.47
Hel.	RP	344.0	1.07	-10.20
		383.0	1.52	-9.82
		400.0	1.09	-10.00
		434.5	1.45	-9.97
		440.0	0.95	-9.97
		452.0	1.25	-10.09
		472.0	1.04	-10.12
		492.5	1.07	-9.48
		500.0	1.63	-9.45
		510.0	1.50	-9.95
		513.5	1.80	-9.48
		535.0	1.81	-9.20
		549.0	1.85	-9.69
		554.0	1.84	-9.91
		557.0	1.90	-9.81
		561.0	1.87	-9.73
		568.0	2.00	-8.86
		571.0	2.18	-8.98
		584.0	2.13	-8.34
		609.0	2.19	-9.55
		723.0	1.10	-10.29
		730.0	1.35	-9.91
		747.0	0.47	-10.41
V.By.	MB1501	72.6	0.66	-5.72
		157.5	-0.34	-5.20
		235.3	-0.84	-5.50
		238.8	-1.01	-5.52
		278.8	-1.78	-5.19
		279.0	-1.67	-5.43
		296.0	-2.60	-5.55
		322.7	-1.36	-3.74
		402.0	1.16	-5.05
		402.4	0.36	-4.49
		426.0	0.25	-4.42
		446.5	0.48	-4.86
		448.0	0.34	-4.76

Formation	Section	Sample Height	$\delta^{13}\text{C}_{\text{VPDB}}$	$\delta^{18}\text{O}_{\text{VPDB}}$
Bât.	T1508	451.4	1.07	-4.95
		452.1	1.38	-4.92
		453.7	1.20	-4.75
		457.5	1.29	-4.83
		489.0	1.04	-4.75
		489.8	1.11	-4.69
		~190 A	3.47	-4.87
		~190 B	3.54	-4.86
		~190 C	3.29	-5.12
	MF1506	67.6	-0.10	-9.75
		68.0	-0.75	-10.20
		72.5	-3.79	-10.74
		83.1	-2.72	-12.80
		A	-3.78	-11.30
		B	-3.48	-11.12
		C	-4.15	-11.19
	MF1507	28.7	-4.26	-12.46
		46.5	-1.77	-14.56
		55.5	-2.37	-14.99
		55.8	-2.50	-15.00
		138.0	-1.99	-14.16
	MF1509	52.8	-3.43	-12.22
		A	-3.68	-11.23
		B	-5.28	-9.55
	MF1510	53.7	-3.20	-11.87
		68.1	-3.63	-11.45
		81.1	-5.19	-11.15
		81.6	-4.89	-11.11
		81.7	-5.77	-11.38
		92.1	-4.09	-10.63
		98.2	-3.21	-11.06

Table S7 $\delta^{13}\text{C}$ in matrix carbonate. Abbreviated formation names: Dra. = Draken Formation; B.In. = Boot Inlet Formation; Mai. = Maieberg Formation; Rf.A = Reefal Assemblage; Hum. = Humboldt Formation; Hel. = Helena Formation; V.By. = Victor Bay Formation; Båt. = Båtsfjord Formation.

Formation	Section	Sample Height	$\delta^{13}\text{C}_{\text{VPDB}}$	$\delta^{18}\text{O}_{\text{VPDB}}$
Dra.	—	A	6.36	-5.57
	—	B	-2.74	-7.99
	—	C	-2.63	-7.19
B.In.	T1516	16.2	2.55	-6.53
	T1522	A	4.88	-7.10
Mai.	MN1500	A	-4.00	-11.01
	MN1500	B	-4.15	-6.64
	MN1500	C	-4.17	-10.90
Rf.A.	—	—	2.79	-6.98
Hum.	—	—	0.78	-10.84
Hel.	RP	344.0	0.95	-7.50
		383.0	1.51	-8.86
		400.0	1.28	-9.18
		434.5	1.41	-9.45
		440.0	1.48	-7.15
		452.0	1.43	-9.38
		472.0	0.66	-7.41
		492.5	2.00	-2.10
		500.0	1.76	-8.31
		510.0	1.84	-8.80
		513.5	1.95	-8.06
		535.0	1.99	-8.22
		549.0	2.15	-7.33
		554.0	2.07	-8.37
		557.0	2.16	-8.09
		561.0	2.10	-8.08
		568.0	1.77	-9.78
		571.0	1.88	-9.85
		584.0	2.02	-8.91
		609.0	2.27	-8.04
		723.0	1.16	-9.74
		730.0	0.55	-11.96
		747.0	0.51	-10.67
V.By.	MB1501	72.6	-0.08	-5.61
		157.5	0.01	-3.38
		235.3	-1.07	-3.17
		238.8	-1.13	-3.98
		278.8	-1.07	-3.73
		279.0	-0.98	-3.50
		296.0	-1.78	-4.59
		322.7	-1.22	-3.46
		402.0	0.62	-2.98
		402.4	0.84	-3.03
		426.0	1.49	-3.74
		446.5	0.13	-5.02
		448.0	0.28	-3.87

Formation	Section	Sample Height	$\delta^{13}\text{C}_{\text{VPDB}}$	$\delta^{18}\text{O}_{\text{VPDB}}$
Bât.	T1508	451.4	1.04	-3.98
		452.1	0.87	-3.99
		453.7	0.83	-4.79
		457.5	1.23	-4.63
		489.0	1.16	-2.69
		489.8	1.09	-3.13
		~190 A	3.17	-4.95
		~190 B	3.22	-4.31
		~190 C	3.06	-4.02
	MF1506	67.6	-2.71	-11.42
		68.0	-2.16	-12.83
		72.5	-2.56	-10.74
		83.1	-2.59	-12.57
		A	-3.24	-7.27
		B	-3.25	-7.62
		C	-3.58	-7.86
	MF1507	28.7	—	—
		46.5	-1.84	-12.82
		55.5	-4.03	-15.01
		55.8	-2.47	-15.00
		138.0	-2.31	-13.07
	MF1509	52.8	-2.62	-7.68
		A	-3.17	-8.44
		B	-5.64	-7.14
	MF1510	53.7	-4.21	-11.01
		68.1	-2.83	-7.31
		81.1	-4.19	-10.38
		81.6	-3.98	-10.39
		81.7	-3.10	-7.84
		92.1	-4.24	-10.83
		98.2	-3.23	-9.75

Table S8 TOC and wt% pyrite in bulk rock. Abbreviated formation names: Dra. = Draken Formation; B.In. = Boot Inlet Formation; Mai. = Maieberg Formation; Rf.A = Reefal Assemblage; Hel. = Helena Formation; V.By. = Victor Bay Formation; Båt. = Båtsfjord Formation.

Formation	Section	Sample Height	TOC (wt%)	Pyrite (wt%)
Dra.	—	B	0.04	0.01
	—	C	0.06	0.15
B.In.	T1522	—	0.15	0.08
Mai.	MN1500	C	0.10	0.04
Rf.A.	—	—	0.08	0.02
Hel.	RP	400	0.01	0.00
		434.5	0.03	0.01
		452	0.12	0.00
		472	0.11	0.00
		510	0.02	0.01
		571	0.04	0.00
		609	0.05	0.00
		723	0.14	0.01
		747	0.04	0.02
V.By.	MB1501	72.6	0.13	0.89
		235.3	0.15	0.26
		322.7	0.08	0.10
		402.4	0.06	0.14
		446.5	0.04	0.03
		452.1	0.06	0.03
		457.5	0.05	0.02
		489	0.04	0.01
		489.8	0.06	0.02
	T1508	~190 A	0.01	0.03
		~190 B	0.07	0.09
		~190 C	0.09	0.06
Båt.	MF1506	67.6	0.19	0.14
		68	0.24	0.10
		72.5	0.12	0.11
	MF1507	46.5	0.06	0.09
		55.8	0.03	0.08
		138	0.03	0.05
	MF1509	52.8	0.05	0.06
		B	0.07	0.01
	MF1510	81.1	0.08	0.02
		98.2	0.04	0.18

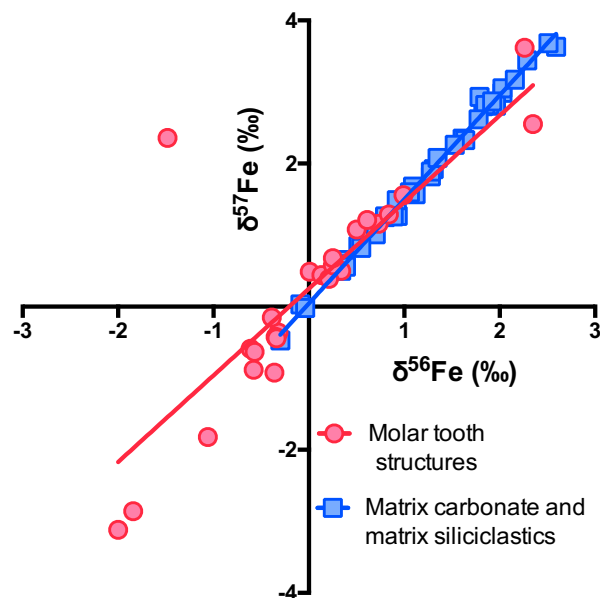


Figure S1 Mass dependent fractionation lines of $\delta^{56}\text{Fe}$ and $\delta^{57}\text{Fe}$ for matrix carbonate and siliciclastics and molar tooth structures. Matrix carbonate and matrix siliciclastics have slope of 1.455, close to the theoretical fractionation of 1.47 (Beard et al., 2004), and $R^2=0.994$. Molar tooth structures have slope of 1.21 and $R^2=0.664$. However, this is the result of erroneous $\delta^{57}\text{Fe}$ measurements due to operating at a low sample concentration of 50 ppb (refer to Section 3.6.6).